THE CONTROL OF CAVITY AND PANEL VIBRATION RESONANCE IN A ROOM WITH VENTILATION DUCT

CHAN SZE MAN

M.PHIL
THE HONG KONG
POLYTECHNIC UNIVERSITY
2010

THE HONG KONG POLYTECHNIC UNIVERSITY

DEPARTMENT OF CIVIL AND STRUCTURAL ENGINEERING

THE CONTROL OF CAVITY AND PANEL VIBRATION RESONANCE IN A ROOM WITH VENTILATION DUCT

CHAN SZE-MAN

A THESIS SUBMITTED IN PARTIAL FULFILLMENT OF

THE REQUIREMENT FOR THE

DEGREE OF MASTER OF PHILOSOPHY

JUNE, 2009

CERTIFICATE OF ORIGINALITY

I hereby declare that this thesis is my own work and that, to the best of my knowledge, it reproduces neither material previously published or written nor material that has been accepted for the award of any other degree or diploma, except where due acknowledgement has been made in the text.

CHAN Sze Man

ABSTRACT

Buildings with double skin façade or using the solar stack ventilation design to achieve natural cooling are the latest sustainable building designs for energy saving. However, sound can enter buildings through the ventilation ducts or openings. It is, therefore, important to take into consideration satisfactory amounts of both noise reduction and daylight when considering natural cooling systems for buildings.

The purpose of this investigation is to design: (1) a silencer with cavity and/or membrane absorbers to control noise in a ventilation duct; (2) a membrane and/or cavity absorber to control Helmholtz resonance in a ventilation space or room. The silencer is designed as a panel absorber system using divided panels with two layers, a transparent plastic membrane and a micro-perforated Plexiglas sheet. The two-layered panel absorber system extends the absorption to lower frequencies as well as maintaining good mid-frequency absorption, and hence becomes a desirable broadband absorber. If ventilation openings exist in a room, it is possible for air flow to generate an infrasound of a significant magnitude in the openings to irritate the people inside. Helmholtz resonance can be controlled using a membrane structure

that is either cavity backed or not. There are significant improvements in low frequency sound reduction when the Helmholtz resonant frequency of the ventilation openings matched with the membrane vibrating resonant frequency.

Formulae with satisfactory accuracy are derived for the panel absorber system with combined layers and the ventilation space with a membrane structure. The agreement between the experimental and theoretical results demonstrates the effectiveness of the formulae.

The new silencer design and membrane absorber have been proved to achieve desirable broadband noise reduction, offer excellent aesthetical properties and at the same time provide a healthier indoor environment in sustainable buildings.

PUBLICATIONS ARISING FROM THE THESIS

1. S.M. Chan and C.F. Ng (2009), Noise control of a ventilation duct by a panel absorber with transparent plastic sheet, *NOVEM2009 Conference (Noise and Vibration: Emerging Method)*. April 5th – 8th, 2009. Keble College, Oxford, UK.

2. S.M. Chan and C.F. Ng (2008), Interaction of nonlinear membrane vibration with acoustic waves, *Twelfth Conference on Nonlinear Vibrations, Dynamics, and Multibody Systems.* June 1st – 5th, 2008. Blacksburg, VA, The Inn at Virginia Tech.

3. C.F. Ng and S.M. Chan (2008), Anti-Symmetric Mode Vibration and Snap-Through Motion of a Curved Beam Subject to Auto-Parametric Excitation , *Twelfth Conference on Nonlinear Vibrations, Dynamics, and Multibody Systems.* June 1st – 5th, 2008. Blacksburg, VA, The Inn at Virginia Tech.

4. Awards:
   ICE Graduates & Students Division Papers Competition 2007, Environmental, Hydraulics and Hydrology Section Merit Award

ACKNOWLEDGEMENTS

I would like to take this opportunity to express my appreciation to my dearest supervisor, Associate Professor C. F. Ng, for his guidance and for the opportunity that he gave me to investigate various challenging engineering problems. The experience and knowledge obtained from those investigations have taught me how to solve new problems with confidence.

I would also like to express my sincere gratitude to Ms. Emily Fung for giving me valuable advices about the experimental setup and technical assistance. I also offer thanks to Mr. Y. W. Lam for his guidance on the operation of the computer software.

Finally, special acknowledgement is due to my family and friends, Ms. Deary Way and Mr. W. K. Lun, for their kind supports and encouragements that allowed me to pursue an academic career.

TABLE OF CONTENTS

LIST OF FIGURES

LIST OF TABLES

LIST OF ABBREVIATIONS

A	Accelerometer
DPPs	Divided Plexiglas Panels
DSF	Double Skin Façade
HAVC	Heating, Ventilation and Air-Conditioner
IAQ	Indoor Air Quality
LPPs	Long Plexiglas Panels
M	Microphone
PMP	Panels with Plastic membrane and Micro-Perforated membrane
TL	Transmission Loss

CHAPTER 1

INTRODUCTION

1.1 Introduction

According to the latest statistics from the Environmental Protection Department (EPD), traffic is a major source of low frequency noise which radiates from highways and railways. Other kinds of low frequency noise and infrasound are produced by machinery, equipment and heating and cooling systems. Low frequency noise shows tonal peaks below 63Hz. There are increasing numbers of complaints from people about infrasound and low frequency hums inside their homes. This low frequency dominant noise not only disturbs daily life, but also distracts our attention from work and makes it impossible for residents living near busy roads and highways to open windows at peak vehicle flow periods. Since walls block higher frequencies rather than lower frequencies, there is a need to implement effective measures to eliminate low frequency noise pollution while at the same time ensuring good ventilation.

In Hong Kong, it is difficult to achieve natural ventilation in residential and commercial buildings due to the number of high rise buildings. In addition, air quality is deteriorating and when this is coupled with the problem of traffic noise the

opportunity to use natural ventilation is reduced. The aim, therefore, is to control the effect of noise in indoor areas and at the same time ensure good ventilation by using natural ventilation like the solar stack ventilation effect in buildings with chimneys (See Appendix I) or double skin façades (DSF) (See Appendix II).

Different approaches have been suggested to minimize the effect of noise pollution such as building noise barriers, modifying building designs and even subsidizing noise victims by installing air conditioning. The last approach is a means of control at the point of the receiver. Although noise can be reduced and even a comfortable environment accomplished, air conditioning is not applicable throughout the year. With the exception of the summer, poor indoor ventilation is unavoidable due to the necessity of keeping windows closed; therefore, a demand exists for a solution that is suitable for all seasons.

The solar chimney has been in use for centuries to improve the natural ventilation of buildings, particularly in the Middle East, as well as by the Romans. In recent years, especially in foreign countries like United States and Turkey, solar chimneys have also been used to improve ventilation in homes. However, this method cannot reduce external traffic noise due to the large opening required for the air inflow. In countries where solar chimneys have been built they are very tall so as to achieve

significant electricity generation. In this study, silencers are applied in the ventilation ducts of buildings with chimneys or DSF to achieve broadband noise reduction (Figure 1-1). As a result, the chimney or ventilation space in buildings with DSF was able to provide enough fresh air required for homes and control the level of noise. This system can be applied to Hong Kong. In summer, Hong Kong is very hot and humid and people usually use air-conditioners to reduce indoor temperature and humidity and exhaust fans for ventilation. This leads to a notably higher level of electrical power consumption from air-conditioning. The solar stack ventilation principle can be applied to reduce heat transfer through the walls and roof, thus easing air-conditioners' cooling load.

Even though it may not be easy to install chimneys on buildings in Hong Kong, the solar stack ventilation principle can still be applied to Hong Kong buildings in the form of noise reduction windows. The window is the weakest part in relation to noise reduction in buildings. Windows with double skin façades (DSF) have the same ventilation effect as solar chimneys. The ventilation effect is due to the formation of air flow caused by the thermal, wind pressure and density differences that exist between the outside and inside of a room. By placing reactive silencers inside double glazed windows (Figure 1-3a), satisfactory performance in relation to both

ventilation and noise reduction can be obtained (Wen, 2008). Noise reduction windows have been on the market since 2002 and have been used in a number of residences, schools and hospitals in China (Figure 1-3b, 1-3c and 1-3d). There was also a research on developing window systems (Figure 1-2) that reduce noise transmission whilst allowing natural ventilation, and enabling the efficient use of daylight (Kang, 2008). The window system consists of acoustic ventilators that use micro-perforated absorbers. He proved that by placing such absorbers between two sheets of glass, noise reduction is significantly improved. This kind of window system is one example of a small scale DSF. A hood hung outside the opening is also very effective at reducing low frequency noise which fortunately has negligible effect on ventilation.

The purpose of this study is to examine the feasibility of applying the transparent panel absorber system, which acts as a silencer, in buildings with chimneys or DSF to provide sufficient air exchange rates and at the same time ensure desirable noise reduction performance, especially for low frequency noise. The transparent panel absorber system can achieve broadband noise reduction and maintain the lighting function of windows. The integrity of the window form can also be maintained. Few researchers have investigated a method to ensure both satisfactory noise reduction

and air flow rate; therefore, this study may help narrow this gap.

Forced and natural ventilation provide more fresh air than air-conditioners and can reduce the accumulation of harmful gases. The transparent panel absorber system is made of Plexiglas and plastic and has many advantages over conventional fibre glass used in air conditioning ducts. It provides better lighting due to its transparency and has less dust and water accumulation, which minimizes the danger of bacteria growth. Unlike fibre glass, it will not cause irritation to workers and occupants. The application of Plexiglas panel absorbers is most suitable for hospitals and schools where patients and children are likely to get sick with bacterial infections.

In summary, low frequency noise exists due to the standing wave and cavity resonance in ventilation ducts or rooms connected to ventilation openings. To control this noise, absorbers using the principle of cavity or panel vibration resonance can be used to dissipate the noise (Figure 1-4).

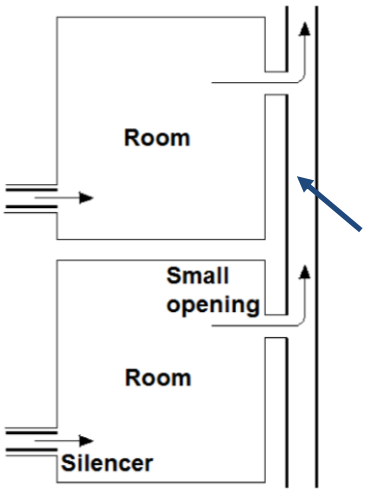

Figure 1-1: Building with a chimney or DSF with silencer inside

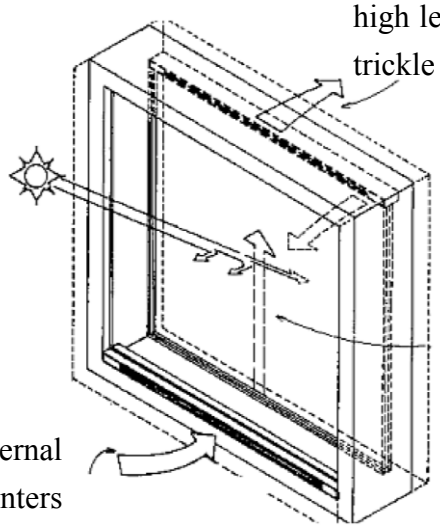

Figure 1-2: Double layer windows using solar stack ventilation principle by Kang [2]

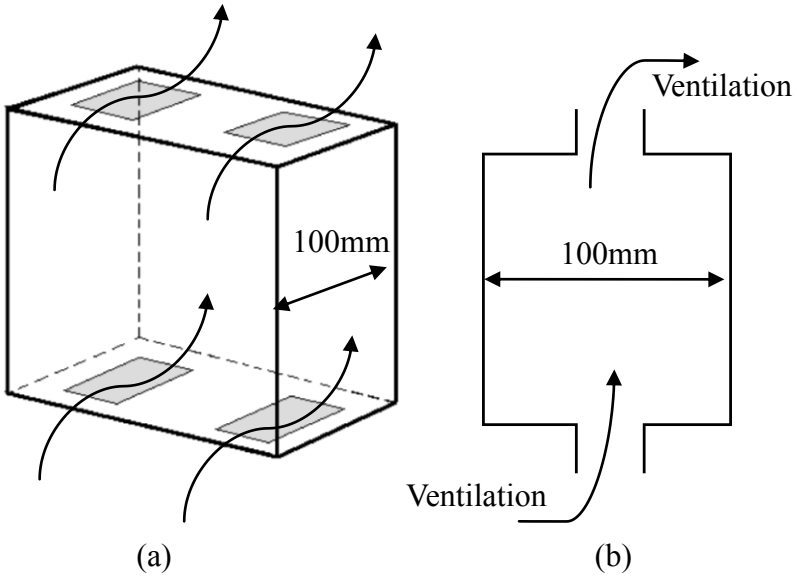

Figure 1-3a: Double window using reactive device: (a) isometric view, (b) side view.

Figure 1-3b: Application of ventilation windows in residences

Figure 1-3c: Application of ventilation windows in a school

Figure 1-3d: Application of ventilation windows in a hospital

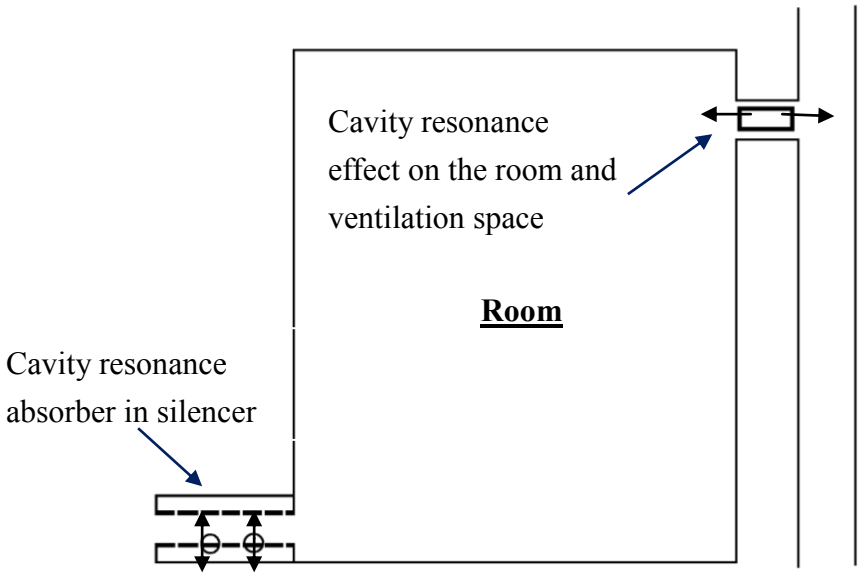

Figure 1-4: Cavity and panel vibration resonance principle in room noise control

1.2 Literature Review

Low frequency noise and infrasound are produced by machinery that is both rotational and reciprocating, including all forms of transport and turbulence. Typical sources might be pumps, air turbulence and fans. This low frequency noise hums inside buildings and resonates through ventilation ducts causing extreme distress to a number of people who are sensitive to its effects. For example, exposure to low frequency noise in the home at night can cause loss of sleep, and experiments have shown that low frequency noise has a significant impact on performance. Effects on mood include a lower social orientation and reduced feelings of happiness.

Low frequency noise control has emerged as a very active research area. Many

studies have shown the effectiveness of noise control in enclosed rooms and other environments for cancelling engine noise and low frequency noise in general. However, there is no research on how both acoustic comfort and ventilation can be achieved. This study asks whether there is any connection between noise reduction and ventilation.

Sound barriers and window insulation are commonly used to control traffic noise but these techniques are mainly effective in cases of middle and high frequency. Much of the high frequency noise that reaches high-rise buildings is absorbed by the air, leaving the lower-frequency component. Sometimes, due to resonance in a room, the low-frequency noise from traffic that is transmitted into a room can become severe because the wavelength is of the order of the room's dimensions.

One of the earliest investigations which applied a silencer to tackle the provision of natural ventilation and acoustic comfort in a building with fixed air vents was conducted (Christopher and Fergus, 2001). He did this by applying a silencer mounted into an air vent inside the wall panel. A reduction of 12–20 dB was reported for high frequency noise, and only a 2–10 dB reduction for low frequency noise. At certain low frequency ranges, the noise was excited to a higher level than before it entered the room. The maximum overall noise reduction was about 16 dB. It should

be noted that research was still focused on the uses of short air vents commonly found in domestic buildings in Australia and the experimental settings are similar to those shown in Figure 1-1. The Australian findings can be treated as references for comparison of the acoustic performance of the silencer in this project.

Recently, the awareness of building environments, including thermal comfort and indoor air quality (IAQ) engineering, has been raised by official authorities. New codes and guidelines for the regulation of lighting and ventilation requirements in the building industry have been published. They focus on treating all possible unacceptable indoor environments, including the improper design of air conditioning systems in domestic areas. It is foreseeable that building requirements will be more stringent in the future; therefore, probing feasible ways to enhance indoor air quality is important.

It is known that low frequency waves entering buildings through ventilation ducts can cause symptoms such as nausea, headaches, fatigue, insomnia and vibration in internal organs. The only effective means to control resonance is to increase acoustic absorption. Porous sound-absorbing materials have been used in ducts to achieve the dissipation of acoustic energy for many years. Dissipative silencers are usually composed of perforated tubes and chambers which are filled with sound-absorbing

materials such as fiberglass and basalt wool. These conventional acoustic materials absorb high-frequency sound energy effectively and transform it into thermal energy; however, they fail to absorb low-frequency sound waves. A silencer using a panel resonator which is constructed of a lightweight stiff foam-cored board with airspace behind it was designed (Ballagh, 1993). When tested, the results showed that the panel resonator achieved better low frequency noise reduction than the expansion chamber. The panel resonator had peaks of 6dB insertion loss at frequencies of 80Hz and 180Hz, which is close to 160Hz, which was the estimated natural frequency of the system. A similar silencer made of wood panel was also suggested. (Wang et al., 2006). Unlike a thin membrane, the resonance frequency of panel is easier to control. However, no panel absorber with transparent material had been studied.

Perforated plates have been used as sound absorption devices for years. The possibility of integrating sound absorption and light transparency was originally proposed for indoor applications. The perforated acrylic glazing mounted in front of windows in the German Parliament building in Bonn was designed(Fuchs and Zha, 1997). More recently, study was conducted to explore the use of micro-perforated plates in silencers for ventilating window systems as well (Kang and Brocklesby, 2005). Another research discussed the construction of a microperforated plastic

membrane; the theory was also applied to glass fibre textiles (Kang and Fuchs, 1999). This treats the membrane and Helmholtz effects in parallel.

The stack effect in solar chimneys or DSF is actually an inexpensive method as it provides adequate air exchange rates for a room by sucking fresh air out while causing the least noise disturbance. It is worth investigating the possibility of combing the cooling function with noise reduction. To do this, it is necessary to carry out an investigation using the solar stack ventilation principle and take into consideration both thermal ventilation and noise control.

1.3 Research objectives

Without mechanical assistance in hot, humid climates, natural ventilation would be the primary strategy for cooling buildings. Solar stack ventilation principle used in chimneys and DSF can achieve natural ventilation. Low frequency noise due to standing wave and cavity resonance exists in rooms and ventilation ducts or openings and annoys residents. The objective of this study is to control the noise, especially low frequency noise, generated in ventilation ducts and openings.

The research objectives are as follows: To investigate:

(1) A silencer with cavity and/or membrane absorber to control noise in a ventilation

duct; and

(2) A membrane and/or a cavity absorber to control Helmholtz resonance in a ventilation space or room.

1.4 The structure of the thesis

The noise control performance of a ventilation duct using the panel absorbers with transparent plastic sheets was investigated in Chapter 2. The transmission loss of the panel absorbers using plastic sheets of different thicknesses was compared. The design of using divided Plexiglas panel system was also introduced and tested. In Chapter 3, the panel absorber was modified into a divided Plexiglas panel with two separated vibrating layers – a top plastic membrane and a middle layer of micro-perforated sheet. This modified design was also tested in a real scale room. The absorption performance of the cloth membrane and the thick perforated Plexiglas sheet was studied in Chapter 4 by impedance tube measurement. The cloth membrane and the thick perforated Plexiglas sheet were treated as a two layer system and its performance was predicted by using the Absorption Coefficient Theory derived in Chapter 3.

In Chapter 5, the control of Helmholtz resonance and standing wave in a duct

ended with a cloth membrane or ended with two layers backed with an air cavity was investigated. Best noise reduction was achieved when the Helmhotlz resonance matched with the vibrating membrane resonance. It was found in Chapter 6 that infrasound can be induced by airflow through small openings in large ventilation ducts. This induced infrasound can be reduced using a membrane absorber introduced in Chapter 5. The interaction of nonlinear membrane vibration with acoustic waves was studied in Chapter 7. The resonant response of the cloth membrane with an increasing one directional tension was also investigated as so to achieve the best Helmholtz resonance reduction.

In Chapter 8, there are sections including the summary of major findings, significance and applications, discussion on limitations and the conclusions.

CHAPTER 2

NOISE CONTROL OF A VENTILATION DUCT BY A PANEL ABSORBER WITH TRNASPARENT PLASTIC SHEET

2.1 Introduction

This chapter presents the design and test of silencer with absorbing elements of transparent plastic panel which achieves effective noise reduction at low and medium frequencies. Transparent material is highly desirable for ventilation devices passing through windows to maximize natural lighting. Noise reduction can be achieved by the dissipation effect of Plexiglas panel which changes the acoustic energy to the vibration energy. Using the smaller divided Plexiglas panels, higher transmission loss can be achieved with a shift in the resonant frequency to 200Hz and 400Hz. Two approaches were applied to calculate the theoretical transmission loss for panel absorbers.

2.2 Literature review

It has been known that low frequency waves entering buildings through ventilation ducts can cause symptoms such as nausea, headaches, fatigue, insomnia and vibration in internal organs. Reactive attenuators using expansion chamber was

proved to overcome the drawbacks of using porous acoustic materials (Ballagh, 1993). The expansion chamber design however achieved a promising attenuation at high frequencies only but had poor noise reduction at low frequency below 250Hz. A high sound insulation ventilating windows which allowed airflow through the window itself was designed (Asdrubali and Buratti, 2005). It was effective for medium and high frequency but not for low frequency sound waves.

Thin membranes can be used to absorb noise at frequency below 250Hz (Cox and Antonio, 2004) (Takahashi et al., 1996). Flexible membrane in duct for noise control was suggested (Huang, 1999). He predicted that the wave dissipation by flexible materials like rubber could outperform typical fibrous duct lining. This was because for panels with substantial structural damping, both flexural and sound waves diminish with distance. The combination of wave reflection and dissipation allowed broadband, low-frequency noise reduction over a short distance. The acoustic behavior of a vibrating metal membrane system was investigated (Frommhold et al., 1994). The metal membrane absorber showed two resonance points, which can be related to a Helmholtz resonance and a plate resonance, achieved satisfactory sound absorption at low and medium frequencies over more than one octave.

A silencer using a panel resonator (Ballagh, 1993) which was constructed of a

lightweight stiff foam cored board with airspace behind. The results showed that the panel resonator achieved better low frequency noise reduction than the expansion chamber. A similar silencer which was made of wood panel was also suggested (Wang et al., 119). Unlike a thin membrane, it was easier to control the resonant frequencies of panel. However, panel absorber with transparent materials has not yet been studied.

2.3 The low frequency sound absorption performance of the Plexiglas panel absorber system between two rooms

2.3.1 Testing of the muffler effect of the Plexiglas panel absorber between two rooms

All measurements were carried out in the coupled reverberation rooms. A ventilation duct (testing duct) which meets the requirement for transmission loss test according to ISO-140 was made with cross-section of 0.35 × 0.35 m² and the total length was 1m. It was installed on a filler wall, which divided the source and the receiving room. The layout plan is sketched in Figure 2-1.

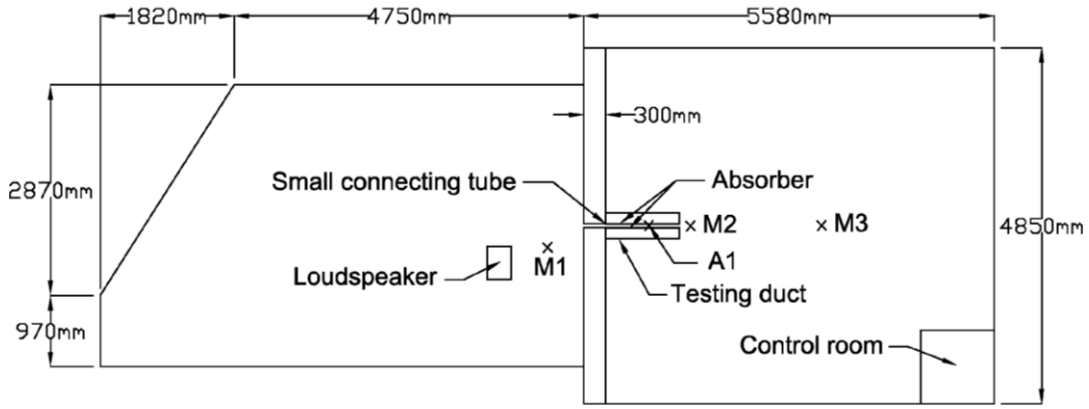

Figure 2-1: Coupled reverberating rooms: rooms dimension detail and layout plan.

Different materials were put inside the testing duct and acted as absorbers to achieve noise reduction. Precautions should be taken when attaching the vibrating Plexiglas sheets to the panel. If not, the actual vibrating mass may be less than expected, and additional losses at the fixings may occur. One solution to that is to attach the edges of the vibrating Plexiglas sheet using resilient foam so that the whole membrane can vibrate including the edges. If such a fixing is used, it is important that the cavity remains air tight.

A test with no absorber inside the duct was also carried out to investigate the effect of muffler. The side view and the cross section of the duct are shown in Figure 2-2.

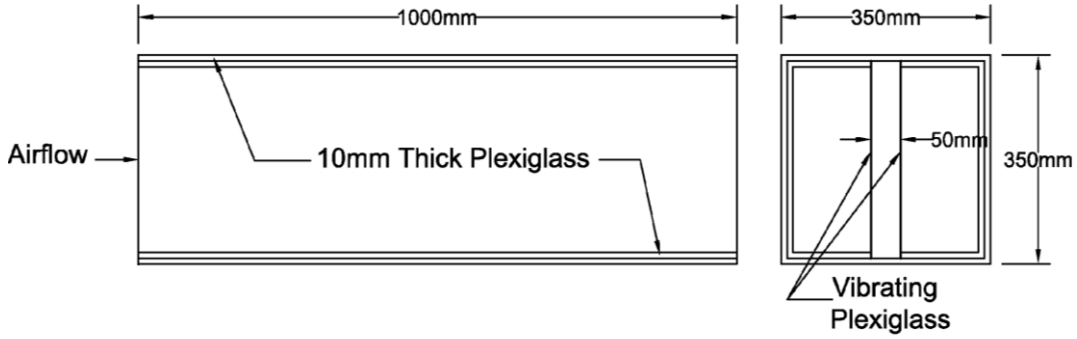

Figure 2-2: (a) Side view of the testing duct (b) Cross section of the testing duct with Plexiglas sheet as a vibrating membrane.

Sound attenuation due to muffler effect happens when there is an sudden expansion or contraction in the cross section of the sound flow path (Figure 2-3). Sound wave of certain wavelengths is then reflected back towards the source and portions of the sound energy can be prevented from being transmitted along the sound flow path. Sound wave passes through the inlet tube then undergoes sudden expansion then contracts again when leaving through the outlet tube. The greater the ratio of expansion or contraction chamber to the inlet or outlet tube is, the greater will be the sound reduction. The equation of transmission loss for the expansion type muffler is as follows.

where

l = Length of muffler, m

$S1$ = Cross-sectional area of inlet chamber, m^2

S2 = Cross-sectional area of muffler, m²

S3 = Cross-sectional area of outlet chamber, m²

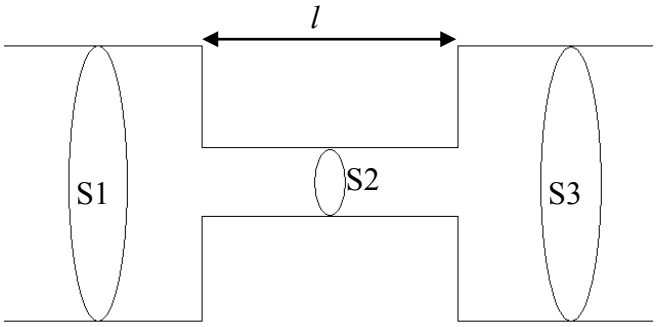

Figure 2-3: Connecting tubes with muffler effect

In the simplest case when *S1* = *S3*, with *s* = *S2*/*S1* and *k* = 2π / λ, the transmission loss is

$$R = 10 \log_{10} \left\{ 1 + \frac{1}{4} (s + \frac{1}{s})^2 \sin^2 kl \right\} \quad (2\text{-}1)$$

Figure 2-4 shows the muffler effect between the coupled reverberating rooms for the case with no absorber inside the testing duct. The target sound reduction is above 25 dB, and the experimental result shows that the acoustic reduction can be above 30dB in the whole frequency range except that in the range 63-100Hz and 200-300Hz. Since there is no absorber present in the testing duct, the sound reduction is mainly due to the muffler effect. The overall performance of muffler is satisfactory. It helps to reduce the traffic noise outside, which mostly exists in high frequency,

since the noise is reflected by the sudden expansion or contraction of the chambers in the muffler. The dips in the noise reduction near 100Hz, 200Hz and 400 Hz are due to the formation of standing wave along the length of the testing duct.

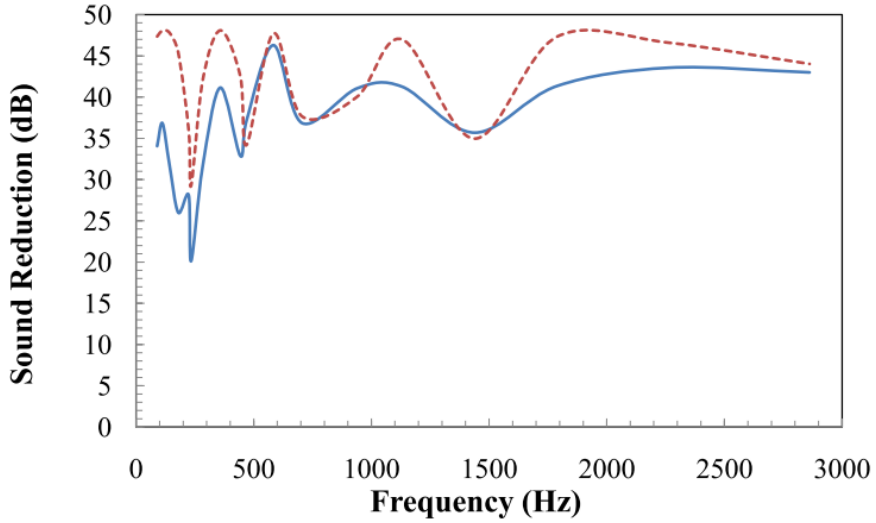

Figure 2-4: Effect of muffler (M3-M1) of the coupled reverberating rooms; – – –, theory; ——, experiment.

2.3.2 Effects of the Plexiglas panel absorber for the whole frequency range

It can be seen from Figure 2-5 that Plexiglas sheets can achieve significantly higher insertion loss than foam at the frequency below 300 Hz. Plexiglas of thickness 5mm has better noise reduction performance for the whole frequency range than that of thickness 10mm. It has peaks at 80Hz and 250Hz with about 25 dB insertion loss. The 10mm thick Plexiglas has the insertion loss higher than 30dB at the frequency range below 300Hz; however the insertion loss deteriorates at high frequencies.

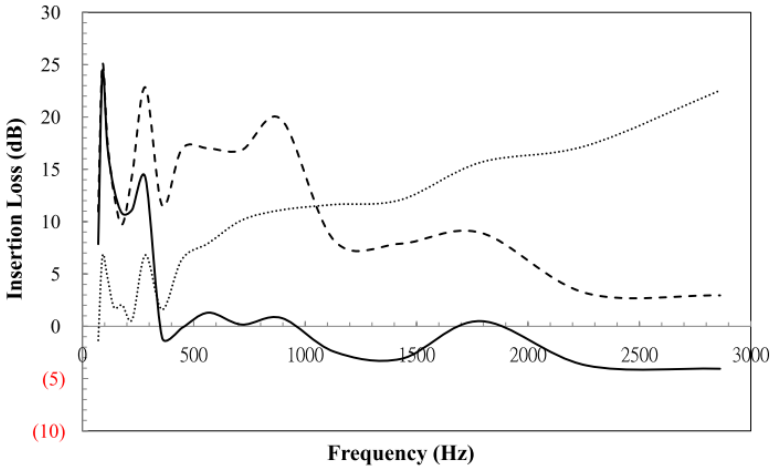

Figure 2-5: Insertion loss of the testing duct using different testing materials; - - -, 5mm thick Plexiglas; ——, 10mm thick Plexiglas; ·····, Foam.

2.3.3 Effect of the Plexiglas panel absorber for low frequencies

To further examine the absorption performance of Plexiglas sheets in the panel absorber in the frequency range of 200-300Hz, another duct system was constructed. The testing duct was designed according to ISO 7235 for the laboratory measurement procedures for ducted silencers. The configuration of the testing duct is shown in Figure 2-6. At both ends of the duct were connected to another duct with cross section 300 × 300 mm² and length of 1m including the anechoic termination. 5mm thick Plexiglas sheets were used as absorbers in the testing duct to achieve low frequency noise reduction. The boundary condition of Plexiglas panel is simply supported. White noise was employed to excite the Plexiglas panel.

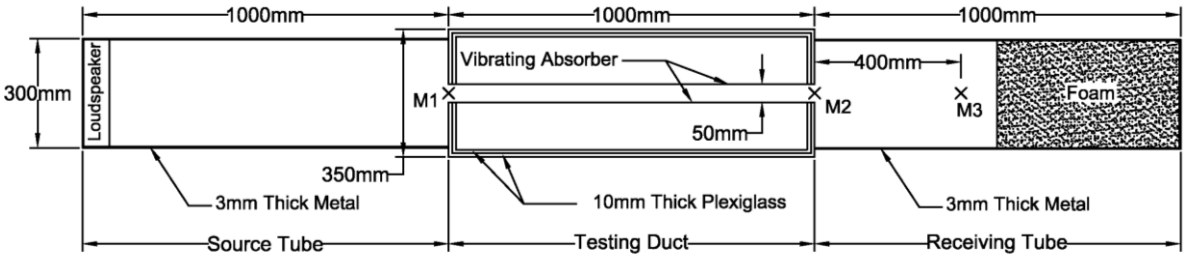

Figure 2-6: The configuration of the duct system.

In order to achieve the best noise reduction, sound energy should be dissipated to become the vibration energy of the panel. The vibrating panels thus have the highest noise reduction at the vibration resonances. A test was carried out (Figure 2-7 and 2-8) to obtain the vibration resonances of the Plexiglas panel.

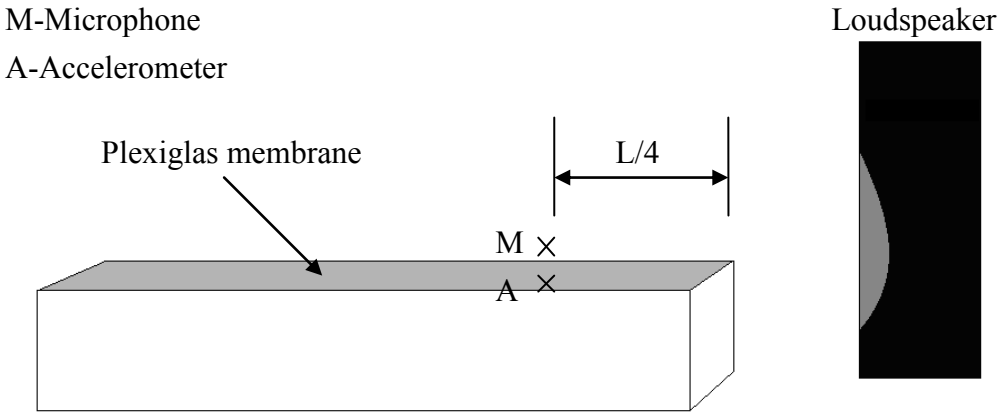

Figure 2-7: Experiment on Plexiglas membrane frequency response

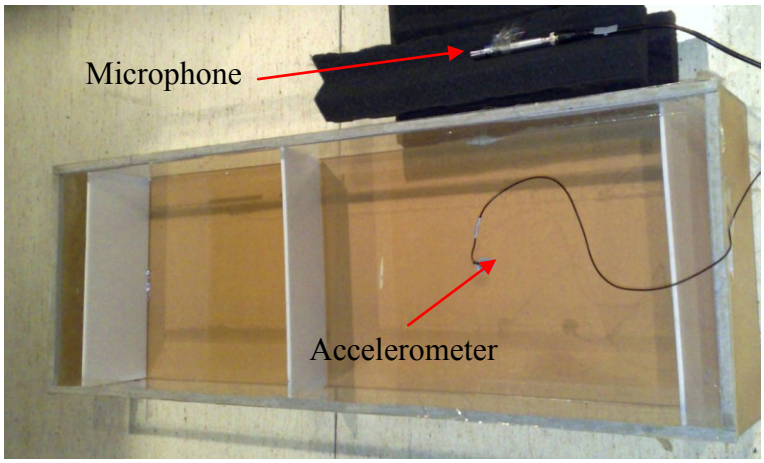

Figure 2-8: Experiment on Plexiglas membrane frequency response

Vibration resonance appears at the frequency where there is a peak at the magnitude of the frequency response together with a 90° phase change. As the findings in Figure 2-9 reveals that the first vibration resonance is at about 70 Hz.

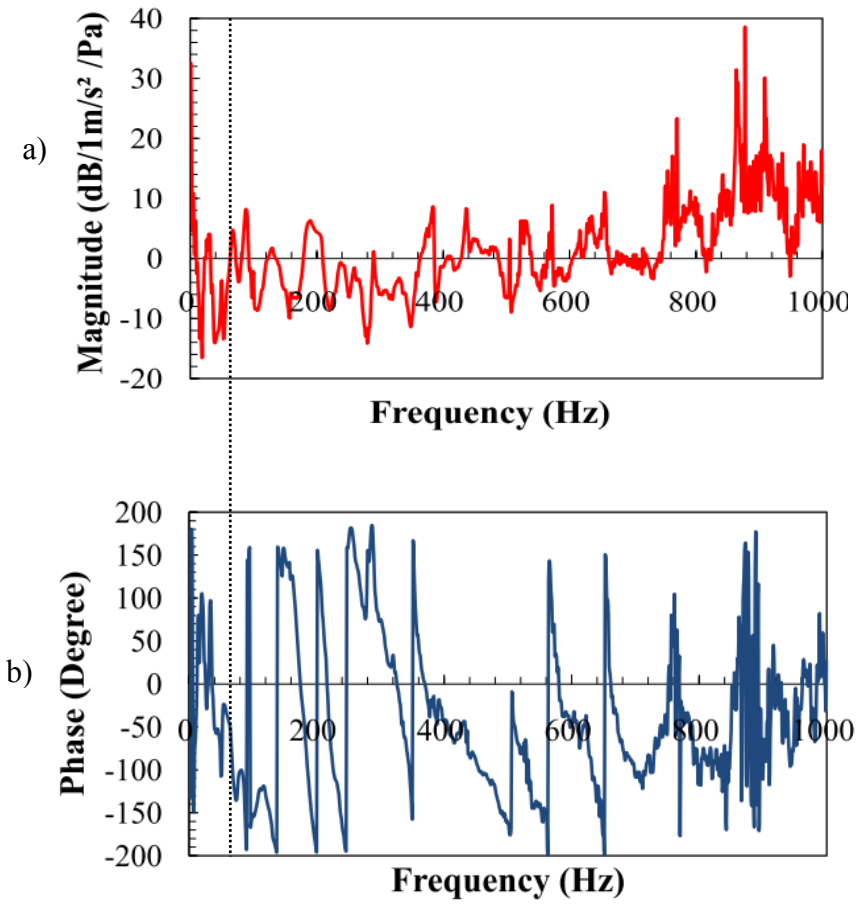

Figure 2-9: The frequency response of a 1m long panel with 5mm thick Plexiglas sheet ; (a) Magnitude; (b) Phase.

2.3.4 Prediction of the resonant frequency using analytical formula

An air-tight and soft material which has mass per unit area of *ms* (kg/m²) with air space *H* (m) and backed behind by a rigid wall is excited into bending vibration with the entrapped air acting as a spring (White and Walker, 1983). If the material permits the propagation of bending waves, this effect has to be added and the resonant frequency is expressed as follows for a rectangular plate whose dimensions are $a \times b$ (m²) with simply supported edge.

$$fr = \frac{1}{2\pi}\sqrt{\frac{\rho c^2}{m_s H} + \frac{\pi^4}{m_s}\left[(\frac{p}{a})^2 + (\frac{q}{b})^2\right]^2 (\frac{Eh^3}{12(1-\sigma^2)})} \quad (Hz) \qquad (2\text{-}2)$$

where p, q are arbitrary positive integers, ρ (kg/m³) is air density, c (m/s) is sound speed, E (kN/m²) is Young's modulus of the plate, h (m) is the thickness and σ is Poisson's ratio. The formula can be used to design a panel absorber for a specified resonant frequency. It can be seen that the resonance frequency increases with smaller dimensions a, b and thicker panels (i.e. larger h).

2.3.5 Prediction of the resonant frequency by finite element method

Finite element method with the help of the software S.A.P. was used to model the plate and air cavity resonant modes (Figure 2-10). Mode 1 has resonant frequency of 77.84 Hz which matches with the experimental result of 70Hz (Figure 2-9). It should be noted that there is one standing wave along the length of 1m inside the cavity (Figure 2-11).

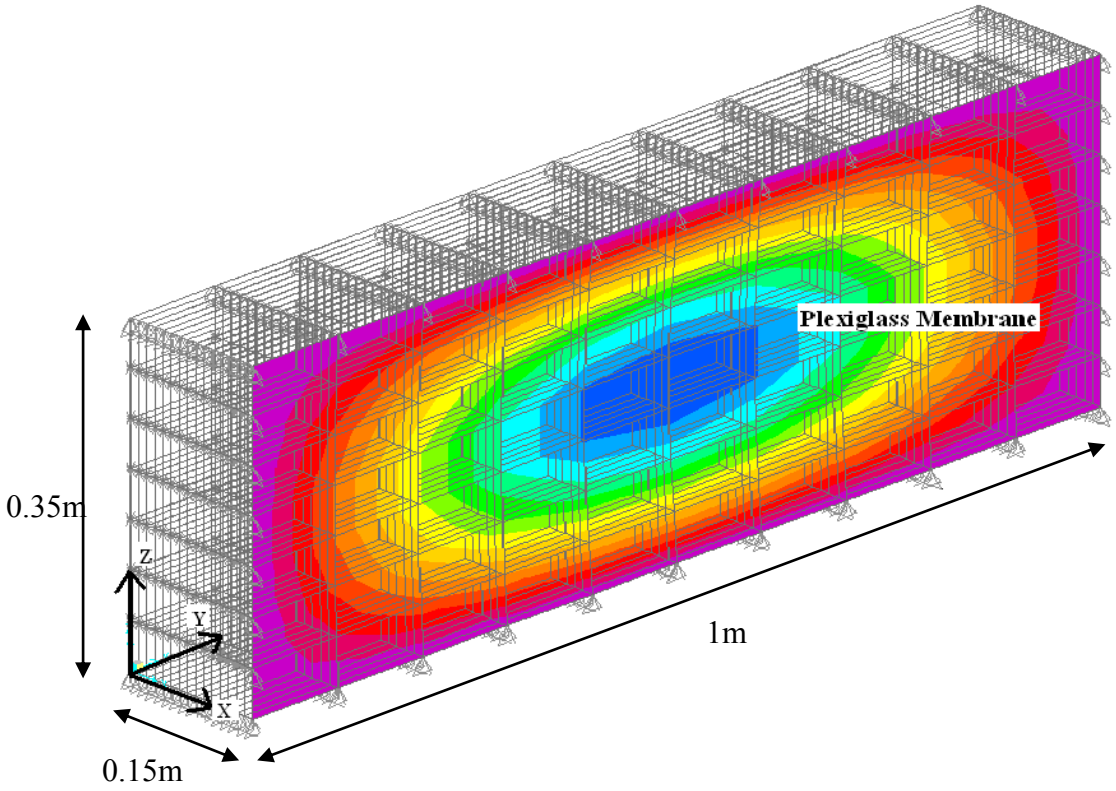

Figure 2-10: Finite element model simulating a panel absorber with Plexiglas membrane

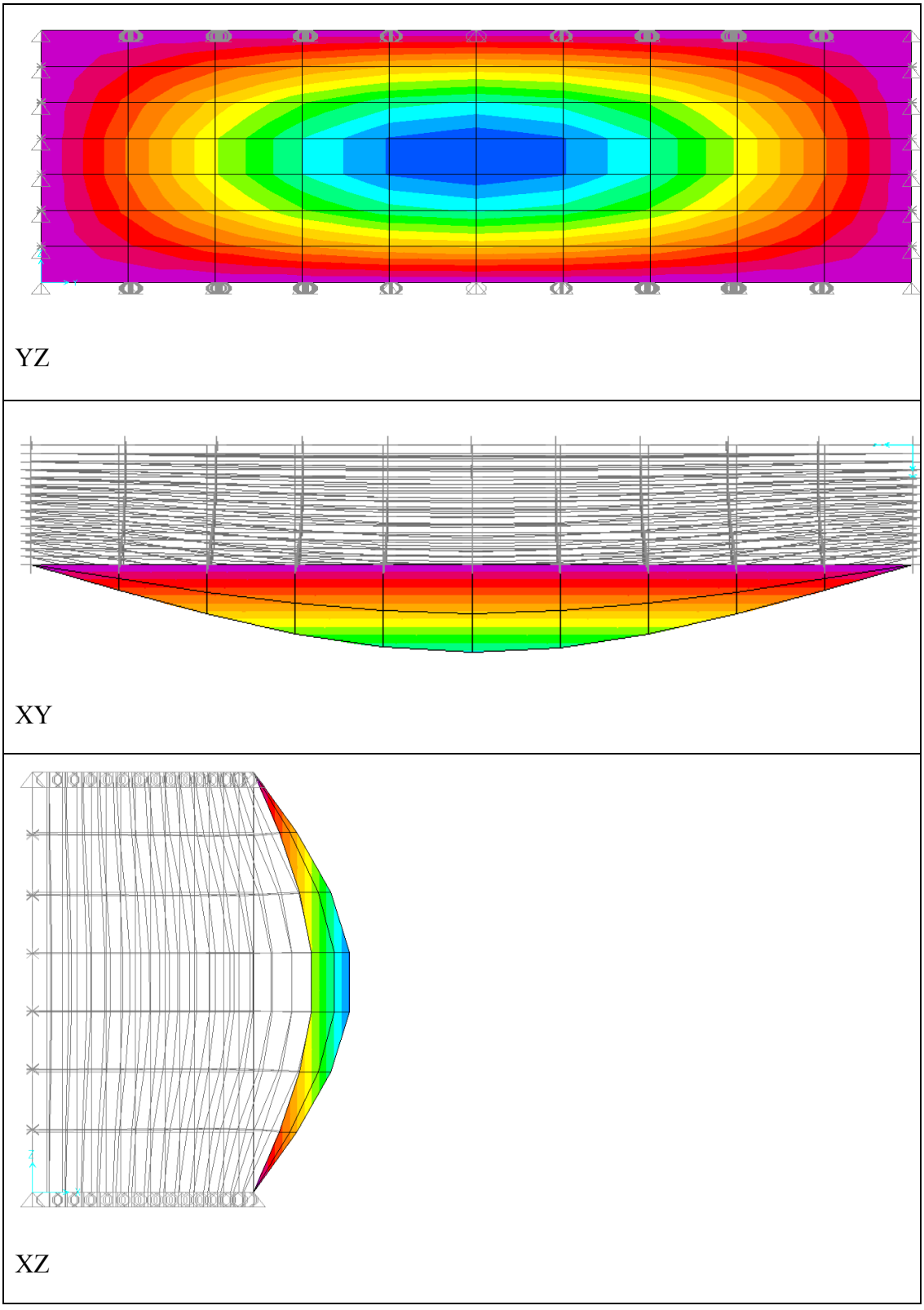

Figure 2-11: Mode shape of Plexiglas membrane vibration: Mode 1

2.4 Designs and tests of the absorption performance of the divided Plexiglas panel system

2.4.1 Experiments on the divided Plexiglas panel system

Since the muffler has unsatisfactory noise reduction in the frequency near 200Hz and 400Hz (Figure 2-4). It is necessary to design a Plexiglas panel system with vibration resonances near 200Hz and 400Hz. Further investigation was conducted on modifying the Plexiglas panel absorber which was made of 10 divided panels. (See Figure 2-12). Due to the short dimension of 0.07m long in each divided panel, the divided panels are predicted to have resonances at 360–400Hz. The cavity for each panel was separated from each other. The configuration of the duct system is shown in Figure 2-13. The end of the duct was connected to the anechoic termination. A long Plexiglas panel of 0.7m long was also used and the vibration resonance is predicted to be 200Hz.

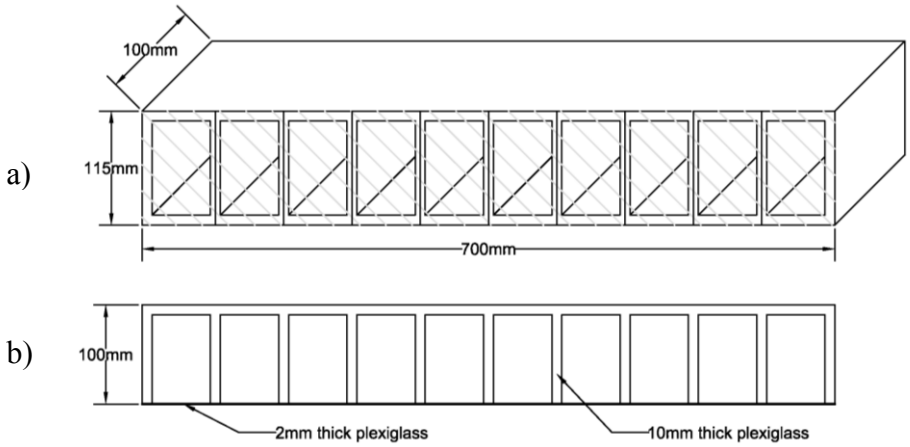

Figure 2-12: (a) Dimensions of the divided Plexiglas panel; (b) Top view of the divided Plexiglas panel.

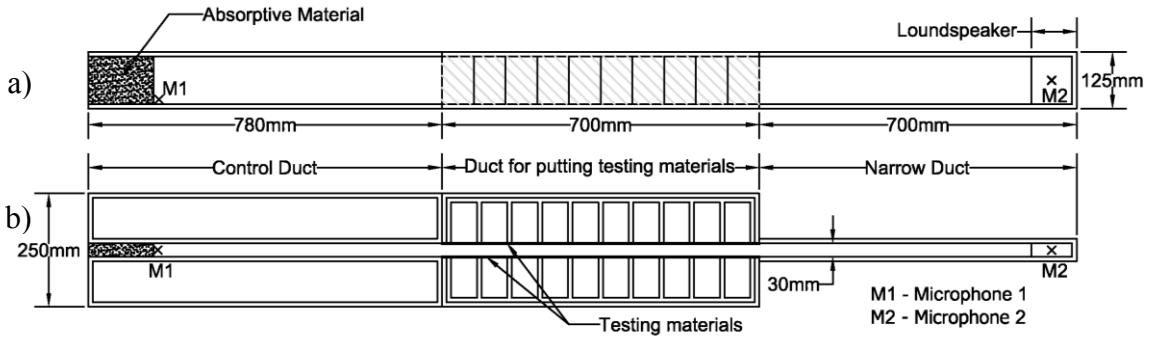

Figure 2-13: Configuration of the duct system: (a) Front view; (b) Top view.

Figure 2-14 shows the comparison of the transmission loss of the testing duct with two divided Plexiglas panels (DPPs) and that with two long Plexiglas panels (LPPs). For the DPPs, there is a peak transmission loss of nearly 40dB in the frequency range from 330 to 420Hz. For the LPPs, there is 25dB transmission loss in the frequency range from 200 to 300Hz. Two peaks of only 35dB are found at 270Hz

and 375Hz. The noise reduction effectiveness was improved using the DPPs with a higher transmission loss peak value.

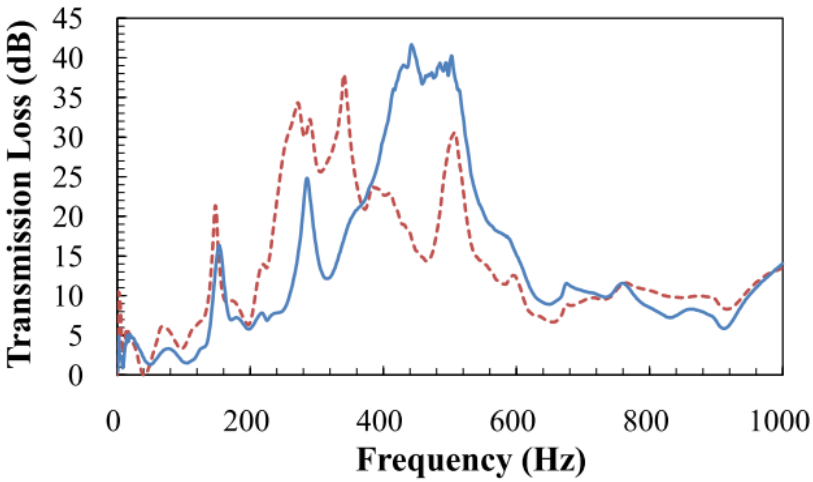

Figure 2-14: The transmission loss of the testing duct using Plexiglas of different configurations; – – – , LPP; ——, DPP.

According to the peak in the frequency response (acceleration/pressure) obtained from the vibration test (Figure 2-15), the vibration resonance for the DPP is 420Hz. For the LPP, the vibration resonance is 248Hz (Figure 2-16). The transmission loss for the DPPs is maximum at the range of 330–420Hz which is near the frequency of the vibration resonance. The LPPs have the highest transmission loss in the frequency range from 200 to 300Hz which is again near the frequency of the vibration resonance.

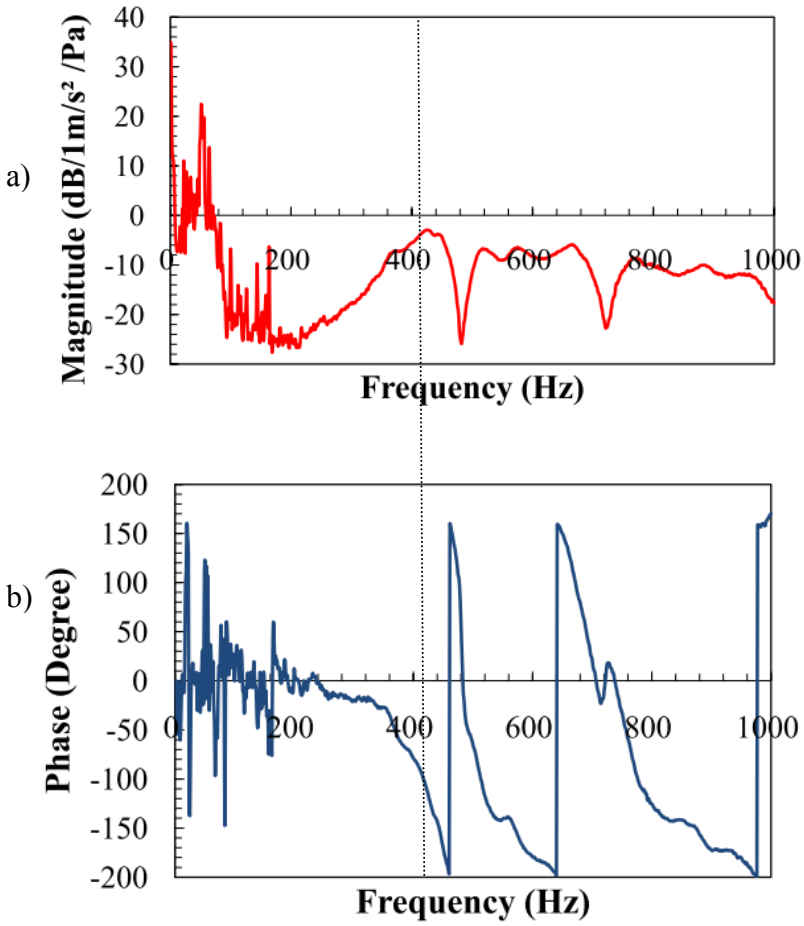

Figure 2-15: The frequency response of the DPP, (a) Magnitude; (b) Phase.

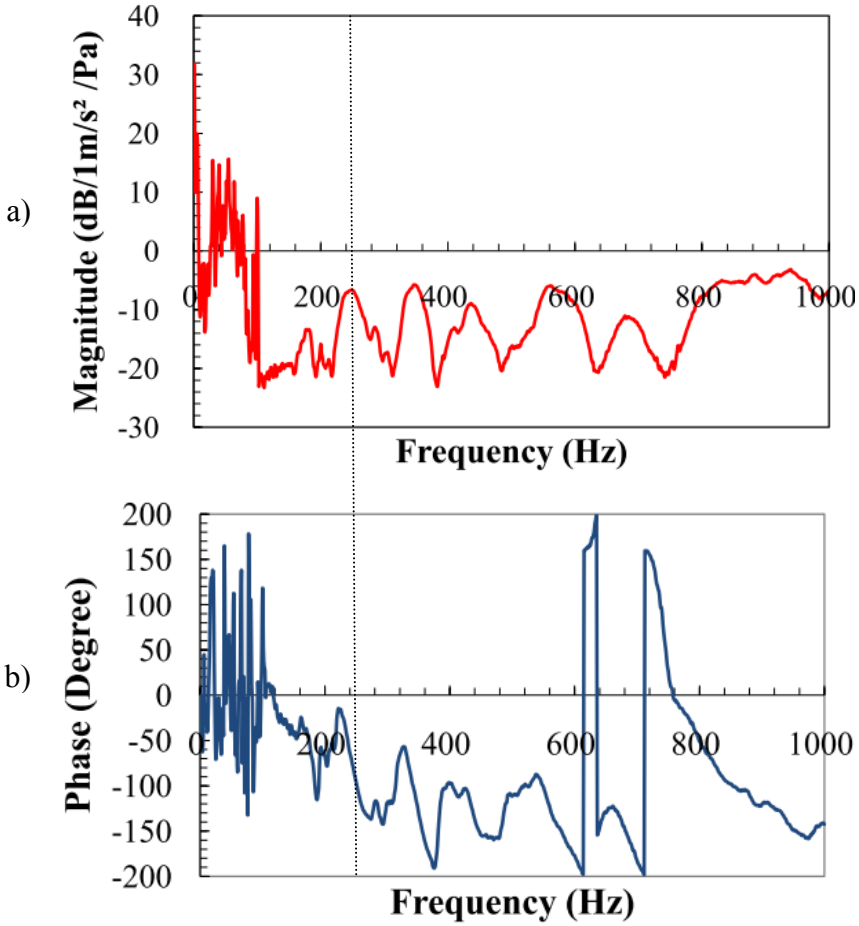

Figure 2-16: The frequency response of the LPP, (a) Magnitude; (b) Phase.

2.4.2 Experiments on the combination of one DPP and one LPP in a duct system

The 0.7m long Plexiglas panel absorber made of 10 separated small panels vibrated more smoothly to absorb the vibration energy of the sound wave with smaller wavelength 0.14m to 0.7m. Results in previous section 2.4.1 (Figure 2-15 and 2-16) found that the DPPs have different resonant frequencies with that of the

LPPs. A testing duct with a combination of one DPP and one LPP was conducted in order to achieve a more broadband noise reduction. One side of the testing duct is filled with a DPP while the other side is filled with a LPP (Figure 2-17). The configuration of the duct system is same as the previous experiment (Figure 2-13).

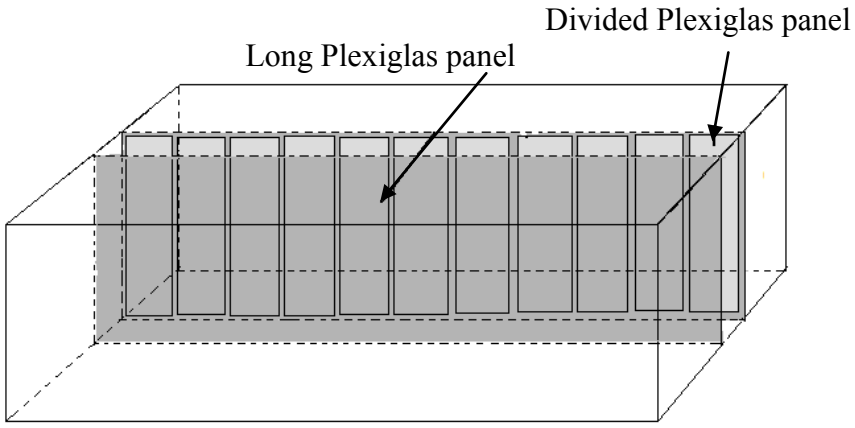

Figure 2-17. Configurations of the testing duct with combination of a DPP and a LPP

The result shown in Figure 2-18 proves that the mixed combination achieves noise reduction of a wider range of frequency from 240Hz to 520Hz with above 20dB transmission loss. The peaks are shaper which existed in the frequency range from 380 to 450Hz with about 30dB transmission loss. It proves that the mixed combination has advantages over the original testing duct configuration (LPP on both sides or DPP on both sides – Figure 2-14). The mixed combination is the best broadband absorber without any sudden minimum points between 240-520Hz.

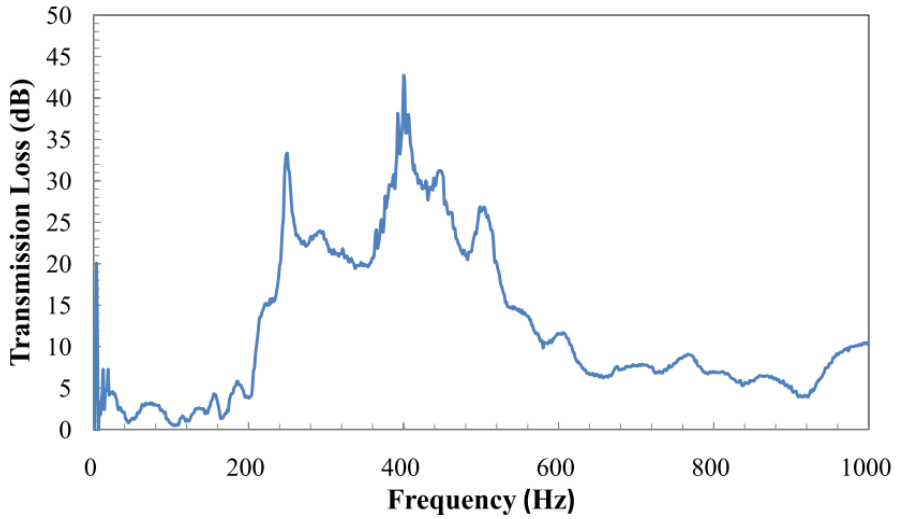

Figure 2-18: The transmission loss of the testing duct with the mixed combination

2.4.3 Experiments on the extended Plexiglas panel system

Further experiments were conducted to investigate the effect of increasing the testing duct length on the sound reduction performance. The DPPs were put in the extended testing duct and the configuration of the extended duct is shown in Figure 2-19. The findings indicate that longer testing duct can obtain better absorption over the whole frequency of interest especially low frequencies (Figure 2-20).

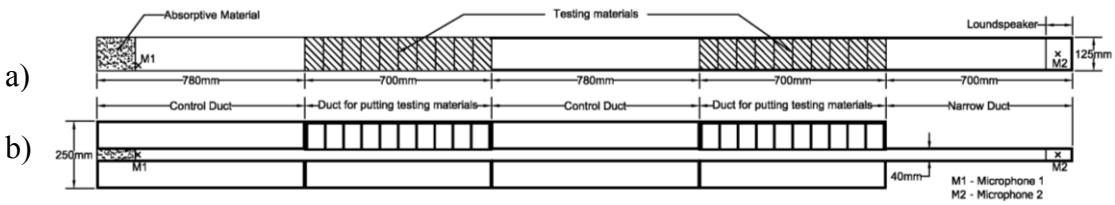

Figure 2-19: Configuration of the extended duct system: (a) Front view; (b) Top view.

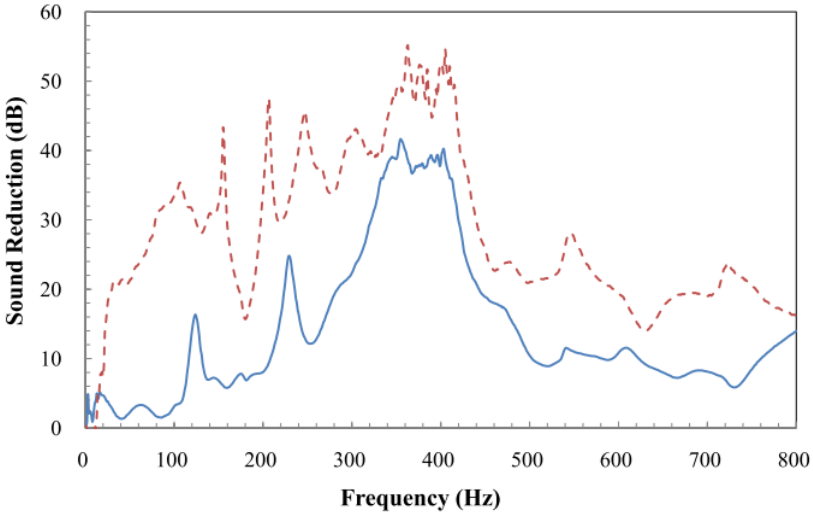

Figure 2-20: Comparison of sound reduction of the DPP in testing ducts of different length; ——, short duct; – – –, long duct.

In order to pursue the most broadband noise reduction performance, the duct system was modified. Two tests with different configurations were conducted (Table 2-1).

	Duct I for putting testing material	Duct II for putting testing material
Configuration 1	DPP on both sides	LPP on both sides
Configuration 2	One side with DPP, one side with LPP	One side with DPP, one side with LPP

Table 2-1: Configuration 1 and 2 in the extended duct

For Configuration 1, a pair of DPPs was put in Duct I and a pair of LPPs was put in Duct II. Configuration 2 is actually the extended version of the mixed

combination (Section 2.4.2 - Figure 2-17) with one DPP and one LPP filled in the two sides of the testing duct. Figure 2-21 shows clearly that configuration 2 achieves more considerable noise reduction performance than that of configuration 1. Configuration 2 works best in the frequency range from 300 to 500Hz with nearly 50dB transmission loss. On the whole, configuration 2 achieves above 30dB transmission loss for the frequency range of 220–530Hz which works as a wider bandwidth noise reduction duct configuration. Though configuration 1 also achieves significant noise reduction performance, it has slightly lower peaks and narrower bandwidth than configuration 2. It can only achieve a peak transmission loss of about 45dB from 250Hz to 350Hz.

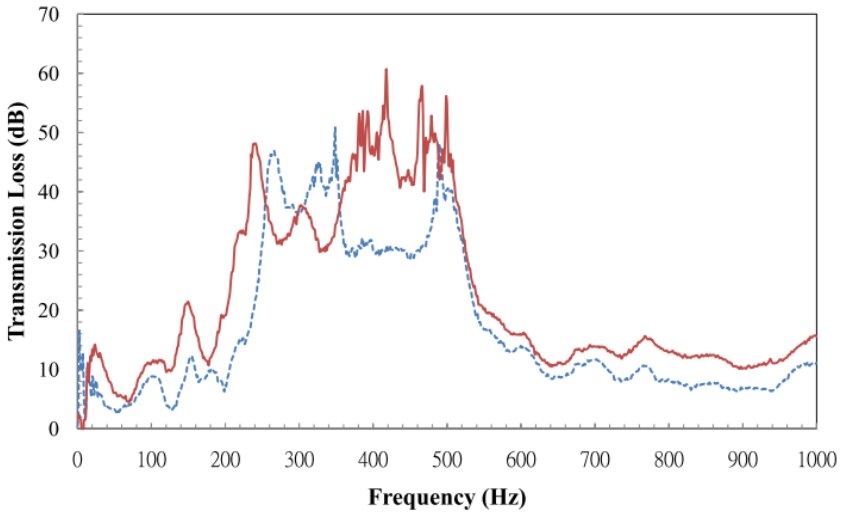

Figure 2-21: The transmission loss of the extended duct with different configurations; – – – , configuration 1; ——— , configuration 2.

2.5 Calculation of the transmission loss of the panel absorbers

2.5.1 Theoretical noise attenuation of non-locally reacting silencer lined with Plexiglas panels by Impedance Method

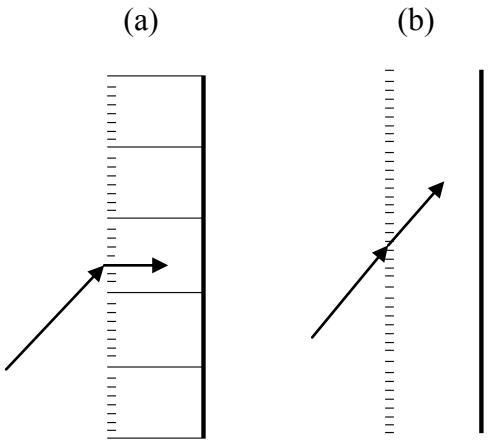

Figure 2-22: Porous sheet-cavity absorber; (a) Locally reacting: Air backing partitioned by means of a partition structure; (b) Nonlocally reacting: No partitions.

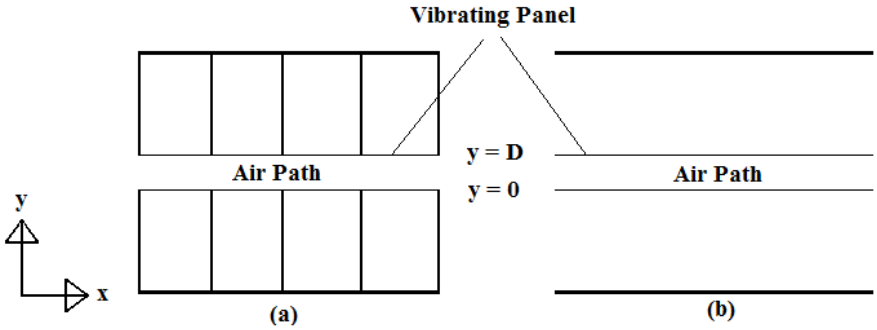

Figure 2-23: Rectangular panel system lined with a vibrating Plexiglas sheet. (a) Locally reacting. (b) Non locally reacting.

The benefit of using the divided Plexiglas panel is that no sound propagation in x direction is assumed due to the separation between each air cavity. Only the effect of the liner on the propagation of the fundamental acoustic mode in the duct is

focused. The sound pressure in the z-direction is assumed to be uniform.

For the locally reacting liner, the input impedance is independent of the distribution of sound pressure along the duct. The problem is then to determine the sound field in the duct subject to the boundary condition of a known normal impedance at $y = D$ and zero normal velocity (infinite impedance) at $y = 0$.

For harmonic time dependent, with x-axis along the duct and the wall at $y = 0$ being acoustically rigid (zero normal velocity amplitude), the complex amplitude of the sound pressure as

$$p(x, y, \omega) = A\,Cos(k_y y) e^{ik_x x} \tag{2-3}$$

where k_x and k_y are propagation constants.

The y-component of the velocity amplitude is

$$u_y = \frac{1}{-i\,\omega\,\rho}\frac{\partial p}{\partial y} = \frac{A}{-i\,\omega\,\rho} k_y\, Sin(k_y y)\, e^{ik_x x} \tag{2-4}$$

The boundary condition at $y = D$ is

$$\frac{u_y}{P} = \frac{\gamma}{\rho c} \tag{2-5}$$

And we then have $\gamma = \dfrac{u_y\,\rho c}{P} = \dfrac{\rho c}{Z} = \dfrac{1}{Z_i}$, where γ is the normalized input admittance, $Z = \rho c\, Z_i$ which is the impedance, ρc is the wave impedance and Z_i is the total normalized input impedance of the sheet-layer combination.

By substitution of Equations (2-3) and (2-4) into Equation (2-5),

$$\frac{u_y}{p} = \frac{\gamma}{\rho c}$$

$$\frac{\frac{A}{-i\,\omega\rho} k_y\, Sin(k_y y) e^{ik_x x}}{A Cos(k_y y) e^{ik_x x}} = \frac{\gamma}{\rho c}$$

$$k_y Tan(k_y y) = \frac{-i\gamma\omega}{c}$$

where $k = \omega/c$ and c is the sound speed. In general, this equation is to be solved numerically.

$$k_y\, D\, Tan(k_y D) = -i\, k\, D\, \gamma \tag{2-6}$$

At sufficiently low frequencies, such that the right hand side of Equation (2-6) is much less than unity, we can use the approximation $Tan(k_y D) \approx k_y\, D$ to obtain the low frequency approximation.

$$\left(k_y\, D\right)^2 = -i\gamma\, k\, D$$

$$k_y{}^2 = \frac{-i\gamma\, k}{D} = \frac{i\gamma\,\omega}{c\, D}$$

Having obtained k_y in terms of the known quantity on the right hand side, the propagation constant k_x for the duct is determined.

$$k_x \equiv k_r + i\, k_i = \sqrt{(\omega/c)^2 - k_y{}^2} = \sqrt{\left(\frac{\omega}{c}\right)^2 + \frac{i\gamma\,\omega}{c\, D}}$$

In fact, the x-dependence of the magnitude of the complex sound pressure amplitude is give by $\left|\frac{P(0)}{P(x)}\right| = e^{-k_i x}$ and the corresponding attenuation in dB is

$$
\begin{aligned}
&TL \\
&= 20Log_{10}\left|\frac{p(0)}{p(x)}\right| \\
&= 20Log_{10}(e)^{k_i x} \\
&\approx 8.72 k_i\, x \\
&= 8.72\,\mathrm{Im}\left(\sqrt{\left(\frac{\omega}{c}\right)^2 + \frac{i\gamma\omega}{cD}}\right)x \\
&= 8.72\,\mathrm{Im}\left(\sqrt{\left(\frac{\omega}{c}\right)^2 + \frac{i\omega}{cD}\left(\frac{1}{Z_i}\right)}\right)x
\end{aligned}
$$

It should be noted that acoustic impedance Z is not constant along the plate due to the non-uniform displacement of the plate. Since the pressure is not distributed uniformly over the plate, the joint acceptance function should be considered when calculating the average acoustic impedance of a panel. The joint acceptance function Jr is a factor which describes the proportion of this force which a particular mode of distortion can accept and convert into the corresponding generalized force.

Suppose a field of plane harmonic waves impinges upon a plate, the wave-fronts making an angle θ with the plate surface.

Consider only the case when the sound wave travels in the direction of the length of the plate without any component of velocity across the width of the plate (Figure 2-24). The wave-fronts make an intercept of λ_l on the plate.

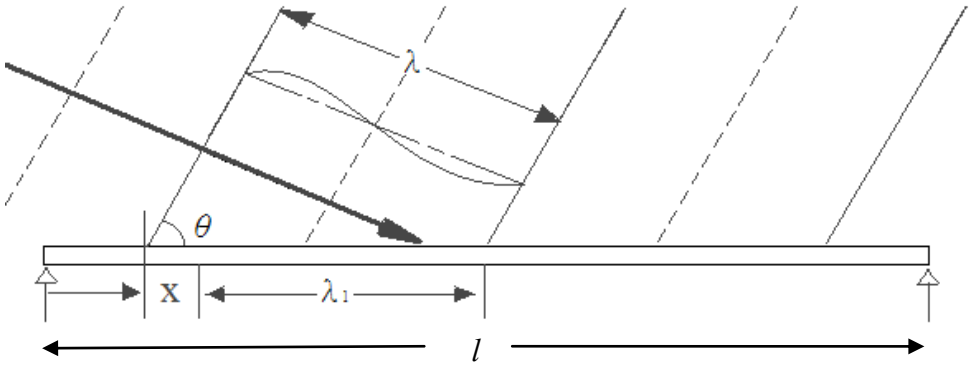

Figure 2-24: Diagram illustrating a sound field impinging on the plate.

The instantaneous pressure at any point along the plate is

$$p(x,t) = p_0 \cos(\omega t - \frac{2\pi x}{\lambda_l} + \phi).$$

The displacement of plate is given by $W = \sin\frac{r\pi x}{l}\sin\frac{\pi y}{b}$

Let r be the number of mode and b (m) be the width of the plate, the generalized force is given by:

$$\begin{aligned} L_r(t) &= \int_0^b \int_0^l p_0 \cos(\omega t - \frac{2\pi x}{\lambda_l})\sin\frac{r\pi x}{l}\sin\frac{\pi y}{b}\,dxdy \\ &= p_0 \frac{2b}{\pi}\int_0^l \cos(\omega t - \frac{2\pi x}{\lambda_l})\sin\frac{r\pi x}{l}\,dx. \end{aligned} \tag{2-7}$$

Evaluating the integral, and replacing l / r by $\lambda_m / 2$ (the half wavelength of the mode of vibration) we find:

$$L_r(t) = p_0 lb \frac{4}{\pi^2}\left\{\frac{\cos\left(\frac{\pi}{2} r\lambda_m / \lambda_l\right)}{r\left|(\lambda_m / \lambda_l)^2 - 1\right|}\right\}\cos(\omega t + \varepsilon) \tag{2-8}$$

And the joint acceptance function is:

$$J_r = \frac{4}{\pi^2}\left\{\frac{\cos\left(\frac{\pi}{2} r\lambda_m / \lambda_l\right)}{r\left|\left(\lambda_m / \lambda_l\right)^2 - 1\right|}\right\} \tag{2-9}$$

Therefore, $L_r(t) = p_0 lbJ_r \cos(\omega t + \varepsilon)$

The actual calculated transmission loss (TL) in dB is

$$TL = 8.72 J_r \,\mathrm{Im}\left(\sqrt{\left(\frac{\omega}{c}\right)^2 + \frac{i\omega}{cD}\left(\frac{1}{Z_i}\right)}\right) x \tag{2-10}$$

Figure 2-25 shows how J_r varies with λ_m/λ_l for the first mode (r = 1). It can be seen that J_r is higher for shorter panel which has smaller λ_m. As shown in Figure 2-26, both curves have peak at about 370 Hz of nearly 40dB noise attenuation which proves the validity of the theory for non-locally reacting silencer lined with Plexiglas panels.

There is a little difference in theoretical and experimental results since problems arise in predicting performance of vibrating panel system, as the absorption from the boundaries is hard to characterize. The design equations for membrane absorbers are often inexact in predicting the resonant frequency. One of the reasons for that may be the physical mass of the membrane is often diffierent from the vibrating acoustic

mass due to the mounting conditions.

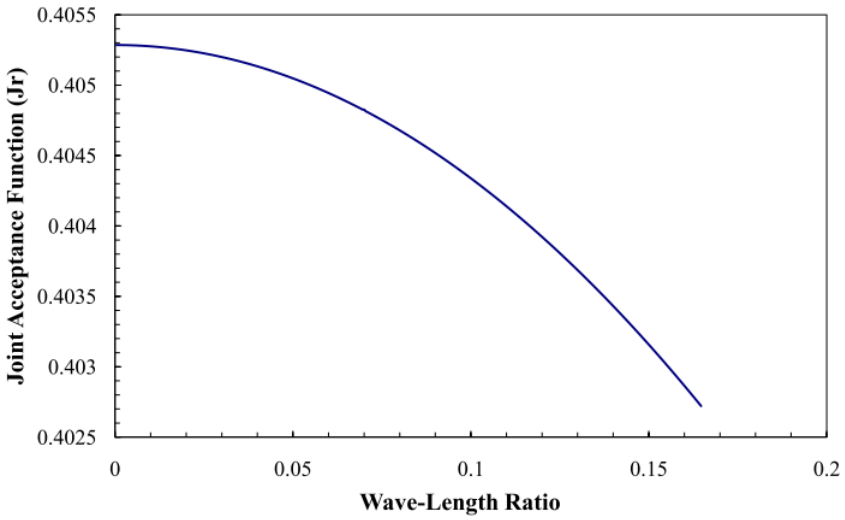

Figure 2-25: The variation of the joint acceptance function, J_r, with the wavelength ratio (λ_m/λ_l)

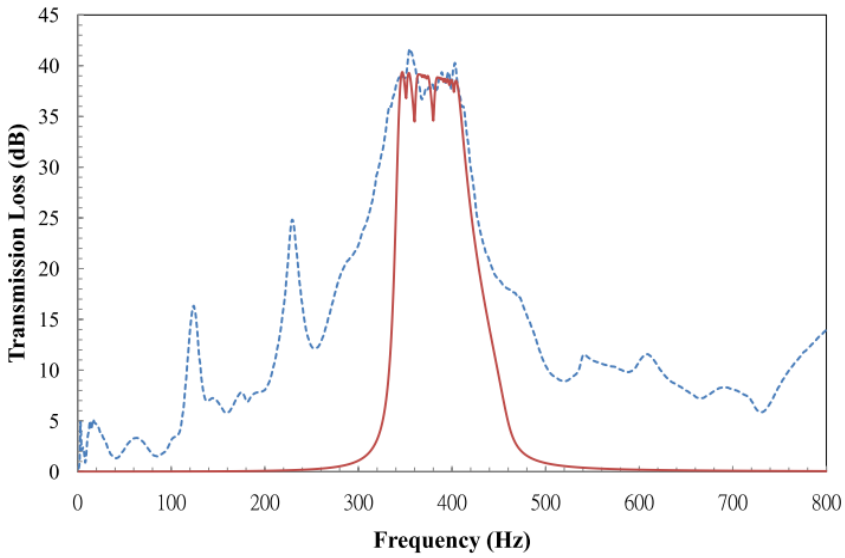

Figure 2-26: Comparison of theoretical and experimental transmission loss for the DPPs; ——, theory; – – –, experiment.

2.5.2 Theoretical transmission loss of silencer lined with Plexiglas panels by Energy Method

The prediction of sound attenuation is developed for a single-pass, rectangular tube with two vibrating membranes on both inner sides along the air path which is depicted in Figure 2-27 with *D* (m) and *B* (m) being the height and width of the air path respectively, and *L* (m) be the total length of the tube. This section presents the approximate simple calculation of transmission loss by Energy Method (White and Walker, 1983).

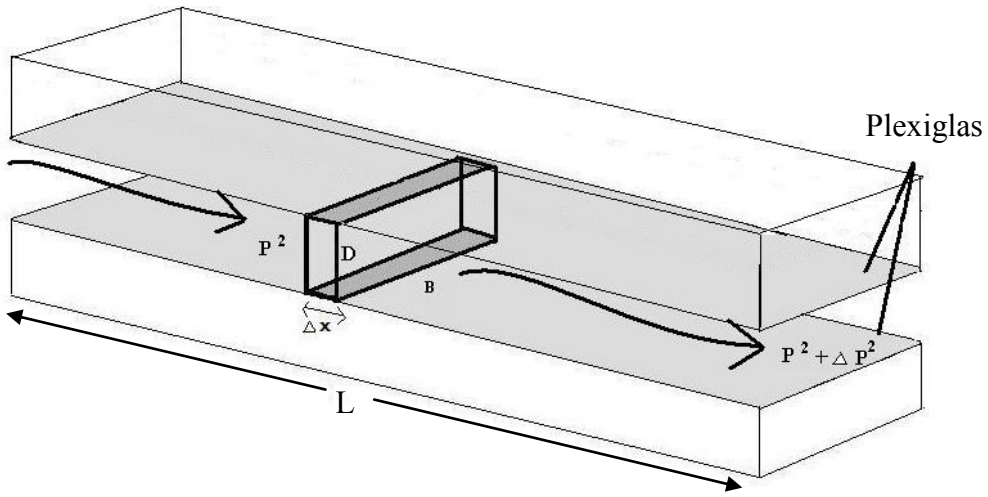

Figure 2-27: Configuration model of the silencer lined with Plexiglas panels

Consider the air inside the air way is divided into small elements (Figure 2-27), each with a length to be △x,

$$Intensity = \frac{P^2}{\rho c}$$

$$Intensity\ Loss = -\frac{\Delta P^2}{\rho c}$$

$$Energy\ Loss = -\frac{\Delta P^2}{\rho c} A, \quad where\ A = B * D \tag{2-11}$$

$$Energy\ Absorbed\ By\ Wall = 2B\Delta x\alpha(\frac{P^2}{\rho c}), \tag{2-12}$$

where Absorption Area = 2B△x and α is the absorption coefficient

By Energy Method, assume Energy Loss = Energy Absorbed by the Wall

Equating Equation (2-11) and (2-12), then

$$-\frac{\Delta P^2}{\rho c} A = 2B\Delta x\alpha(\frac{P^2}{\rho c})$$

Therefore, $P^2 = C_1 e^{-\frac{2\alpha}{D}L}$

Having $P_1^2 = C_1$ and $P_2^2 = C_1 e^{-\frac{2\alpha}{D}L}$ respectively, transmission loss can be calculated by finding $\left(\frac{P1}{P2}\right)^2$. Hence, dividing P_1^2 by P_2^2,

$$\left(\frac{P1}{P2}\right)^2 = e^{\frac{2\alpha}{D}L} \tag{2-13}$$

Transmission Loss

$$= 10Log_{10}(\frac{P1}{P2})^2$$

$$= 10Log_{10}e^{\frac{2\alpha}{D}L} \qquad \text{By Equation (2-13)}$$

$$= \frac{2\alpha}{D}(10)(Log_{10}e)L$$

$$= \frac{8.72\alpha}{D}L$$

Therefore, we have

$$\text{Transmission Loss } = \frac{8.72\alpha}{D} L \tag{2-14}$$

where

$$\alpha = \frac{4R1Rn}{(R1 + Rn)^2 + Xn^2}$$

$R_1 = \rho_0 c$ where R_1 is the acoustic impedance for air at 20°C

Rn is the acoustic impedance for the panel and $Z = Rn + Xn\,j$

For vibrating panel with single degree of freedom,

m: Modal Mass (Kg)

k: Modal Stiffness (N/m)

C: Modal Damping Constant (N/m/s)

S: Surface Area of Panel (m^2)

$$Z = \frac{\text{Pr}\,essure}{Velocity} = \frac{c}{S} + \frac{k - m\omega^2}{S\omega} j \tag{2-15}$$

Since $Z = Rn + Xn\,j$

By Equation (2-15), we have $Rn = \frac{c}{S}, Xn = \frac{k - m\omega^2}{S\omega}$ (2-16)

Since the pressure is not distributed uniformly over the plate, the joint acceptance function should be considered when calculating the average acoustic impedance of a panel.

Therefore, the actual calculated transmission loss (TL) in dB is:

$$TL = \frac{8.72 * \alpha * J_r * L}{D} \tag{2-17}$$

where α is the absorption coefficient and J_r is the joint acceptance function.

The followings are the comparisons of theoretical and experimental results for different panel absorbers:

A. Long Plexiglas panels of 1m long (Figure 2-2)

The value of m, k and c for theoretical calculation are as follows:

m = 1.00625kg

$k = m\omega^2 = m(2\pi f)^2$ where f = 77.84Hz and 163.29Hz

$c = 2\xi m\omega = 2 \times 0.02 \times m \times 2\pi f$ where f = 77.84Hz and 163.29Hz

Figure 2-28 shows how J_r varies with λ_m/λ_l for the first mode (r = 1). It can be seen that J_r is higher for shorter panel which has smaller λ_m. The comparison of theoretical and experimental results is shown below. The results in Figure 2-29 show good agreement between the theoretical and experimental results. The shapes of the two curves are very similar with the peak value at about 80Hz. Though the theoretical peak is calculated to be slightly higher than that of the experiment, the theory can be used as an approximation in the design of silencer with various sizes Plexiglas panels.

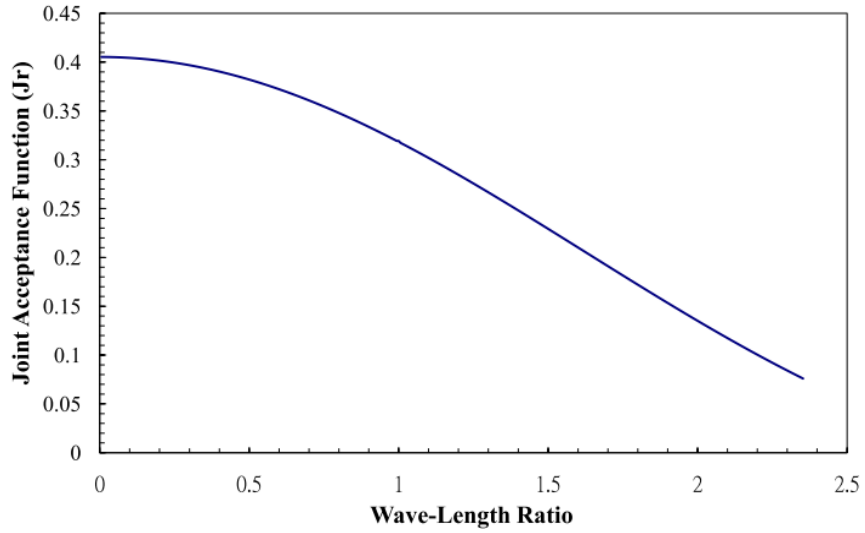

Figure 2-28: The variation of the joint acceptance function, J_r, with the wavelength ratio (λ_m/λ_l).

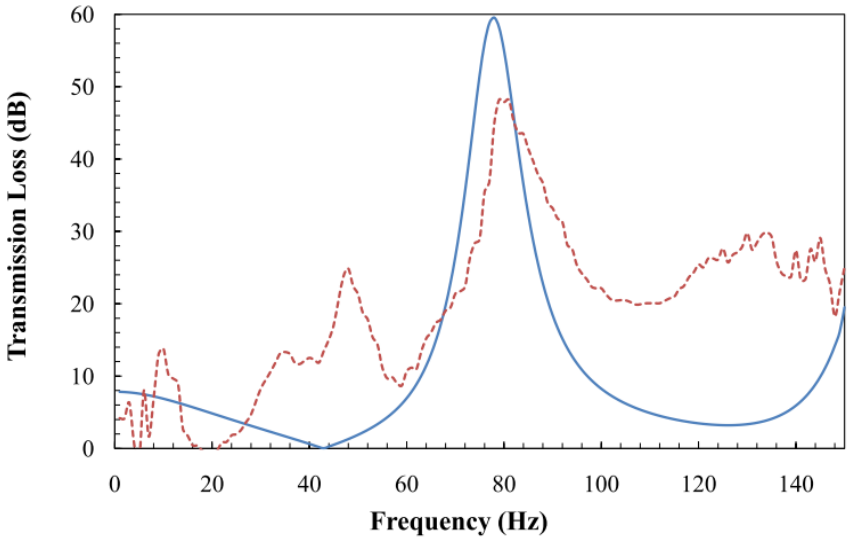

Figure 2-29: Comparison of theoretical and experimental transmission loss for the long Plexiglas panels; ——, theory; - - - , experiment.

B. Long and Divided Plexiglas panels of 0.7m long (Figure 2-12)

The value of m, k and c for theoretical calculation of Long Plexiglas panel are as follows:

$m = 0.100625kg$

$k = m\omega^2 = m(2\pi f)^2$ where f = 210Hz and 275Hz

$c = 2\xi m\omega = 2 \times 0.08 \times m \times 2\pi f$ where f = 210Hz and 275Hz

The value of m, k and c for theoretical calculation of Divided Plexiglas panel are as follows:

$m = 0.100625kg$

$k = m\omega^2 = m(2\pi f)^2$ where f = 360Hz, 370Hz, 380Hz, 390Hz and 400Hz

$c = 2\xi m\omega = 2 \times 0.08 \times m \times 2\pi f$ where f = 360Hz, 370Hz, 380Hz, 390Hz and 400Hz

Long Plexiglas panel was divided into 10 separated equal divisions and named as divided Plexiglas panels. Theory was applied and the graphs for the comparison of the theoretical and experimental transmission loss for the long and divided Plexiglas panels are in Figure 2-30 and Figure 2-31 respectively. The theoretical and experimental curve shapes are very similar though the peak transmission loss values are not exactly the same.

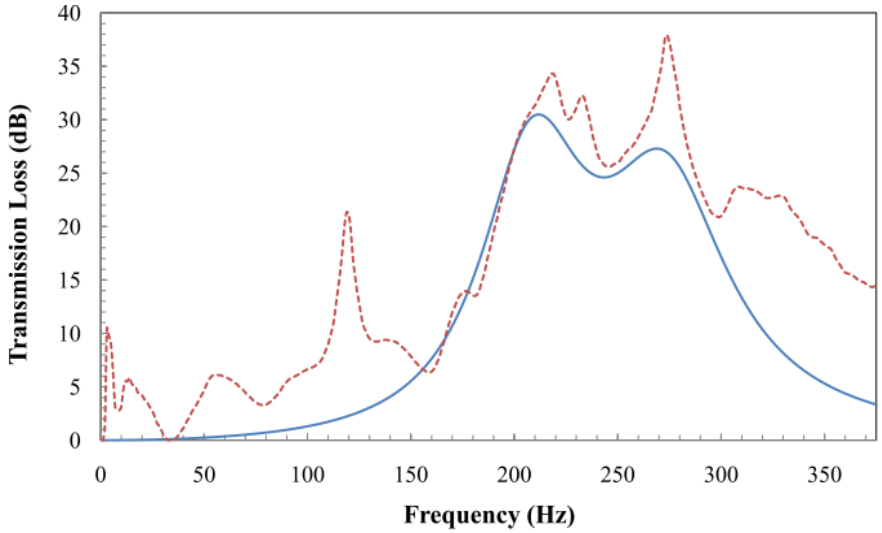

Figure 2-30: Comparison of theoretical and experimental transmission loss for the long Plexiglas panels; ——— , theory; - - - - , experiment.

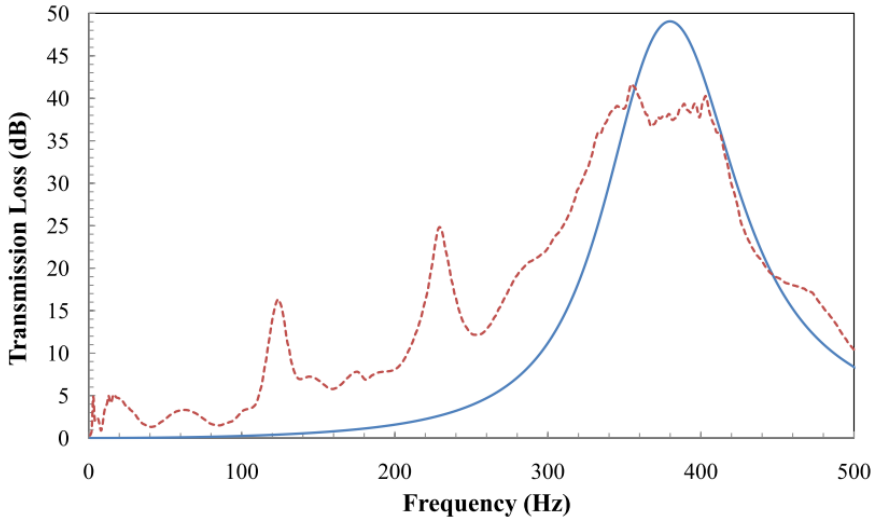

Figure 2-31: Comparison of theoretical and experimental transmission loss for the divided Plexiglas panels; ——— , theory; - - - - , experiment.

2.5.3 Comparison of the two approaches in calculating the transmission loss

Though the Energy Method is well know for years, the calculated transmission loss values are slightly overestimated or underestimated. Using the impedance

method, not only the curve shapes of experiment and theory matched with each other, but also the peak values show identical results. Therefore, the impedance method is preferred in the calculation of the transmission loss for panel absorber system.

2.6 Summary

Noise reduction can be achieved by the muffler effect and by changing the acoustic energy to the vibrational energy of the vibrating Plexiglas sheets in each divided panel. The primary losses most likely come from within the Plexiglas sheet or friction at the fixings between the Plexiglas sheet and the supporting structure of the panel system. There is a shift in of the resonant frequency when using the divided panels instead of the long panels. The divided panels obtained best sound reduction at the frequency range from 330–420 Hz with higher peak values which compensate for the poor performance of muffler at 400Hz. Thus a broadband noise reduction can be achieved by a testing duct combining effect of muffler and panel absorbers of various sizes. Transmission loss calculated by the theory shows good agreement with the experimental results and thus the theory can be used to design the panel absorber for specific frequency range from 50–500 Hz.

CHAPTER 3

THE ABSORPTION PERFORMANCE OF THE DIVIDED PLEXIGLAS PANEL WITH TWO SEPARATED VIBRATING LAYERS

3.1 Introduction

It is known that medium to high frequency sound at homes can be eliminated easily by furniture, people and surface elements in the room; the most important task is to achieve good absorption at medium to high frequencies as well as low frequency range. Absorption of low frequency noise requires thick material, such that most sound absorbing linings, typically a few centimeters thick, are ineffective at the low frequencies. As proved in Chapter 2 that divided Plexiglas panel (DPP) performs better than that of long plesiglass panel (LPP) with a higher peak value and slightly wider absorption bandwidth, the DPPs are further modified to achieve broadband noise reduction. A new design was obtained by applying a plastic membrane together with a micro-perforated sheet on the top and in the middle of the DPPs respectively.

This chapter presents the combination of vibrating membrane resonance and Helmholtz mechanisms in a single transparent panel absorber system which achieves broadband noise reduction. A theoretical method for predicting the absorption of this structure is described and the theoretical predictions results are compared with the

experimental measurements with good agreement. Experimental results clearly show that this panel absorber made of membrane together with resonator extends the absorption at low frequencies while maintaining the good absorption at mid frequencies as well.

3.2 Literature Review

The control of sound transmission through a panel has received widespread attention with the emphasis of producing increased attenuation by passive and reactive of active means. Passive sound control methods that dissipate propagating acoustic and/or structural waves through various damping mechanisms do not require an external supply of control energy. Foams and visco-elastic constrained damping layer are some of the examples. Usually, these methods work well at relatively high frequencies, where the wavelengths are short enough to produce significant strain in the damping device. At low frequencies, the amount of material needed for effective control of sound/ vibration becomes economically infeasible, considering most of the applications are weight and volume sensitive. Reactive materials and devices, which include semi-passive or tuned absorbers, are devices that provide significant attenuation over limited frequency bands by transferring energy from the acoustic

field into a resonant system. An experimental investigation was carried out on the performance characteristics of a new device, called Re-Active Passive, which combined active, re-active and passive technologies packaged into a single unit to achieve broadband performance (Thomson, 1981). Although active-control was applied to low frequency range and worked quite well due to low modal density of the structure, a feed-forward controller was used and it required the consumption of electricity. Therefore, it was not a cost-effective method to achieve broadband noise reduction.

Perforated plates have been used as sound absorption device for years. Perforated plates can be considered as a lattice of short tubes, where the pitch of adjacent tubes is small compared with wavelength of propagating sound, but larger than the hole diameter (Cox and Antonio, 2004). It is assumed that when sound flows through the holes, there is no motion in the plate itself, and the hole radius is larger than the boundary layer thickness. If the perforations of a Helmholtz resonator are made small enough, then losses will occur due to viscous boundary layer effects in the perforations. Since in reality the size of holes required is so small as to make the production difficult. To extend the bandwidth, multiple layers can be used and each layer is then tuned to a different frequency range.

The technology is based on the well-known acoustic principle Helmholtz resonator. Helmholtz resonator is named after the German physician and physicist Hermmann von Helmholtz (1821-1894). When sound waves, defined as compressed air, hit the perforated surface an overpressure arises on the front of the perforated plates. To equalize the pressure, the compressed air is forced through the micro perforations, and viscous forces between the very small perforations and the air causes friction. Hence the sound waves are absorbed and transformed into heat without use of any porous fiber-materials.

An impedance tube test was conducted to measure the normal acoustic impedance of perforated sheets with through-flow in a high intensity sound environment (Salikuddin et al., 1994). There were experimental results for perforated samples covering a range of hole diameters and porosities with constant through-flow and acoustic intensity. Results proved that both resistance and reactance decrease with increasing porosity and the absorption coefficient increases with decreasing hole diameter. To achieve this, the perforations must be millimeter in diameter so that they are comparable to the boundary layer thickness but at the same time maintain a suitable porosity. It is then possible to achieve absorption without using a porous material. This becomes a useful technique because the perforated

sheet can be made from transparent acrylic or glass and so form a clear absorber. From the academic viewpoint, this is a neat device because the physics of the system is very simple.

Profiled absorbers can obtain better sound absorption (Wu et al., 2006). Profiled absorbers are periodic surface structures with rigid constructions, which consist of wells separated by thin walls. The wells have the same width, but different depths in one period. By optimizing the positions of perforated plates in the constant depth wells and the depth sequence of variable depth wells, the well-tuned and well-distributed resonant frequencies can be obtained. Great effort is needed to balance the number of constant wells and the number of variable wells in order to get better coupling at the low frequency range as well as high frequency range.

A theoretical method was developed for predicting the absorption of a device which could be micro-perforated plastic membrane or glass-fibre textile mounted over an airtight cavity (Kang and Fuchs, 1999). The basic idea of the theory is to regard an open weave textile or a micro-perforated membrane as a parallel connection of the membrane and apertures. Although theories for membrane absorbers, micro-perforated plate absorbers and their combination have been developed, there is still no theory for panel absorbers with one membrane and one

micro-perforated plate layer separately mounted over an air cavity. It is possible to combine the membrane and Helmholtz resonator effect and apply it on the panel absorber system. Results show that the absorption range can be much extended. This chapter demonstrates the feasibility of using transparent panel absorbers with both vibrating plastic membrane and micro-perforated sheet backed by an air cavity to achieve broadband sound absorbing performance in ventilation ducts.

3.3 Calculation of the absorption coefficient of the panel absorber system with a top plastic membrane and a middle layer of micro-perforated sheet (PMP)

This part presents the theoretical method for the combination of one layer of plastic membrane and one layer of micro-perforated membrane (**P**lastic membrane **and M**icro-**P**erforated membrane – **PMP**) mounted over the same airtight cavity. In order to modify the absorption, the acoustic impedance of the structure can be adjusted by varying the appropriate parameters of the membrane and the perforated sheet apertures.

Consider the top membrane, for a tension-free membrane mounted at some distance from a rigid wall, the normal specific acoustic impedance of the membrane normalized by ρc can be calculated by

$$Z_M = \frac{R_M + jM_M}{\rho c} = r' + j\omega(\frac{m'}{\rho c}) \quad (3\text{-}1)$$

where

R_M is the specific acoustic resistance of the membrane (Ns/m³)

M_M is the specific acoustic reactance of the membrane (Ns/m³)

ρ is the density of air (kg/m³)

c is the sound velocity in air (m/s)

m' is the surface density of the membrane (kg/m^2)

r' is the normalized specific acoustic resistance of the membrane, which depends mainly on mounting conditions (Ns/m³)

Consider the perforated sheet, according to Maa's theory, the acoustic resistance of the apertures becomes significant when the apertures are very small. Consequently, it is not necessary for micro-perforated absorbers to provide extra acoustic resistance using porous materials. According to Maa, for normal incidence, the normalized specific acoustic impedance of the apertures can be calculated by

$$Z_L = \frac{R_L + jM_L}{\rho c} = r + j\omega m \quad (3\text{-}2)$$

With

$$r = \frac{g_1}{d^2}\frac{t}{p}K_r$$

$$m = 0.294(10^{-3})\frac{t}{p}K_m$$

$$K_r = \sqrt{1+\frac{x^2}{32}} + \frac{x\sqrt{2}}{8}\frac{d}{t}$$

$$K_m = 1 + \frac{1}{\sqrt{9+\frac{x^2}{2}}} + 0.85\frac{d}{t}$$

$$x = g_2 d\sqrt{f}$$

where

t is the membrane thickness (mm)

d is the aperture diameter (mm)

p is the aperture ratio (aperture area/membrane area, %)

g_1 and g_2 are constants.

The normal specific acoustic impedance of the air behind the testing specimen, again normalized by ρc is

$$Z_D = -j\ ctg\left(\frac{\omega D}{c}\right) \tag{3-3}$$

where D is the distance (m) from the membrane or perforated sheet to the rigid wall.

Therefore, overall normal specific acoustic impedance of the membrane backed with an air cavity is

$$Z = Z_M + Z_D = r' + j\left(\frac{\omega m'}{\rho c} - ctg\left(\frac{\omega D}{c}\right)\right) \tag{3-4}$$

And the overall normal specific acoustic impedance of the perforated sheet backed with an air cavity is

$$Z = Z_L + Z_D = r + j\left(\omega m - ctg\left(\frac{\omega D}{c}\right)\right) \tag{3-5}$$

The normalized specific acoustic impedance of the combination of the two separated layers of plastic membrane and perforated sheet backed by the same air-cavity can be calculated by

$$Z = r' + j\left[\frac{\omega m'}{\rho c} - ctg\left(\frac{\omega D_1}{c}\right)\right] + \frac{ctg^2\frac{\omega D_1}{c}}{r + j\left[\omega m - ctg\left(\frac{\omega D_2}{c}\right) - ctg\left(\frac{\omega D_1}{c}\right)\right]} \tag{3-6}$$

where D_1 (m) is the membrane to perforated sheet distance and D_2 (m) is the perforated sheet to the rigid wall distance.

The absorption coefficient can then be calculated by the well-known formula:

$$\alpha = \frac{4\,\mathrm{Re}(Z)}{[1 + \mathrm{Re}(Z)]^2 + [\mathrm{Im}(Z)]^2} \tag{3-7}$$

The parameters put into the equations have values as follows: for membrane backed with air cavity, m'=0.325kg/m² and D=0.075m; for perforated sheet, t=1mm, d=1mm, p=1.8%, g_1=0.2 and g_2=0.6 and D=0.075m; for the combination of two separated layers backed with air cavity, m'=0.325kg/m², t=1mm, d=1mm, p=1.8%,

g_1=0.2, g_2=0.6 and D_1=0.025m and D_2=0.075m. Figure 3-1 shows the comparison of the absorption coefficient of plastic membrane, micro-perforated sheet and PMP backed by an air cavity. It can be seen that PMP helps to increase additional damping and hence improve absorption at peaks together with wider absorption bandwidth. The PMP achieves much better absorption at lower frequency range with a higher peak value of nearly 1 at 200–300 Hz.

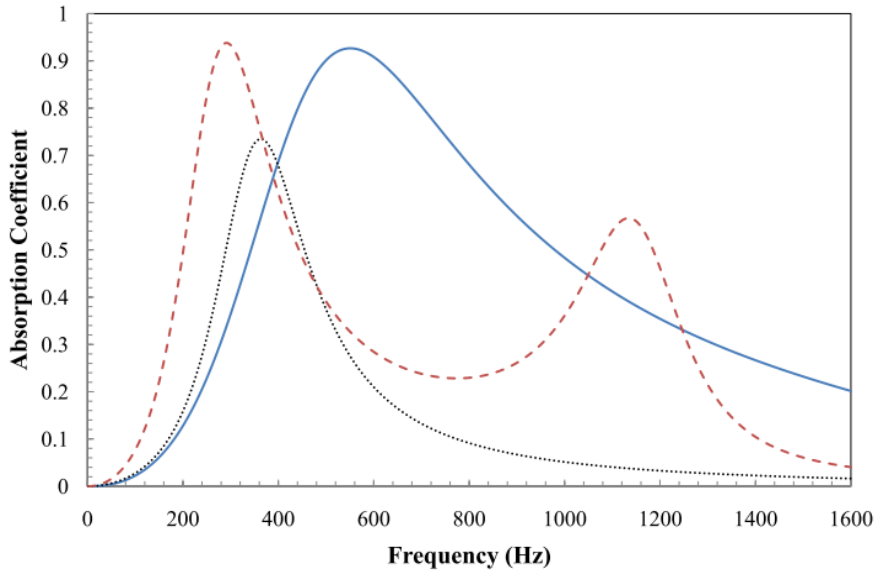

Figure 3-1: The theoretical absorption coefficient of material backed by an air cavity; ——— , plastic membrane,••••••••••, micro-perforated sheet; – – – , PMP.

By treating the PMP backed by an air cavity as a spring mass system and by the equation: *Force* $=\rho\, c\, Z\, V$ where Z is the normal specific acoustic impedance (Ns/m³) and V is the velocity (m/s). The relationships of the velocity of membrane and that of micro-perforated sheet can be found by $V_2 = \left\{\dfrac{Z_{D1}}{Z_{D1}+Z_L+Z_{D2}}\right\}V_1$

where

Z_L is the normal specific acoustic impedance for micro-perforated sheet (Ns/m³)

Z_{D1} is the normal specific acoustic impedance for air cavity between the two layers (Ns/m³)

Z_{D2} is the normal specific acoustic impedance for air cavity between the inner micro-perforated sheet and the rigid wall (Ns/m³)

The graph displayed in Figure 3-2 shows the relationships of V_2/V_1 and frequency. V_2 is greater than V_1 in the frequency range of 200–500Hz which means that air flow reaction is caused by micro-perforated sheet cavity absorber. For the frequency higher than 500Hz where V_1 is approximately the same as V_2 means that air flow is due to membrane action.

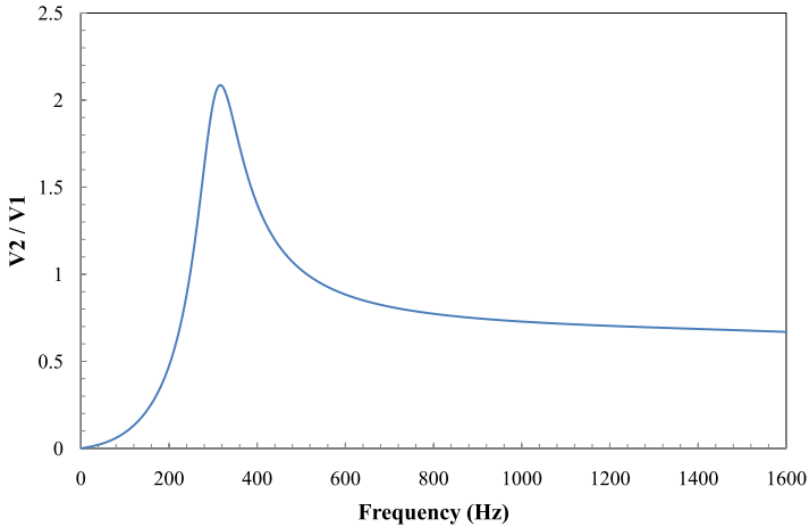

Figure 3-2: The relationships between V_2/V_1 and frequency.

Since the relationships between the parameters for the absorption characteristics of the PMP structure are rather complicated; it is difficult to examine the effects of those parameters on the absorption characteristics of the PMP. In this section, therefore, a series of parameter studies on the PMP structure is presented. According to Equation (3-7), it is seen that the absorption characteristic of the PMP structure is dependent on the membrane to micro-perforated sheet separation distance (D_1), the air cavity depth backed behind the micro-perforated sheet (D_2) and the surface density of the plastic membrane (m'). However, there are some constraints on the parameters for the design optimization: e.g. the plastic membrane and micro-perforated layers thickness cannot be too small, in order to guarantee a reasonable mechanical strength and durability for the whole panel. Using the appropriate parameters are the key ingredients to a broad band absorber. The effects of these parameters are thus analysed below based on a series of theoretical calculations.

The effect of membrane surface density (m') is demonstrated in Figure 3-3. As expected, with increasing surface density, the resonant frequency becomes smaller. Designed membrane surface density of 3.09kg/m² was chosen so as to achieve better absorption at low frequencies.

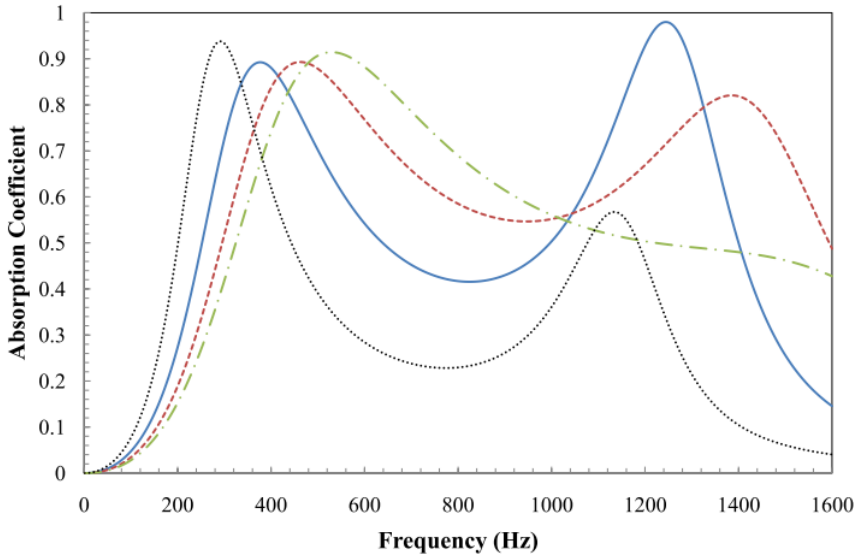

Figure 3-3: The theoretical absorption coefficient of the PMP with different membrane surface density (*m'*); ····· , designed *m'*(0.325kg/m²) , ——— , 1/2 designed *m'*; – – –, 1/4 designed *m'*; — · — , 1/8 designed *m'*.

The effects of membrane to perforated sheet separation distance (D_1) on noise absorption are shown in Figure 3-4. The results obtained suggest that the membrane to micro-perforated sheet distance will not affect the first resonant frequency but the second one instead. With a greater separation distance, the second resonance shifts to the left and gets closer to the first resonant peak. In order to pursue the objective of obtaining good absorption along a wide frequency range, the separation distance (D_1) of 0.025m is chosen.

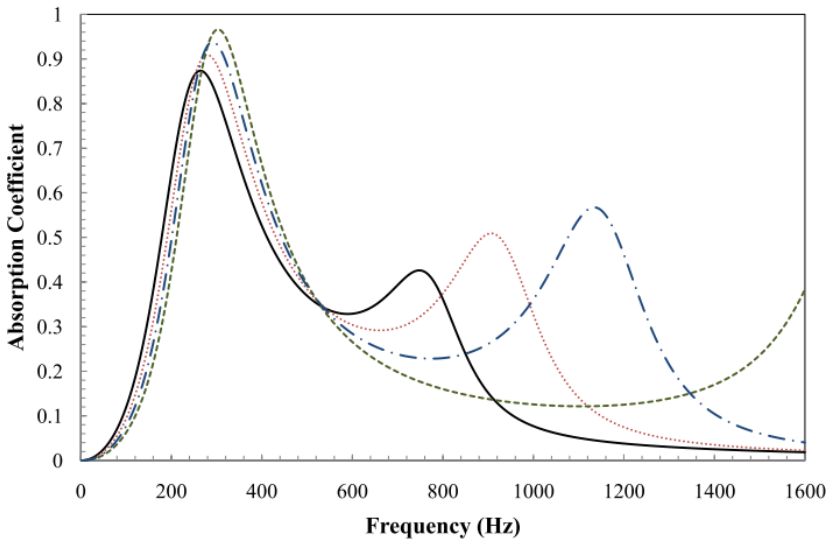

Figure 3-4: The absorption coefficient of the PMP with different membrane to perforated sheet distance (D_1); , D_1 = 0.01m; , designed D_1 = 0.025m; , D_1 = 0.04m, , D_1 = 0.06m.

3.4 Impedance tube measurements

To validate the theory, a series of measurements was carried out in an impedance tube test. A plastic membrane and a micro-perforated Plexiglas sheet samples (Figure 3-5) were built inside an impedance tube of 100mm diameter to verify the prediction model. The plastic membrane has parameter of m'=0.325kg/m² and the micro-perforated sheet has parameters of t=1mm, d=1mm and p=1.8%. In the measurements, the samples which had the same cross section as that of the impedance tube were stuck on the frame inside the impedance tube (Figure 3-6 and Figure 3-7). A special device was used to clamp samples inside the impedance tube to eliminate air leakage. The plastic membrane to the micro-perforated sheet distance

(D_1) and the air cavity depth behind the micro-perforated sheet (D_2) were varied to achieve the optimization of broadband sound absorption. The frequency of maximum sound absorption decreases as the air cavity behind the micro-perforated sheet (D_2) increases. The comparisons between theoretical calculation and measurements are also presented.

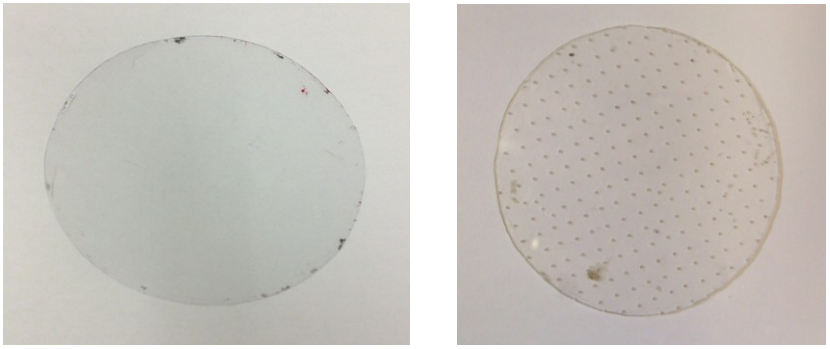

Figure 3-5: Front view: (a) plastic membrane; (b) micro-perforated sheet

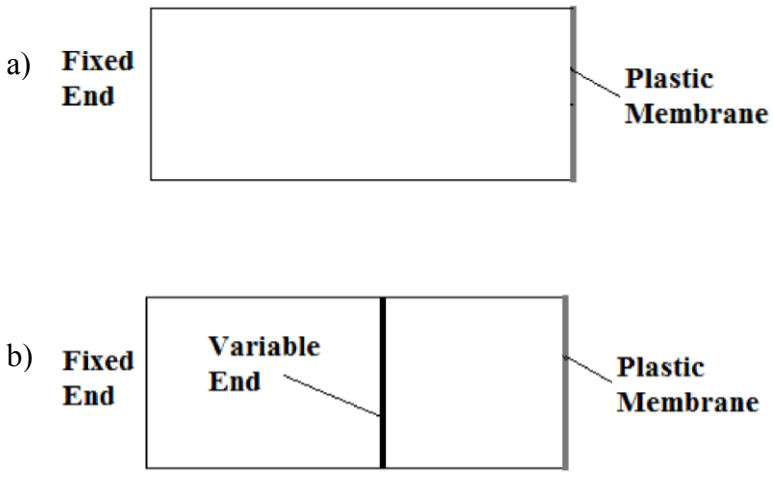

Figure 3-6: Configuration of the impedance tube test for plastic membrane: Top view (a) fixed end; (b) variable end.

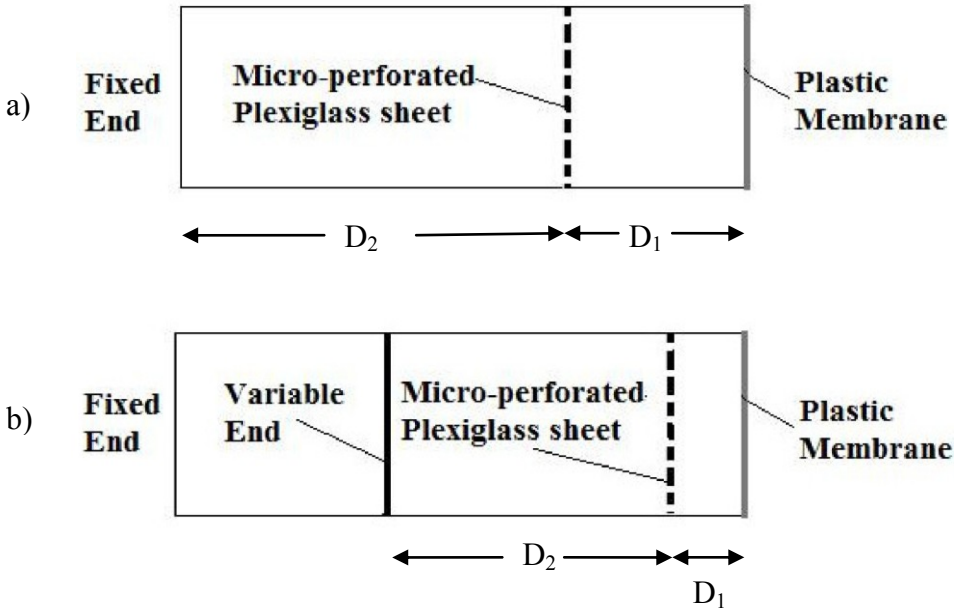

Figure 3-7: Configuration of the impedance tube test for PMP structure with variable micro-perforated sheet: Top view (a) fixed end; (b) variable end.

Figure 3-8 compares the absorption performance of the plastic membrane with different air cavity depth (*D*) of 0.01m, 0.05m and 0.075m respectively (experiment configuration shown in Figure 3-6). Results points out that larger air cavity depth (*D*) shifts the resonant frequency to the lower frequency region.

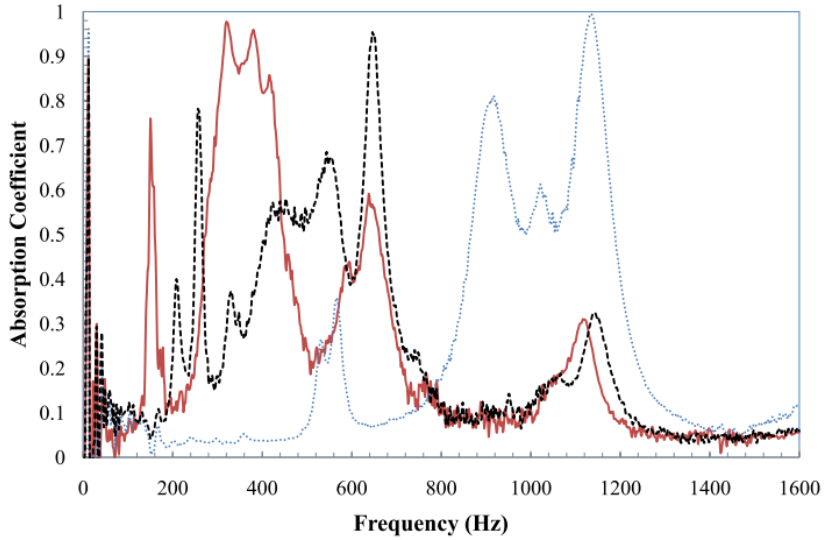

Figure 3-8: The absorption coefficient of plastic membrane with different air cavity at the back (D); ——— , 0.075m, – – – , 0.05m; ····· ,0.01m.

The absorption ability of the micro-perforated sheet is compared with that of PMP with fixed air cavity at the back (D_2=0.075m). The impedance tube test configuration was same as in Figure 3-7a. Results are shown in Figure 3-9. Without the top plastic membrane layer, the absorption coefficient of the micro-perforated Plexiglas sheet is above 0.6 for the frequency range from 400Hz to 1100 Hz with a peak absorption coefficient value of 0.9 at about 500Hz. When the top plastic membrane layer is applied, the peak absorption coefficient shifts to the left and reaches the highest value of nearly 1 at 300Hz. The PMP has broader absorption bandwidth but its absorption ability fluctuates more along the whole frequency range.

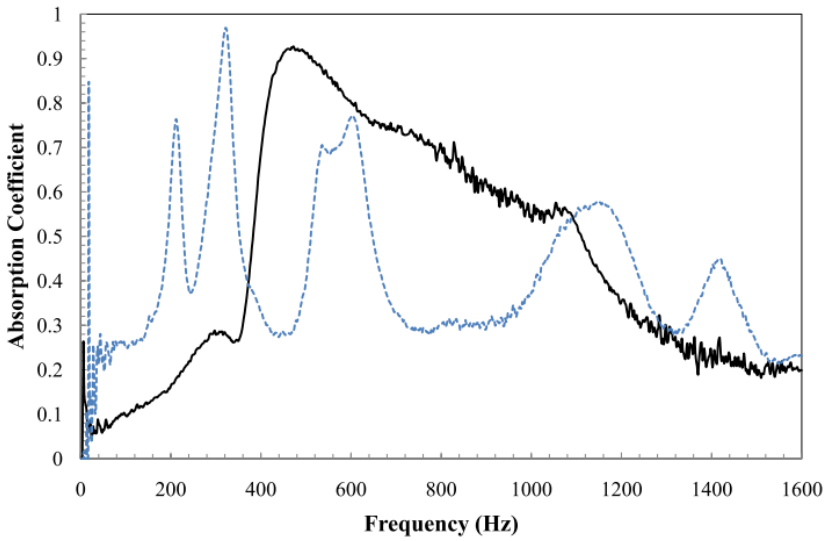

Figure 3-9: The absorption coefficient of different absorbers with same micro-perforated sheet to rigid end distance (D_2=0.075m); ——,micro-perforated sheet, – – –, PMP.

Figure 3-10 is the comparison of the absorption coefficient of the PMP with fixed membrane to perforated sheet distance (D_1=0.025m) but different air cavity depth behind the perforated sheet (D_2) (experiment configuration shown in Figure 3-7). The findings indicate that an increase in the air cavity at the back (D_2) improves sound absorption at the lower frequency range.

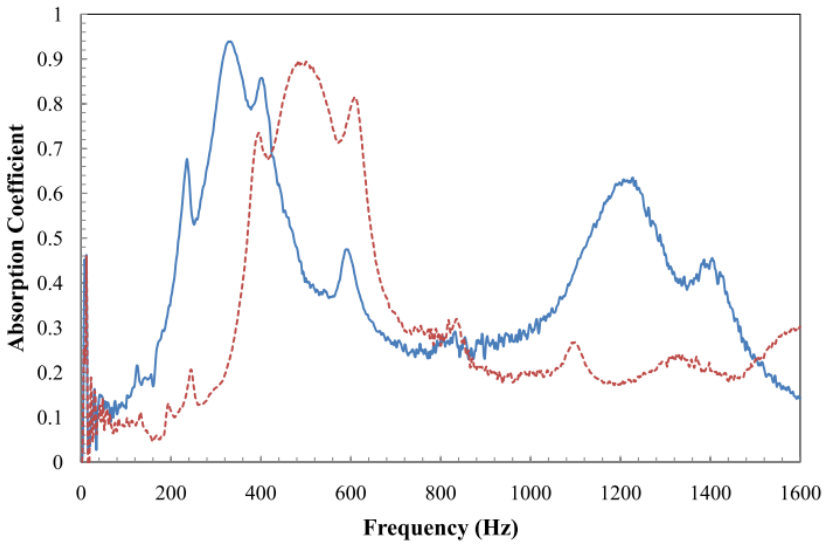

Figure 3-10: The absorption coefficient of the PMP with fixed membrane to micro-perforated sheet distance (D_1=0.025m) but different micro-perforated sheet to rigid end distance (D_2); – – –,0.015m, ———, 0.075m.

Figure 3-11 shows the comparison of the absorption coefficient for the cases with fixed air cavity behind the perforated sheet (D_2) and variable membrane to perforated sheet distance (D_1) (experiment configuration shown in Figure 3-7). It can be seen that the resonant frequencies and the peak absorption values for both cases are very similar. However, the absorption performance for the case with shorter D_1 deteriorates from about 700Hz.

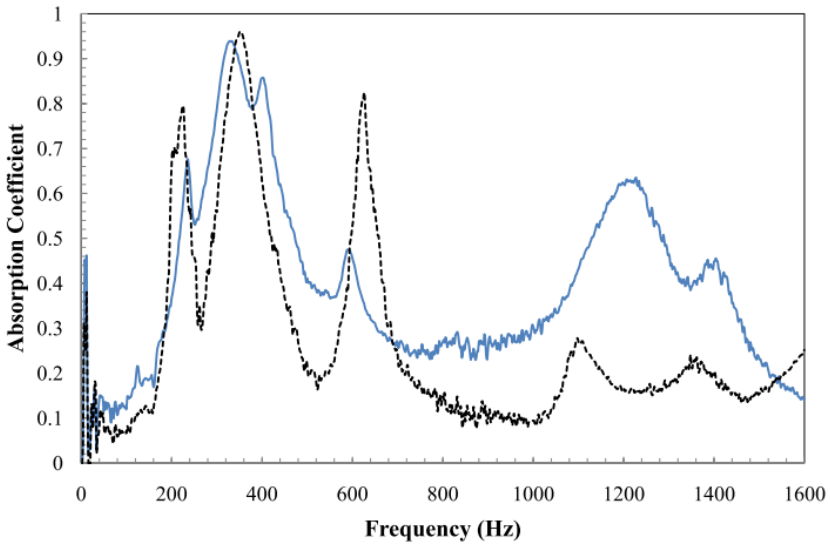

Figure 3-11: The absorption coefficient of the PMP with fixed micro-perforated sheet to rigid end distance (D_2=0.075m) but different membrane to micro-perforated sheet distance (D_1); – – –, 0.01m, ———, 0.025m.

From the above results, the parameters for PMP were chosen to be D_1=0.025m and D_2=0.075m. Figure 3-12 shows the comparison of the experimental absorption coefficient of different absorbers. With only a plastic membrane can achieve a maximum absorption coefficient value of 0.95 for a small frequency range of 300–500Hz. When applying resonator only, the absorption coefficient peak of nearly 1 is achieved in frequency range of 500–700Hz. Using PMP, a broader bandwidth can be achieved from 200–1400 Hz, where the average absorption coefficient is around 0.5. The curve shape of PMP is similar to that of plastic membrane with same first resonant peak value while the second resonance for PMP is much more

significant. The second resonant frequency for PMP is near 1100–1400Hz with absorption coefficient of about 0.6.

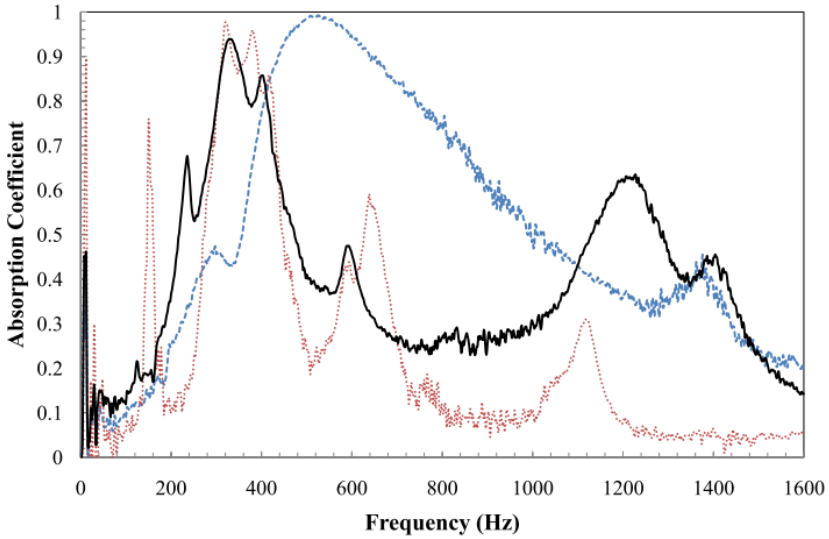

Figure 3-12: The absorption coefficient of different absorbers backed by an air cavity; ····· , plastic membrane, – – – , micro-perforated sheet; ——— , PMP.

Another experiment was conducted to examine the effect of membrane surface density (m') on the absorption performance (experiment configuration same as Figure 3-6). It is shown in Figure 3-13 that the surface density affects the resonant frequencies for the same air cavity depth. Membrane with larger surface density gives a result of better absorption at the lower frequency range with comparatively higher peak absorption value. Since high frequency sound can be eliminated easily by many traditional methods, it is desirable to apply the membrane with larger

surface density to the panels in order to obtain better low frequency absorption.

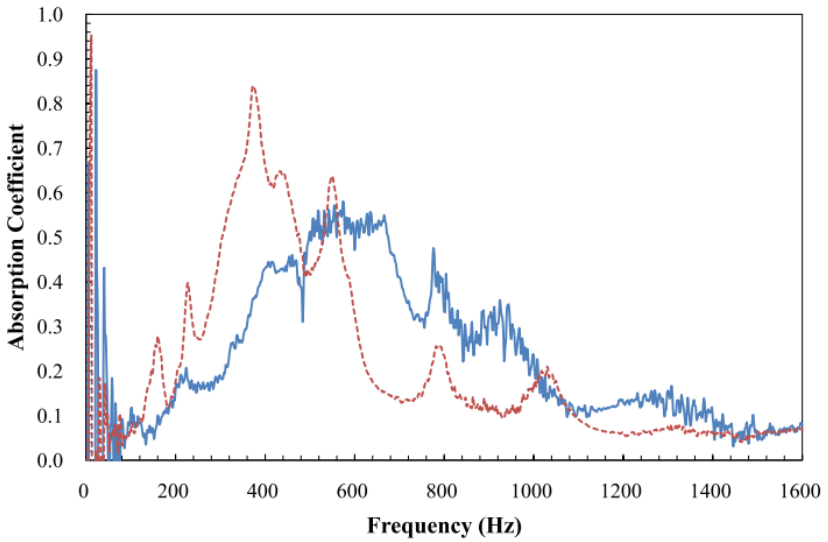

Figure 3-13: The absorption coefficient of the plastic membrane with different surface densities (*m'*); – – –, 3.09kg/m², ——— , 0.325 kg/m².

Figure 3-14 shows the comparison of the absorption coefficient of PMP using top plastic membrane of different surface densities (experiment configuration same as Figure 3-7). Results show that the PMP with larger surface density achieves noise reduction at wider bandwidth with the frequency range from 200Hz to 1400Hz whereas membrane with smaller surface density has frequency range of 300–1300Hz. Membrane with larger surface density obtains significant improvement at low frequency range of around 300–500 Hz with absorption coefficient of nearly 0.9.

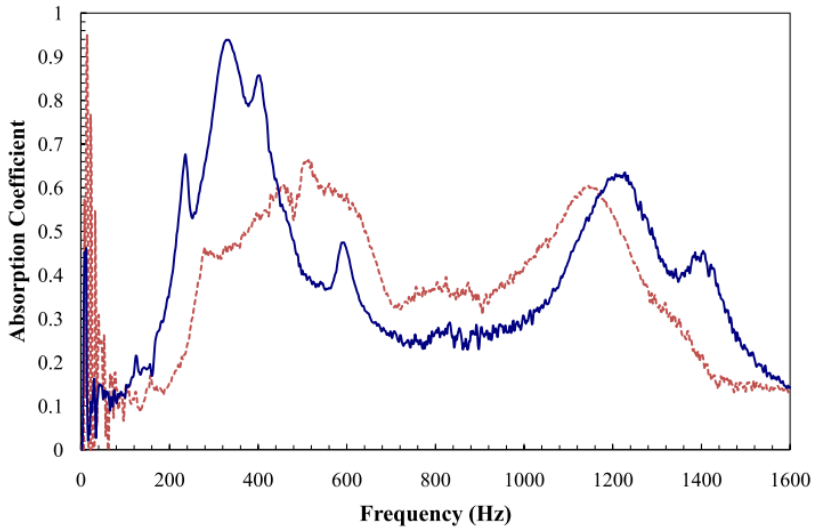

Figure 3-14. The absorption coefficient of the PMP with top plastic membrane with different surface densities; ——, 3.09kg/m², – – –, 0.325 kg/m².

3.5 Experiments on investigating the absorption performance of a panel absorber with PMP in a testing duct

By the formula developed (Section 3.3) and the impedance test results (Section 3.4), the optimized parameters can be chosen. The designed membrane thickness is 0.5mm with surface density of 3.09kg/m². The dimensions of the rectangular micro-perforated Plexiglas plate are 10.5 × 6 cm² with mass 7.493g. The parameters of plate are porosity p=1.8%, t=1mm, d=1mm. The holes were drilled mechanically. The device provides absorption through high viscous losses as air passes through the small holes. This inherent damping eliminates the need for fiberglass or other porous materials in the air cavity. The surface is transparent when looked at from straight on,

but at oblique angles the holes become more apparent, although the surface is still translucent. Overly small perforations should be avoided, otherwise additional resistive losses in the perforations is likely to decrease the performance as too large the resistivity will lower the absorption ability. The separation distance between holes is 5mm. Micro-perforated sheets are placed 0.025m away from the plastic membrane on the top (i.e. D_1=0.025m).

The position of the micro-perforated plate in the divided panel is important for the resonant frequency. Changing the position of the plate from bottom to the top of the panel, the first resonant frequency of the panel is gradually decreased. The maximum depth controls the lowest frequency sound absorption. The micro-perforated sheet was fixed at 0.075m from the rigid end (D_2) for this study to guarantee a good performance at low frequencies (Figure 3-15 and 3-16). The panels were put inside a testing duct which has the same configuration as previous experiment in Chapter 2 (Section 2.4.1 - Figure 2-13).

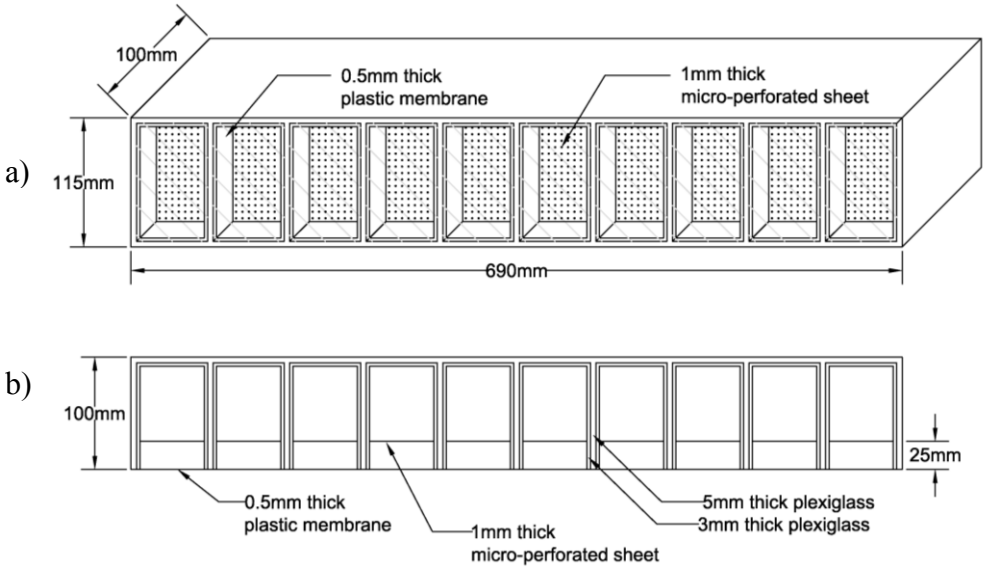

Figure 3-15: Dimensions of the divided Plexiglas panel with one membrane layer and one layer of micro-perforated sheet; (a) isometric view, (b) top view.

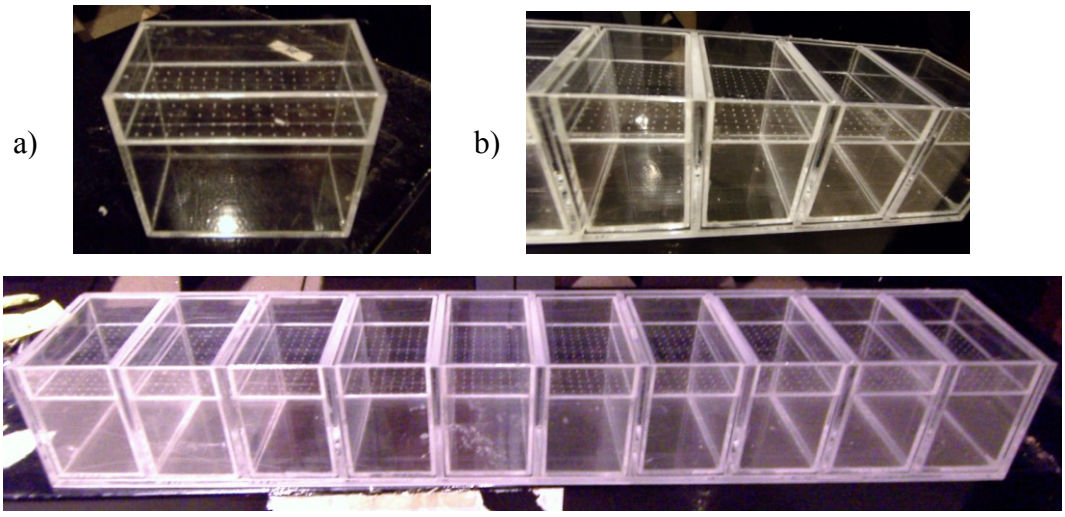

Figure 3-16: (a) A division of the divided Plexiglas panel; (b) small divisions put into the divided Plexiglas panel; (c) divided Plexiglas panel

The findings in Figure 3-17 reveal that the DPP works best only in the frequency range from 400 to 500 Hz with about 40dB sound reduction. For the case

of the PMP, a wider bandwidth of noise reduction can be achieved from around 200Hz to 750Hz. The peaks are near 300Hz with of 60dB sound reduction. The result has confirmed the usefulness of the new design (PMP) in gaining additional low frequency absorption.

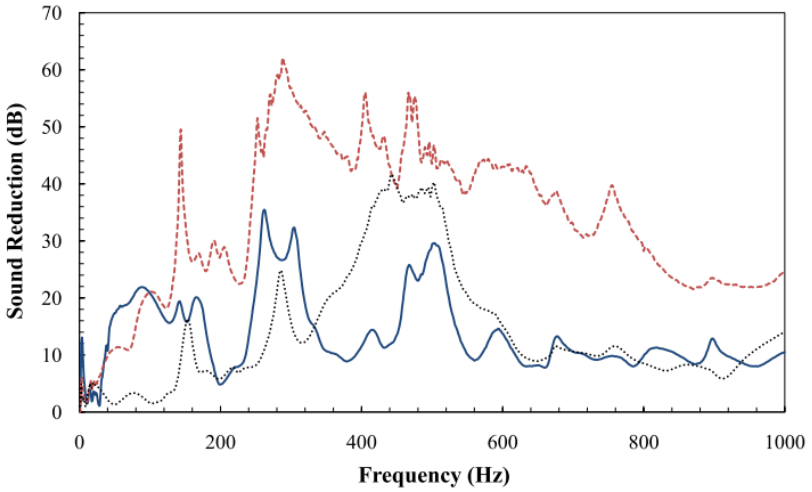

Figure 3-17: Sound reduction of Plexiglas panels in the testing duct using different absorbers; ····· , DPP; ——— , LPP; – – – , PMP.

Further experiments were conducted to investigate the effect of increasing the testing duct length on sound reduction performance. PMP was put in the extended testing duct and the configuration of the extended duct was same as previous experiments in Chapter 2 (Section 2.4.3 – Figure 2-19). The findings indicates that the extended duct can obtain better absorption over the whole frequency of interest

especially low frequencies (Figure 3-18). As is shown in Figure 3-18, the bandwidth for the PMP in the extended duct is about 80–900Hz with over 30dB sound reduction.

Another experiment was conducted to compare the sound reduction performance of the extended duct with and without absorber and the result is shown in Figure 3-19. There are significant improvements in sound reduction when using absorber inside the extended duct with more than 30dB sound reduction achieved in the frequency range from 200 to 1000Hz together with a peak value of 50dB at around 300Hz. However, the sound reduction performance is not considerable at frequencies below 200Hz which reveals the fact that the absorber cannot bring benefit at frequencies below 200Hz.

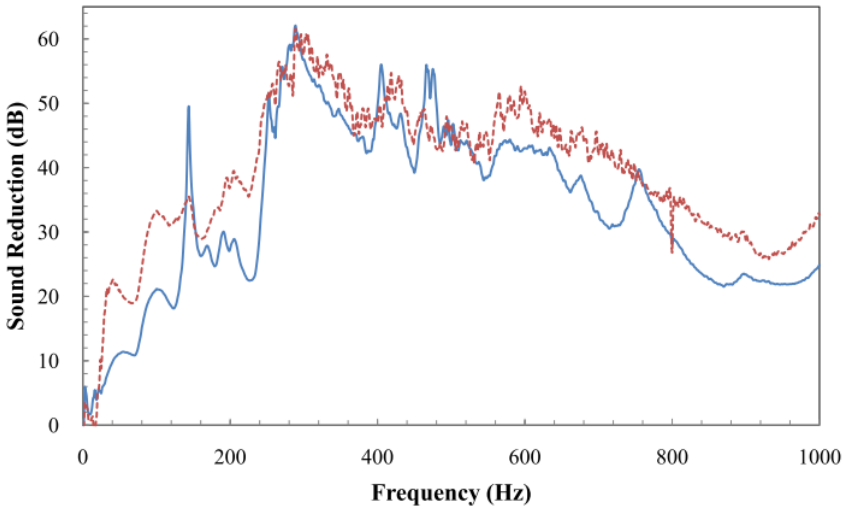

Figure 3-18: Sound reduction of the divided Plexiglas panel with PMP for testing ducts of different length; ——— , short duct; – – – , long duct.

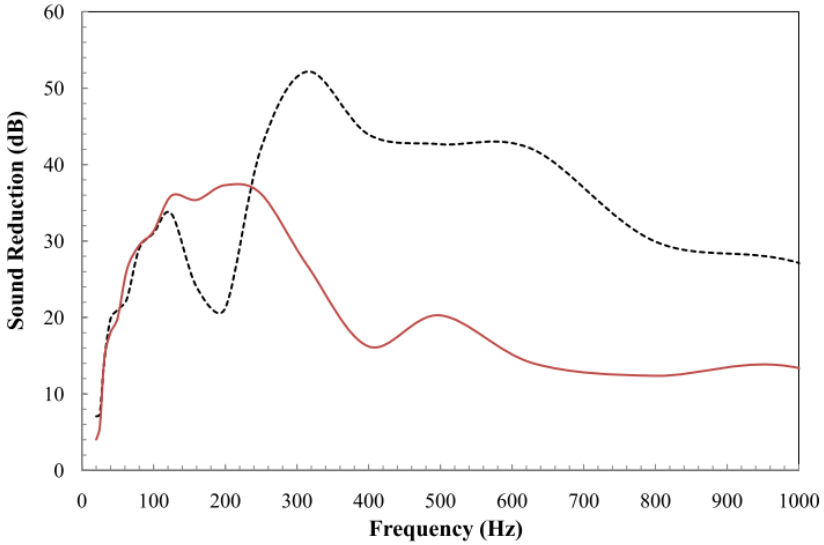

Figure 3-19: Sound reduction of the divided Plexiglas panel with PMP (Absorber) in the extended duct system; ——, no Absorber; – – –, absorber.

Different absorbers were put inside the extended duct for comparison of the absorption ability. As is shown in Figure 3-20, the DPP can achieve noise reduction only at a particular frequency range of 400–500 Hz. The divided panels with plastic membranes instead of Plexiglas sheets can perform better with noise reduction from 250Hz to 650 Hz. When the PMP and the divided panels with only top plastic membrane are compared, the divided panels with only top plastic membrane can achieve higher insertion loss values but narrower bandwidth. The bandwidth for the PMP is about 200–760Hz. The data provides evidence that the PMP widens the bandwidth towards the high frequency range and improves significantly the absorption in low frequency range.

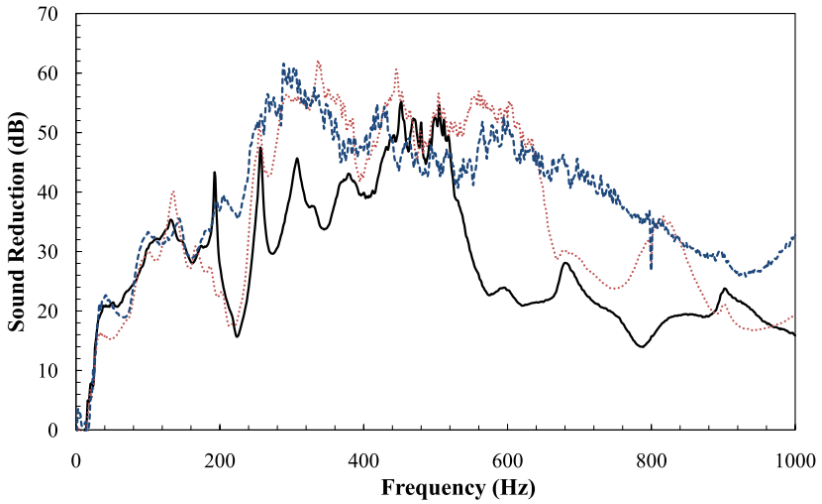

Figure 3-20: Sound reduction of Plexiglas panels in the extended testing duct using different absorbers; ——, DPP; ·····, divided plastic membrane; – – –, PMP.

The concept of optimized constant depth of micro-perforated sheet inside panel can contributes to better absorption than with micro-perforated plate fixed at the top of the cavity. The micro-perforated sheet parameters are also a key factor for sound absorption. As the holes enlarge, the open area increases leading to greater absorption at higher frequencies; there is also a slight increase in resonant frequency. As the open area decreases, additional low frequency absorption is generated mainly due to the increased stiffness of the spring in the unit cell as the volume reduces. The high frequency absorption decreases because the proportion of solid parts of the perforated sheet increases, and these parts reflect high frequency sound. Increasing the cavity depth causes the stiffness of the spring to decrease, and consequently the peak absorption decreases with frequency.

Therefore, it is important to get the perforated sheet with the correct hole size and open area. Consequently, the micro-perforated sheet often has to be specifically constructed for acoustic purposes, which makes it more expensive than if stock items could be used.

3.6 Comparison of theoretical and experimental results in the testing duct

Figure 3-21 shows the comparison between theoretical and measured absorption coefficients for the micro-perforated Plexiglas sheet. It can be seen that the calculated and measured absorption coefficients are almost the same. Figure 3-22 shows the comparison of theoretical and experimental absorption coefficient for plastic membrane. Both curves have the highest peak at the same frequency range at about 300–400Hz. Apart from the highest peak at 300–400Hz in Figure 3-22, there are several peaks with smaller magnitude which may be generated by different membrane vibration modes or by imperfect mounting condition. Similar results are shown in Figure 2-14 for the 0.7m long Plexiglas panels of 2mm thickness.

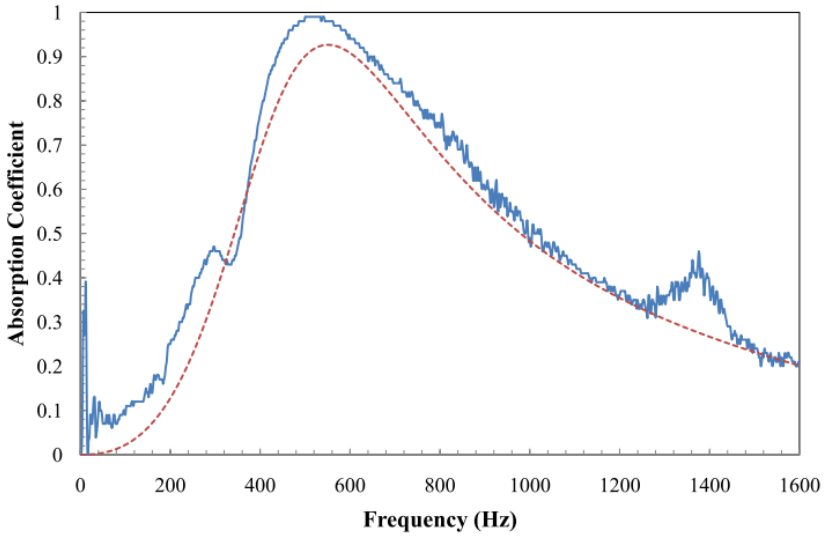

Figure 3-21: Comparison of theoretical and experimental absorption coefficient for micro-perforated sheet; - - -, theory; ——— , experiment.

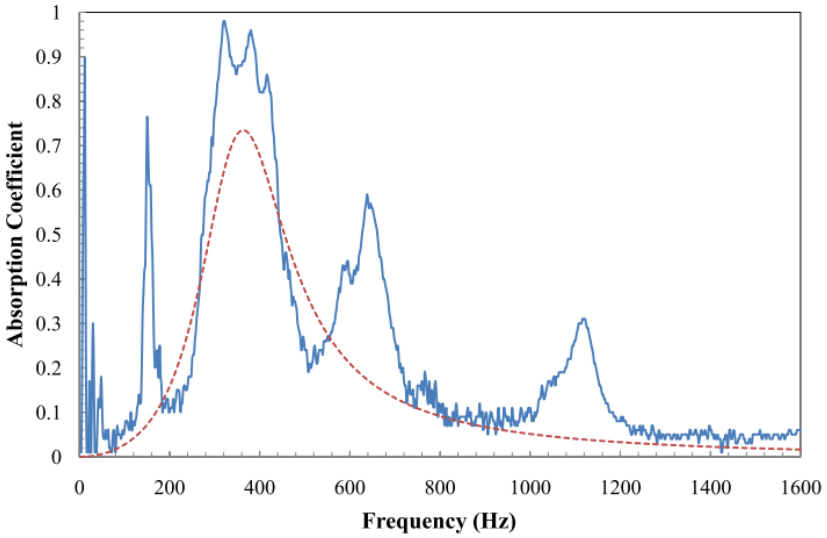

Figure 3-22: Comparison of theoretical and experimental absorption coefficient for membrane;- - - , theory; ———, experiment.

Figure 3-23 shows the comparison of theoretical and experimental absorption coefficient for PMP. It reveals that both curves are well-matched with each other which prove the validity of the theory for PMP. The peak absorption coefficient of the theoretical result is almost the same as that of the experimental result with a value of above 0.95 in the frequency range from 300 to 400 Hz. As expected, when there is a combination of these two layers, the low frequency range of absorption can be extended and the frequency range of absorption is much wider than that of a single layer.

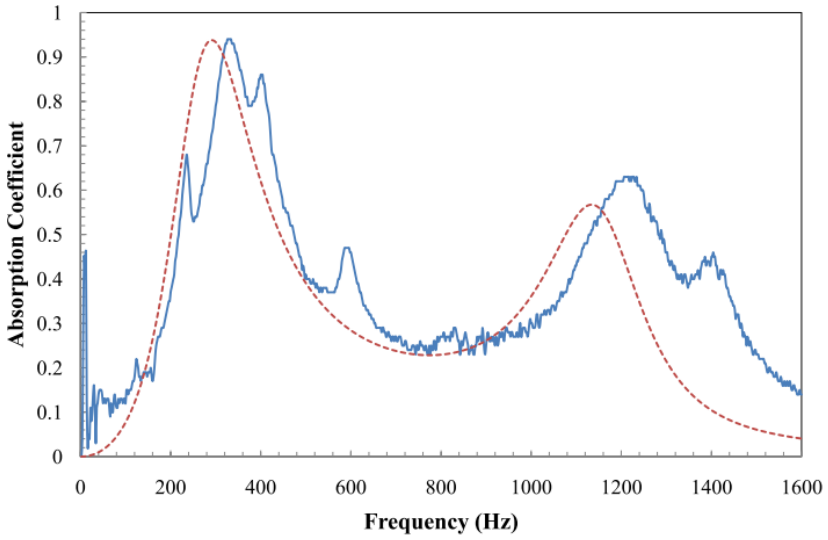

Figure 3-23: Comparison of theoretical and experimental absorption coefficient for PMP; – – –, theory; ——, experiment.

3.7 Experiments on investigating the absorption performance of a panel absorber with PMP in a real scale room

To further examine the absorption performance of PMP, an experiment was carried out in a real scale room. The room dimensions and the configuration of the testing duct are shown in Figure 3-24. The panel absorbers (PMP) are put in the testing duct which is the same as the previous experiment in this Chapter – Section 3.5. One end of the testing duct was connected to the real scale room while the other end is connected to a 0.7m long duct with a loudspeaker as termination. A control experiment was carried out by a testing duct without panel absorber. That testing duct provided a pathway having same dimension as that provided by PMP putting in the testing duct.

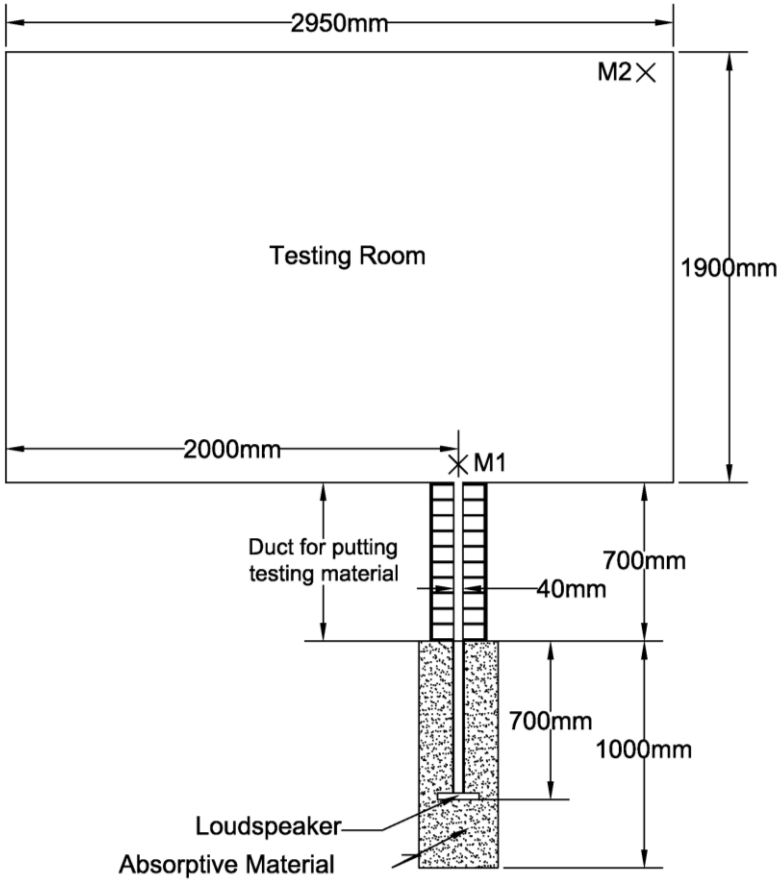

Figure 3-24: Testing room dimensions and configuration of the testing duct

The sound pressure level measured in the opening of the testing duct (M1) is shown in Figure 3-25. PMP has poor absorption performance for the frequency below 200Hz. It performs best in the frequency range from 400 to 800Hz. Both control and PMP fell to its lowest point at frequency 500Hz which is due to muffler effect. On the whole, using PMP achieves 30dB lower than using the control. The sound pressure level measured in the corner of the room (M2) is shown in Figure

3-26. PMP cannot help sound reduction at the frequency below 200Hz but performs very well in the frequency range from 200 to 1000Hz. PMP has an average sound pressure level of 10dB above 200Hz while the control has an average sound pressure level of 40dB. PMP can have 30dB more sound reduction than the control. Again, both control and PMP fell to its lowest point at frequency 500Hz which is due to muffler effect.

Referring to Figure 3-26, it can be seen that only 10- 20dB is measured at M2 using PMP. The peaks values are mainly due to the formation of standing wave due to the room dimensions (3m x 1.9m), where the transmission loss will be lower at about 90Hz, 180Hz, 270Hz, 360Hz, etc.

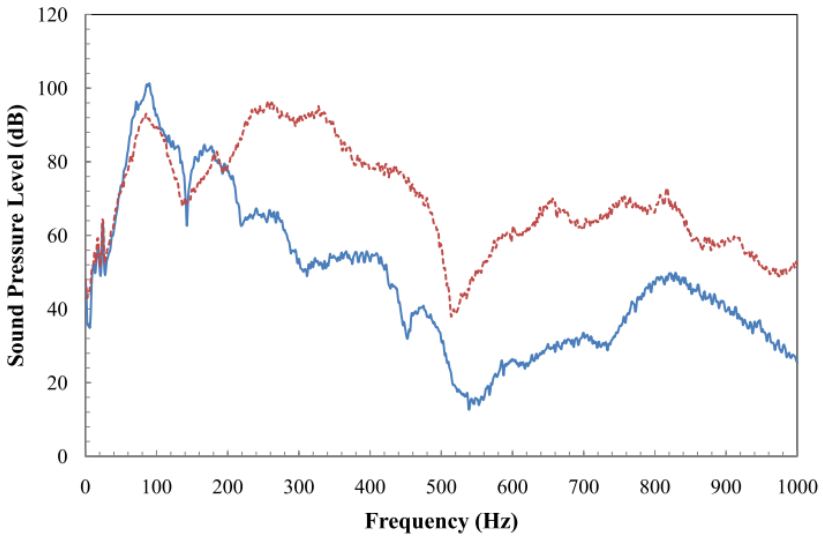

Figure 3-25: The sound pressure level measured in the opening of the testing duct (M1); ——— , PMP ; - - - - , control.

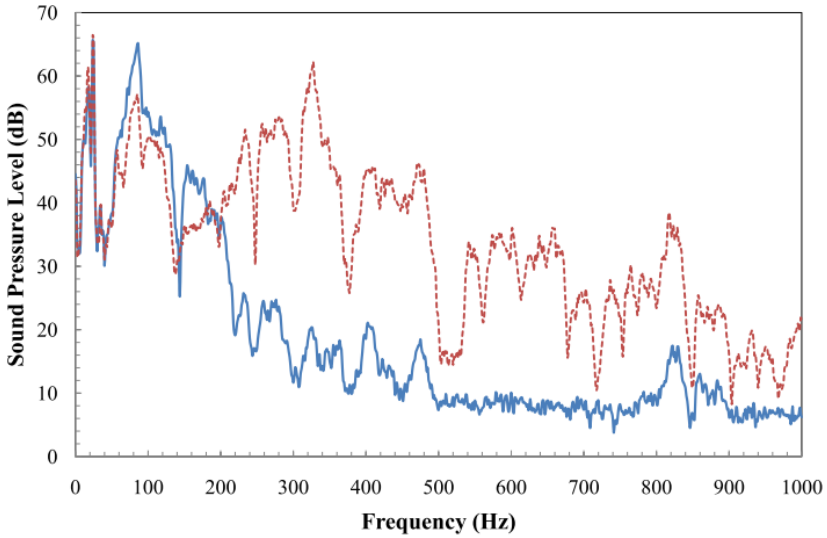

Figure 3-26: The sound pressure level measured at the corner of the testing room (M2); ——— , PMP ; – – – , control.

3.8 Summary

This chapter has examined the sound reduction performance using the new optimized panel absorber system with a combination of two layers - a plastic membrane and a micro-perforated Plexiglas sheet. Good agreement between theoretical and experimental results is found.

The Plexiglas panels in the extended duct using PMP can achieve about 55dB sound reduction at the frequency range of 200Hz to 400Hz and about 40dB sound reduction for the frequency range after 400Hz, and then deteriorate at higher frequencies. Using PMP in full scale room can also obtain an average insertion loss of 30dB.

The new optimized structure combined plastic membrane and micro-perforated plate extends the absorption to lower frequencies as well as maintaining good mid-frequency absorption, and hence becomes a considerably better broadband sound absorber. The Plexiglas sheet and plastic membrane are both resistant to moisture, bacteria and fungi and so can be used in place of traditional fabric upholstered systems. Due to its fiber-free property, the panel absorber system does not emit health impairing particles. Another significant benefit of the panel absorber system is that it can be maintained easily and has longer product lifetime compared to conventional fibrous absorbers.

CHAPTER 4

THE ABSORPTION PERFORMANCE OF THE CLOTH MEMBRANE AND THE THICK PERFORATED PLEXIGLAS SHEET

4.1 Introduction

It is possible to gain absorption at low to mid-frequencies by using the phenomenon of resonance. Resonant absorbers can be membrane absorber or Helmholtz resonator, placing the device at the boundaries will improve their effectiveness. Membrane absorber can be a sheet of material such as plastic or plywood which then vibrates as a spring system. The spring is provided by the air enclosed in the cavity. By changing the vibrating mass and the stiffness of the air spring, the resonant frequency of the device can be tuned, and absorption is maximum at the resonant frequency. A membrane absorber converts the high sound pressure fluctuations typically found at wall surfaces and in corners into selective absorption in the modal frequency range. The mechanism of Helmholtz resonator has been described in the previous chapter (Chapter 3).

Resonant absorbers are commonly employed to treat low frequency room modes and as parts of silencers within ventilation systems. The purpose of this chapter is to

examine the absorption performance of the cloth membrane as membrane absorber and the 13mm thick perforated sheet as Helmholtz resonator.

4.2 Literature Review

Perforated plates have been used as sound absorption device for years. The impedance characteristics of perforates are important not only in aircraft engine liner designs, but also in a number of other applications; namely, cooling systems for electrical, electronics and laser system requiring control flow, etc (Salikuddin et al., 1994). A micro-perforated panel was made out of a thick panel in order to overcome the lack of appropriate strength required for room walls (Sakagami et al., 2008). However, thick micro-perforated panels are usually not efficient because the resistance and/or reactance becomes too high. Trial production of thick micro-perforated panel and measurements of their normal absorption coefficients were carried out. Results showed that efficient absorption can be given with a thick micro-perforated panel by using a tapered perforation.

The problem with the above mentioned perforated panel systems are getting broadband absorption. In the absorption test of a micro-perforated panel, an additional sound absorption peak was unexpectedly found around the low-frequency

range (50–100 Hz) due to the panel vibration effect (Lee and Swenson, 1992). As it relies on resonance, the absorption will be limited to low to mid-frequencies, whereas an ideal clear absorber would probably be the one that covered the entire speech frequency range.

Interestingly, a paper reported that poorly constructed structures could provide high absorption below the lowest resonant frequency (Fujiwara and Miyajima, 1995). It is speculated that this additional absorption came from cracks in the well bottoms forming Helmholtz resonators with air cavities behind. This inspired the idea that using perforated plates in some wells could significantly extend the absorption range towards the lower frequencies by adding mass to the system and so lowering the resonant frequency. However, the structure cannot provide broadband frequency absorption.

There are less than two dozen fundamental experimental membrane vibration studies found in the literature (Jenkins and Korde, 2006). The simplest cases have even not yet been thoroughly investigated. This is partly due to the extreme flexibility and lightness of membranes and an advanced non-contact measurement methods are thus required.

4.3 Impedance tube measurements of the absorption performance of the cloth membrane backed with an air cavity

The surface density of the cloth membrane (Figure 4-1) is about 0.399 kg/m². The cloth membrane is fitted to the size of the impedance tube (Figure 4-2). Two parameters are investigated: the depth of the air cavity behind the membrane (*D*) and the surface density of the membrane (*m'*). It is shown in Figure 4-3 that the cloth membrane backed with a greater air cavity obtains better absorption at lower frequencies. With the largest air cavity of 0.7m, the first resonance is at around 82Hz with absorption coefficient of nearly 1. When using a 0.3m air cavity, the first resonance shifts to 200Hz with absorption coefficient of about 0.9 and the resonant peaks are comparatively further away from each other. There is only one resonant peak for the 0.1m air cavity which happens at about 290Hz with 0.85 absorption coefficient.

Figure 4-1: Front view of the cloth membrane

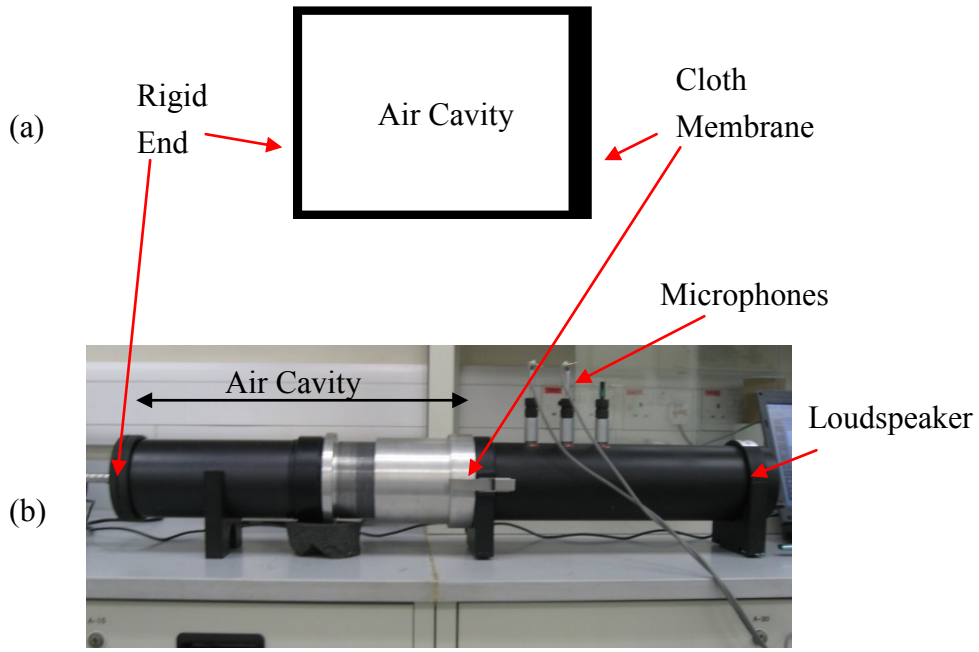

Figure 4-2: Side view of the cloth membrane in an impedance tube test

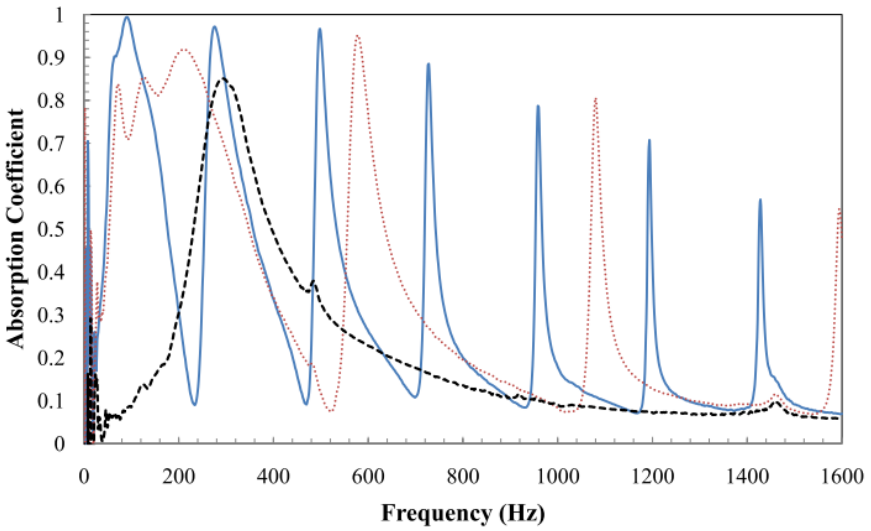

Figure 4-3: Comparison of the absorption coefficient of the cloth membrane backed behind with different air cavities (D) in an impedance tube test; ——, D=0.7m; ·····, D=0.3m; – – –, D=0.1m.

The findings in Figure 4-4 indicate that using the cloth membrane with greater surface density has adverse effect on the absorption coefficient. The membrane with smaller surface density (m'=0.399kg/m²) obtains its first resonance at around 78Hz with 0.75 absorption coefficient. The absorption coefficients for the first fifth resonances are above 0.7. For the membrane with greater surface density (m'=1.596kg/m²), the first resonance obtained is at about 172Hz with 0.62 absorption coefficient. Apart from the first resonance, membranes of different surface densities have similar resonant frequencies. In marked contrast to the membrane with smaller surface density, the absorption coefficients obtained after the third resonance of the heavier membrane are only 0.1.

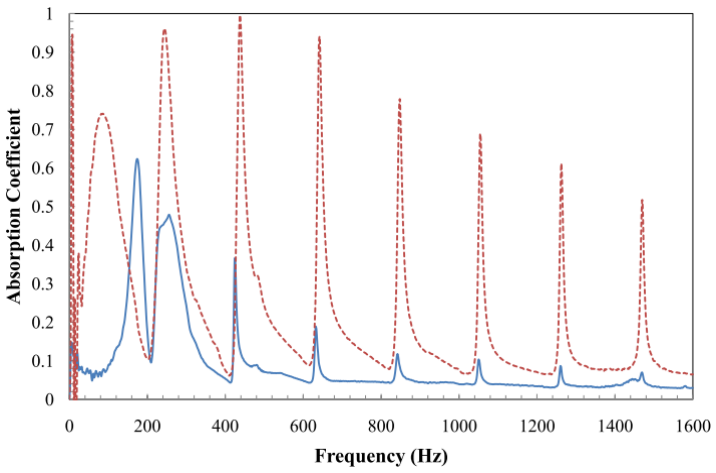

Figure 4-4: Comparison of the absorption coefficient of the cloth membrane with different surface densities (m') with a 0.8m air cavity backed behind (D=0.8m); ——— , m'=1.596 kg/m²; - - - , m'= 0.399 kg/m².

To further prove the validity of the formula in calculating the absorption coefficient of the resonant absorber with membrane backed with an air cavity developed in Chapter 3 Section 3.3 Equation (3-4) and Equation (3-7), a comparison of theoretical and experimental results is carried out. Fortunately, it can be seen from Figure 4-5, Figure 4-6 and Figure 4-7 that the formula for finding the absorption coefficient of any membrane type is valid. Though the theoretical coefficient values are lower than that of the experiment for the case of a 0.3m air cavity, the experimental and theoretical resonance peaks are well-matched with each other. There is a good accuracy obtained from the comparison of the theory and impedance tube measurements for the membrane samples. One of the keys to obtain good comparisons between theory and measurements is to get good quality samples. Even apparently small imperfections in the samples can lead to large measurement errors.

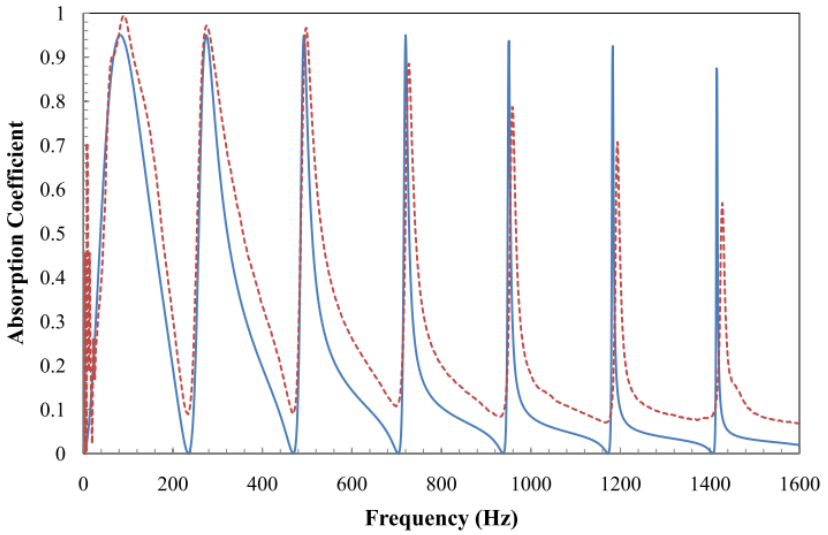

Figure 4-5: Comparison of the theoretical and experimental absorption coefficient of the cloth membrane with an air cavity (D=0.7m); ——, theory; – – –,experiment.

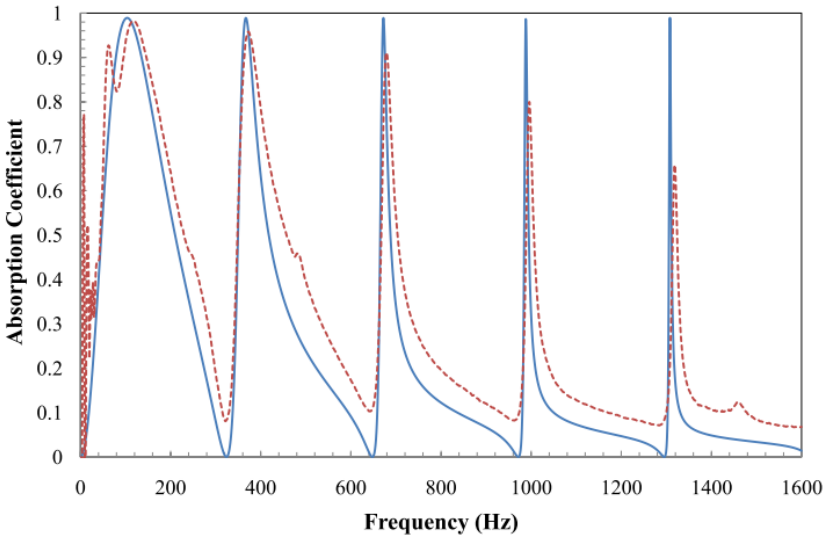

Figure 4-6: Comparison of the theoretical and experimental absorption coefficient of the cloth membrane with an air cavity (D=0.5m); ——, theory; – – –,experiment.

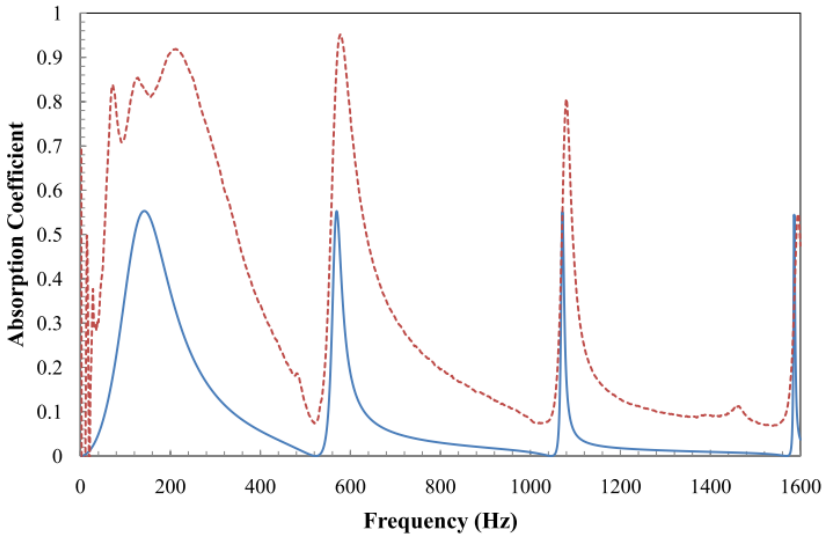

Figure 4-7: Comparison of the theoretical and experimental absorption coefficient of the cloth membrane with an air cavity (D=0.3m); ——, theory; – – –, experiment.

4.4 Impedance tube measurements of the absorption performance of the 13mm thick perforated sheet

The perforated sheet is 13mm thick with 1.5mm as the radius of the holes. The separation distance between holes is 10mm (Figure 4-8). The perforated sheet is fitted to the size of the impedance tube (Figure 4-9). It is shown in Figure 4-10 that the thick perforated sheet backed with a larger air cavity (D) obtained better absorption at lower frequencies. The first resonance is at about 45Hz with absorption coefficient of nearly 1 for the case of the largest air cavity of 0.8m. When the air cavity is 0.4m, the first resonance shifts to 70Hz with absorption coefficient of 1 and

the resonance peaks are comparatively further away from each other. For the case of the 0.2m air cavity, the first resonance is 110Hz with only two resonance peaks in the frequency range below 1600Hz.

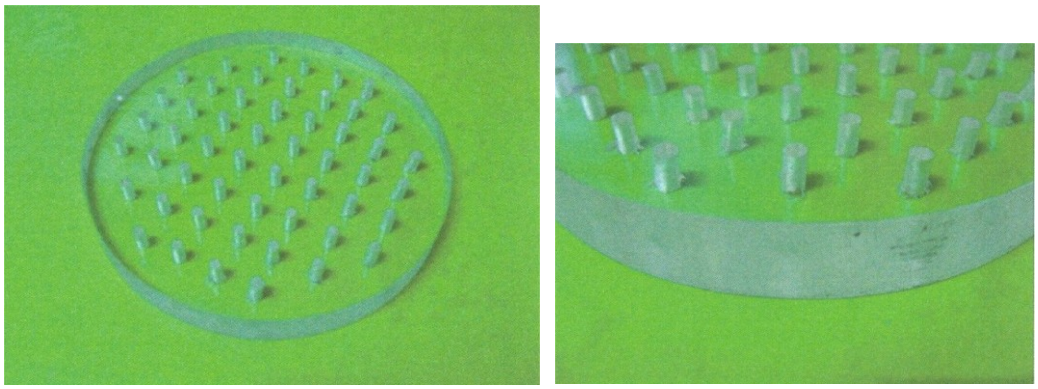

(a) (b)

Figure 4-8: Thick perforated sheet; (a) front view, (b) side view

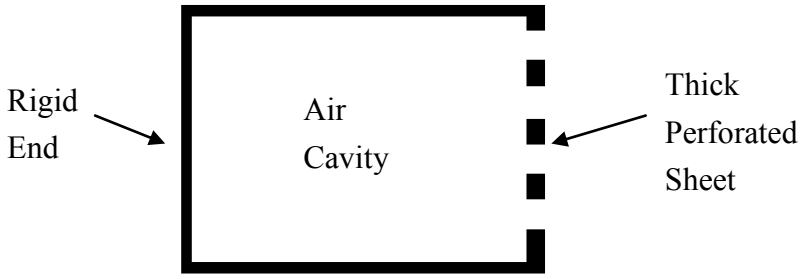

Figure 4-9: Side view of the thick perforated sheet in an impedance tube test

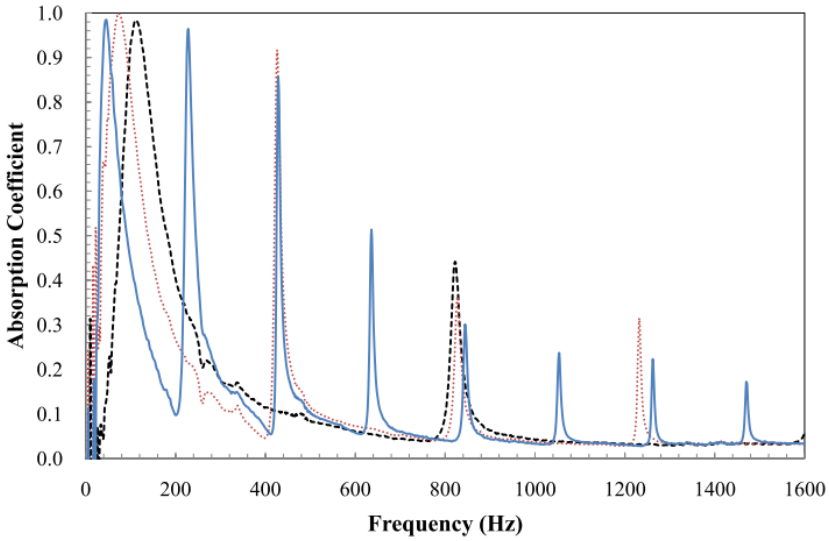

Figure 4-10: Comparison of the absorption coefficient of the thick perforated sheet backed behind with different air cavities (D) in an impedance tube test; ——— , D=0.8m; ····· , D=0.4m; – – – , D=0.2m.

The formula in calculating the absorption coefficient of the resonant absorber with perforated sheet backed with an air cavity was developed in Chapter 3 Section 3.3 Equation (3-5) and Equation (3-7). Theoretical results are compared with that obtained in the impedance tube test. It can be seen from Figure 4-11, Figure 4-12 and Figure 4-13 that the experimental and theoretical resonance peaks are well-matched with each other. There is a good accuracy obtained from the comparison of the theory and impedance tube measurements for the samples though some of the theoretical resonance peak values are higher or smaller than the experimental values.

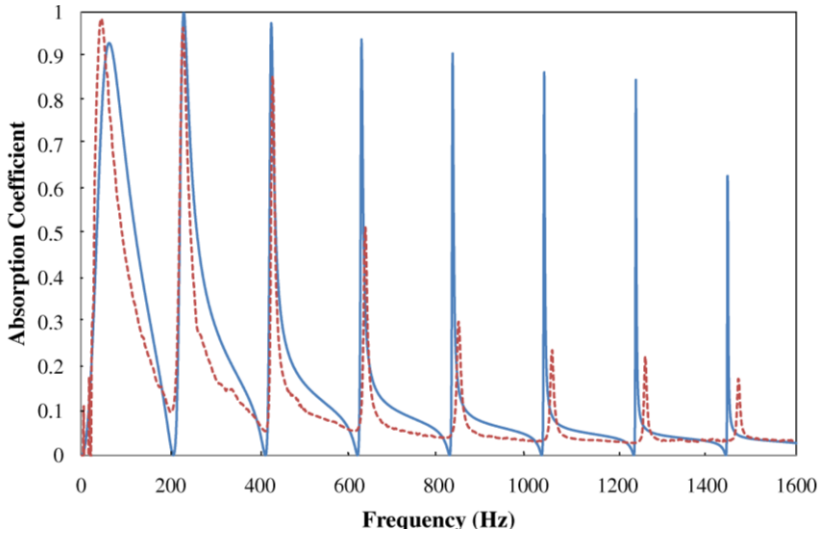

Figure 4-11: Comparison of the theoretical and experimental absorption coefficient of the thick perforated sheet backed behind with a 0.8m air cavity (D=0.8m); ——— , theory; – – – ,experiment.

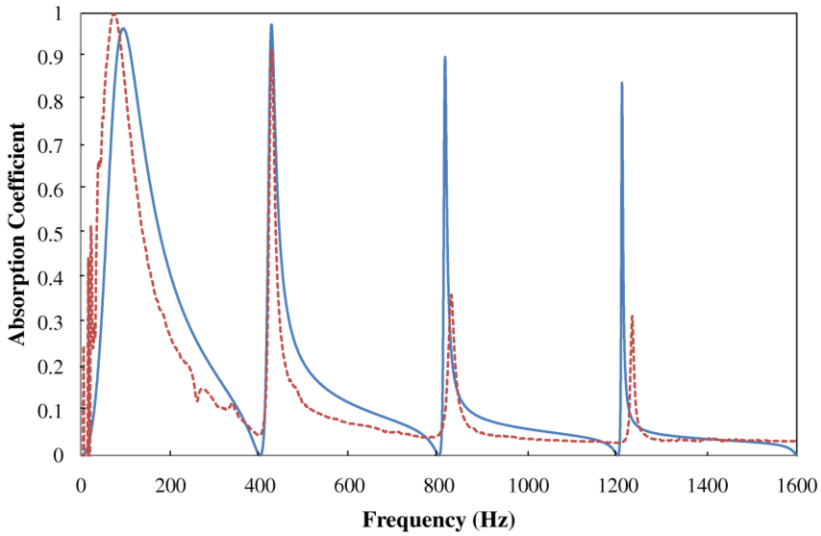

Figure 4-12: Comparison of the theoretical and experimental absorption coefficient of the thick perforated sheet backed behind with a 0.4m air cavity (D=0.4m); ——— , theory; – – – ,experiment.

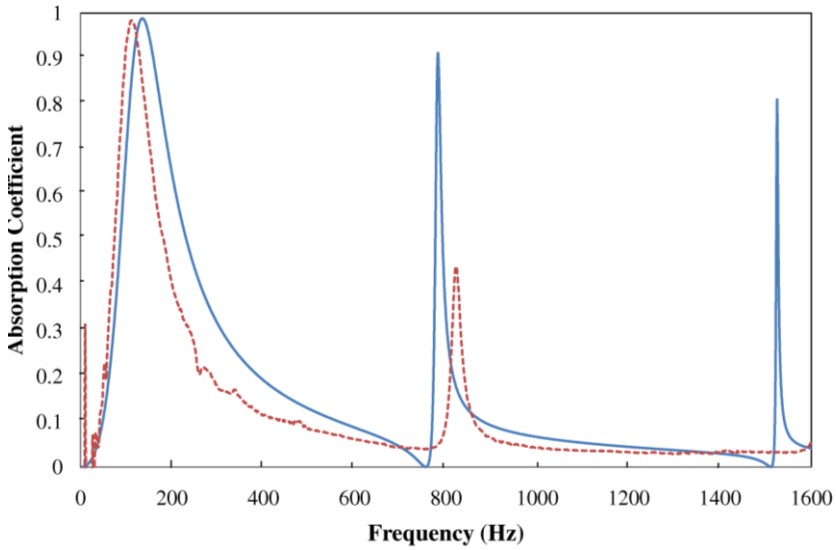

Figure 4-13: Comparison of the theoretical and experimental absorption coefficient of the thick perforated sheet backed behind with a 0.2m air cavity (D=0.2m); ——— , theory; – – – ,experiment.

Figure 4-14 shows the comparison of the absorption coefficient of the 13mm thick perforated sheet, the cloth membrane and the plastic membrane used in the previous chapter (Chapter 3 – Figure 3-5(a)) in an impedance tube test. It can be seen that the 13mm thick perforated sheet achieved the best absorption performance at lower frequencies of around 40–70Hz. The cloth membrane and plastic membrane work best at about 70–110Hz and 160–190Hz respectively.

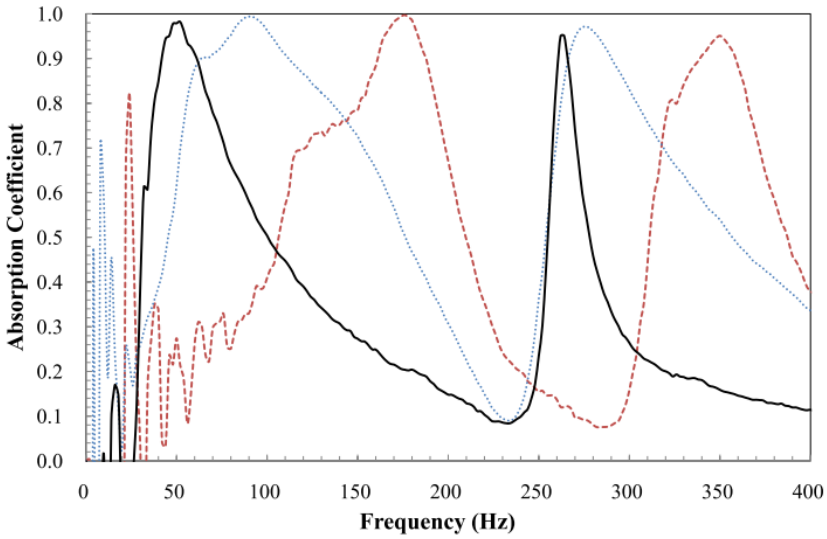

Figure 4-14: Comparison of the absorption coefficient of different resonant absorber backed behind with a 0.7m air cavity (D=0.7m); ——, 13mm thick perforated sheet; ·····, cloth membrane; – – –, plastic membrane.

4.5 Prediction of the absorption performance of the two-layered absorber system by the absorption coefficient theory

This section is an attempt to investigate the absorption performance of the double layer system (One layer of cloth membrane and one layer of 13mm thick perforated sheet backed behind by an air cavity) using the absorption coefficient theory developed in Chapter 3 in Section 3.3 – Equation (3.6) and Equation (3.7). The cloth membrane is assumed to be the top layer while the perforated sheet is the middle layer (Figure 4-15). Two parameters are investigated: the air cavity distance behind the perforated sheet (D_2) and the distance between the cloth membrane and the thick

perforated sheet (D_1). Figure 4-16 and 4-17 show that with fixed cloth membrane to thick perforated sheet distance (D_1=0.04m), increasing the air cavity behind the thick perforated sheet allows the first resonance to shift to lower frequencies. The graph for the double layer system with a 0.8m air cavity behind the perforated sheet indicate that it performs best at around 50Hz with absorption coefficient of nearly 0.96.

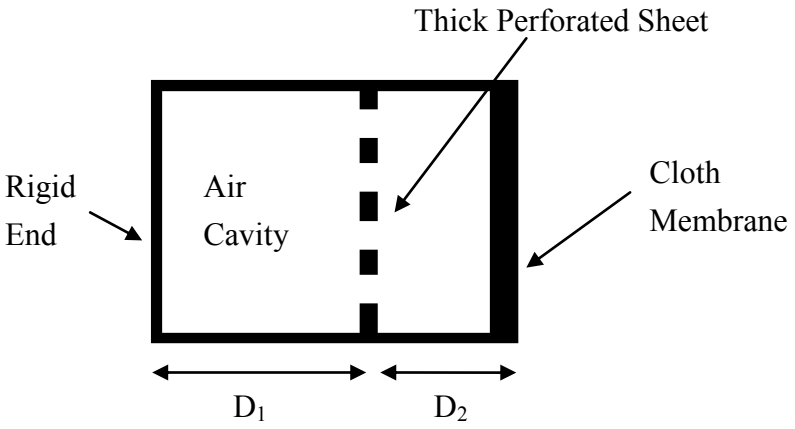

Figure 4-15: Configuration of the double layer system

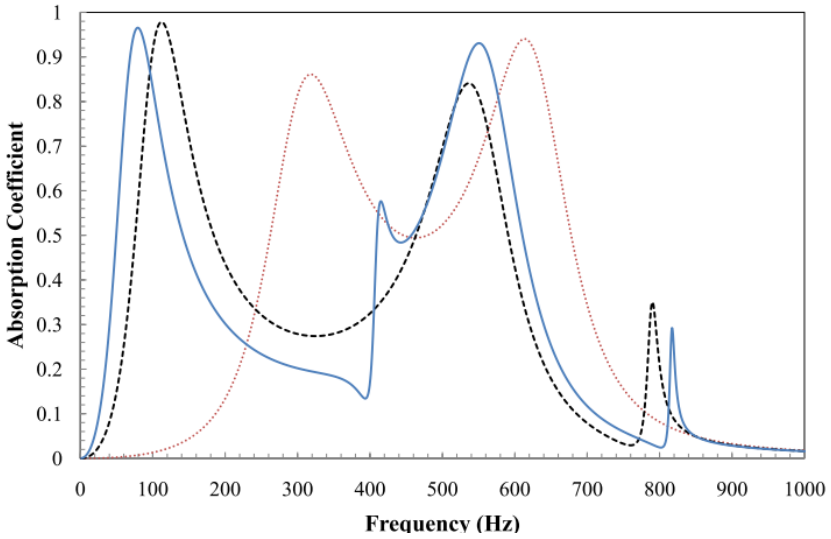

Figure 4-16: The absorption coefficient of the double layer system with D_1=0.04m; ——, D_2=0.4m; – – –, D_2=0.2m; ····· , D_2=0.05m.

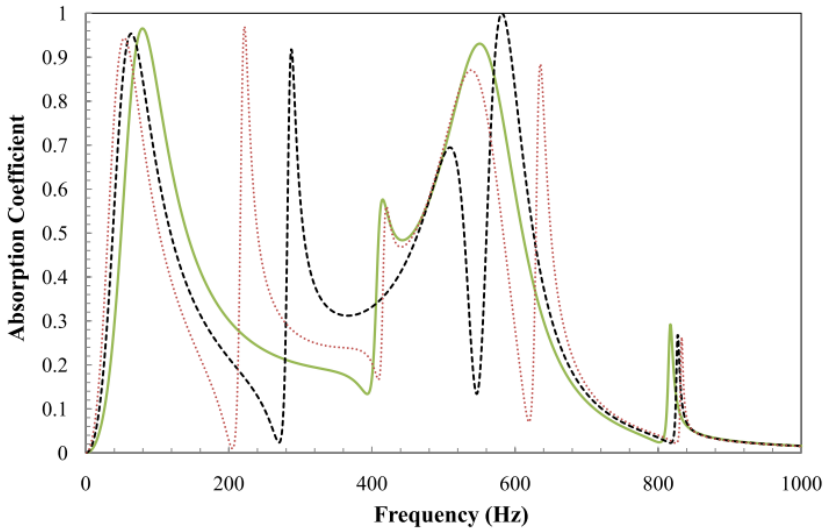

Figure 4-17: The absorption coefficient of the double layer system with D_1= 0.04m; ····· , D_2=0.8m; – – –, D_2=0.6m; ——, D_2=0.4m.

Figure 4-18 and 4-19 show that for the double layer system with a fixed air cavity behind the thick perforated sheet (D_2=0.8m), increasing the inner cavity distance between the cloth membrane and thick perforated sheet (D_1) helps to obtain better absorption in lower frequencies. However, too large the inner cavity causes adverse effect on the absorption coefficient as that shown in the case with 0.06m inner air cavity which has only about 0.05 absorption coefficient.

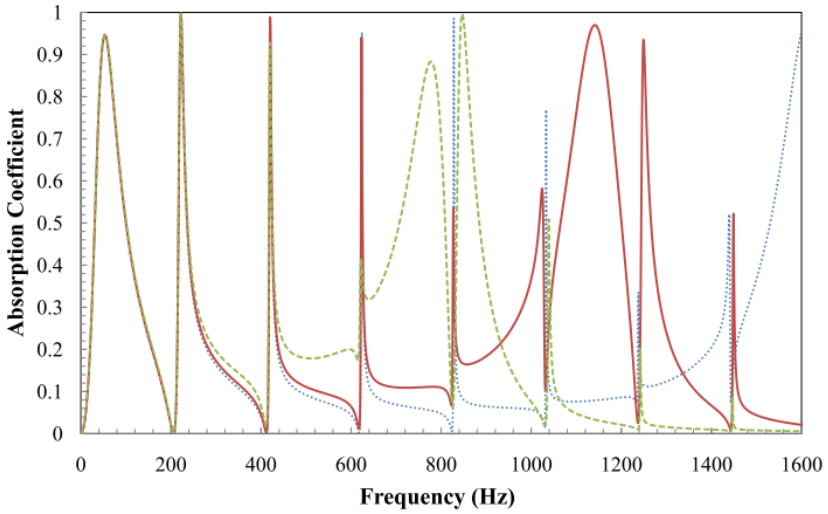

Figure 4-18: The absorption coefficient of the double layer system with D_2=0.8m; – – –, D_1=0.02m; ——, D_1=0.01m; ·····, D_1=0.005m.

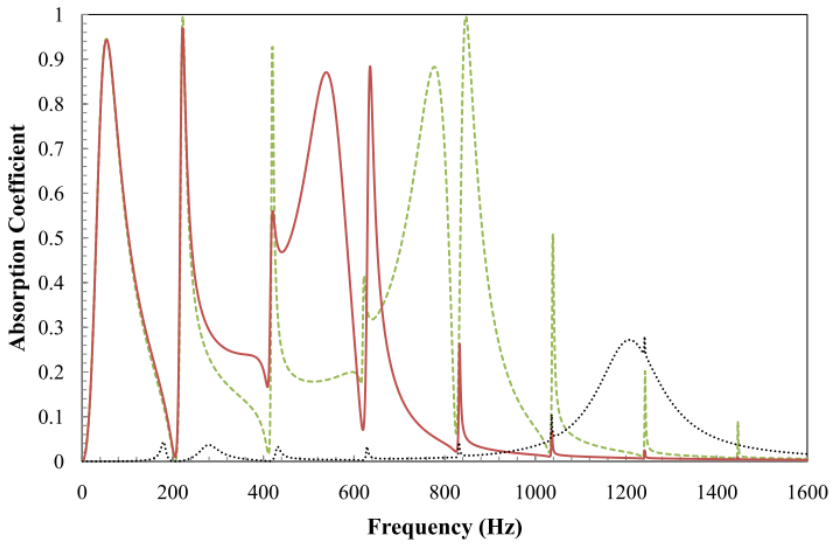

Figure 4-19: The absorption coefficient of the double layer system with D_2=0.8m; ····· , D_1=0.06m; ——, D_1=0.04m; - - - , D_1=0.02m.

4.6 Summary

As proved in the above experiments with a larger air cavity backed behind membrane or perforated sheet achieves lower frequency sound reduction. Cloth membrane backed with a 0.7m air achieve resonance from 70Hz to 110Hz while the thick perforated plate with the same air cavity obtains resonance from about 40Hz to 70Hz. Using both cloth membrane and thick perforated plate with suitable D_1 and D_2 can improve the sound absorption bandwidth. Having the air cavity of 0.8m backed behind the thick perforated sheet (D_2=0.8m) and a cavity of 0.04m between the cloth membrane and thick perforated sheet (D_1=0.04m), the first resonance of 50Hz can be achieved with absorption coefficient of nearly 1.

The low frequency sound absorption problem can be solved using a resonant absorber, such as the cloth membrane design, the thick perforated sheet design or a design of combining both a cloth membrane and a perforated sheet backed with an appropriate air cavity.

CHAPTER 5

THE CONTROL OF HELMHOLTZ RESONANCE AND STANDING WAVE IN A DUCT

5.1 Introduction

Porous absorbent has been used for sound absorption for a long time. The effect of porous absorbent depends on where it is placed. Ideally, it should be placed where the particle velocity is a maximum. Porous absorption works primarily by viscous losses as sound penetrates the small pores. For this to be maximized, the air motion must be at its greatest where the particle velocity is largest.

Low to mid-frequency absorption is difficult to achieve with porous absorbers because of the thick and large size of the material and porous absorbers placing at room boundaries are inefficient as the particle velocity is low. Luckily, using the phenomenon of resonance can help to gain absorption at low to mid-frequency. For many resonant absorbers, placing the device at the boundaries will improve their effectiveness. Resonant absorbers are commonly employed to treat low frequency room modes and as parts of silencers within ventilation systems.

In this chapter, a design combining the concept of Helmholtz mechanism and membrane absorber was investigated for sound reduction which can be applied in

small to medium rooms for noise reduction. The cloth membrane and the perforated sheet were placed at one end of the testing duct. Theoretical and experimental measurements were compared. The Helmholtz mechanism in this chapter was presented by the air pumping in and out of the small tube connecting the loudspeaker and the testing duct. The cloth membrane in Chapter 4 which have been proved to have reasonable low frequency absorption performance was used as the membrane absorber in this chapter.

5.2 Literature review

The holes in perforated plate act as Helmholtz mechanism are narrow enough to have significant viscous and thermal losses together with additional resonances created where absorption can be high(Cox and Antonio, 2004). Membrane absorber is a sheet of material which vibrates as a spring system. A membrane absorber converts the high sound pressure fluctuations typically found at wall surfaces and in corners into selective absorption in the modal frequency range.

5.3 Sound pressure level measurements inside a duct system with a rigid end

5.3.1 Prediction of the standing wave and Helmholtz resonances by experiments using a signal generator

An experiment (Figure 5-1) was carried out to demonstrate the theory for both standing wave and Helmholtz resonances. The testing duct was 2.8m long with the inner dimensions of 10.5 x 10.5 cm^2. The duct was filled with foam particles with one rigid end while the other end had a 0.09m long circular tube of 5cm diameter connecting to the loudspeaker (Figure 5-2). Microphones were placed inside the circular tube and at the rigid end of the testing duct respectively.

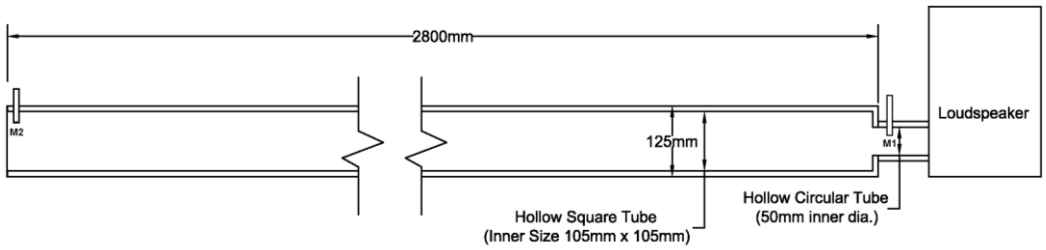

Figure 5-1: Configuration of the testing duct system

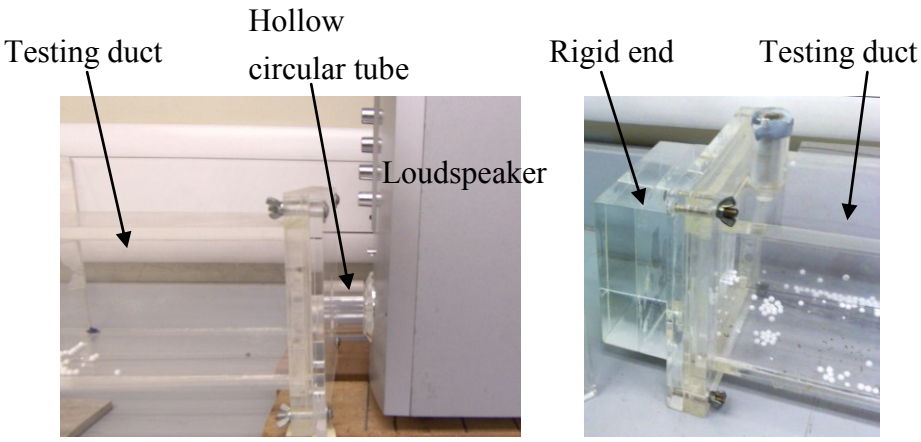

Figure 5-2: (a) Hollow circular tube collecting the testing duct to the loudspeaker; (b) rigid end of the testing duct

Foam particles vibrate with different amplitudes at different positions subjecting to different sound pressures. The standing waves in the testing duct appeared as the nodes and antinodes. When the sound pressure is minimal, the foam particles vibrate most vigorously; the least vibration of the foam particles, the higher is the sound pressure level. By adjusting the frequency and observing the particles vibrating pattern, the standing wave resonances can be found.

Helmholtz resonance is the phenomenon of air resonance in a cavity. When air is forced into a cavity, the pressure inside it increases. Once the external force that forces the air into the cavity disappears, the higher-pressure air inside will flow out. However, this surge of air flowing out will tend to over-compensate, due to the

inertia of the air in the neck, and the cavity will be left at a pressure slightly lower than the outside, causing air to be drawn back in. This process repeats with the magnitude of the pressure changes decreasing each time. The air cavity then acts like a piston pushing fro and back. The experimental Helmholtz resonance can be found by the frequency adjustment and observing the particles moving like pistons in and out of the 0.09m long small tube connecting the testing duct and the loudspeaker.

The formula for calculating the Helmholtz resonance (Figure 5-5) is $fr = \frac{c}{2\pi}\sqrt{\frac{S}{VL}}$, where L and S are the length (m) and the cross-sectional area (m^2) of the small connecting tube respectively, V is the volume of the testing duct (m^3) and c is velocity of sound (m/s).

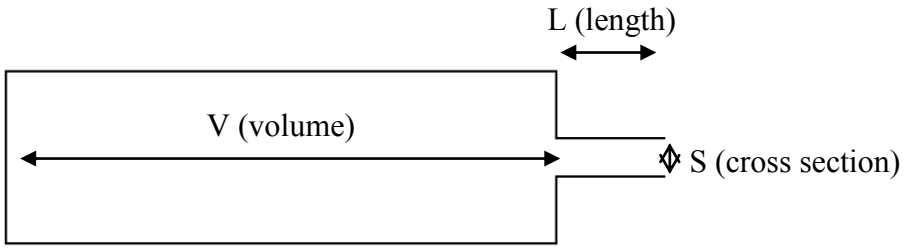

Figure 5-5: Parameters of the Helmholtz resonance theory

For the theoretical Helmholtz resonance,

L= 0.09 m, S= $0.025^2\pi$ m^2 and V= 0.105^2 x 2.8 m^3

$$fr = \frac{c}{2\pi}\sqrt{\frac{S}{VL}} = \frac{340}{2\pi}\sqrt{\frac{0.025^2\pi}{0.105^2 * 2.8 * 0.09}} = 45.5Hz$$

Table 5-1 below shows the comparison of the standing wave resonances found by theory calculation and experiments. It is found that both results are well-matched except for the case of the first standing wave resonance. A possible explanation for the difference in results is that there is the formation of the Helmholtz resonance combining with the first standing wave.

At frequency 45Hz, it can be seen that the foam bubbles pumping in and out of the small circular tube violently which implies 45Hz is the pure Helmholtz resonance of the small circular tube (Figure 5-6). This result also matches with the above calculated Helmholtz resonance. At frequency 85Hz, there is a half standing wave formed by the foam bubbles and at the same time foam bubbles pump in and out of the small circular tube at a smaller magnitude (Figure 5-7). The air cavity inside the connecting tube produces less Helmholtz effect which can still slightly reduce the effective length for the standing wave formation. Thus the first experimental standing wave resonant frequency 85Hz differs from the first theoretical standing wave resonant frequency of 61Hz. Another reason for the difference is the personal error in observing the Helmholtz piston effect and the standing wave effect while adjusting the signal generator.

Helmholtz effect decreases with increasing frequency. At frequency 125Hz, foam bubbles formed one complete standing wave (Figure 5-8). The minor Helmholtz effect has only negligible effect on the standing wave motion. Thus both theoretical and experimental results match well.

Standing wave resonant frequencies (Hz)		
	Calculation by resonant peaks theory	Experimental results
f1	61	45,85
f2	122	125
f3	183	185

Table 5-1: Comparison of calculated and experimental standing wave resonances

Figure 5-6: Helmholtz effect inside the testing duct for the frequency of 45Hz

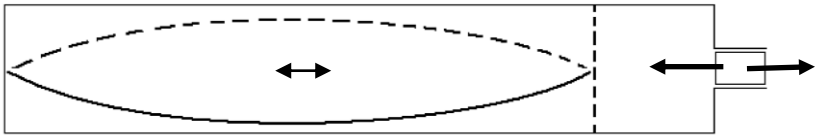

Figure 5-7: Helmholtz effect combining with the standing wave resonance for the frequency of 85Hz

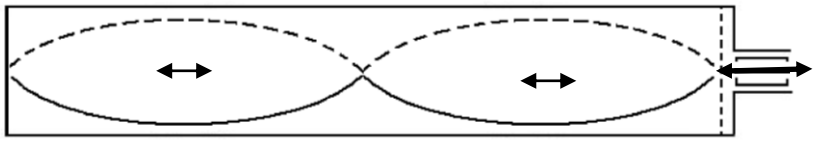

Figure 5-8: Standing wave for the frequency of 125Hz

5.3.2 Calculation of the sound pressure level in a duct system with a rigid end

The resonant properties of the duct system are investigated in this part. The testing duct is driven by a loudspeaker which applies force onto the duct system. The loudspeaker has its own impedance so both the mechanical behavior of the loudspeaker and that of the duct should be considered when calculating the resonances of the duct system. The loudspeaker gives out sound and causes the air inside the connecting tube moving like a piston. The air piston acts like a damped, harmonic oscillator. Figure 5-9 below demonstrates the driver-duct system where loudspeaker is the driver and provides force (F) to the air piston inside the small connecting tube of mass m. s is the spring constant of the driver and R is the damping constant of the driver where $R = 2\zeta\omega m$ with ζ as the damping coefficient of the driver.

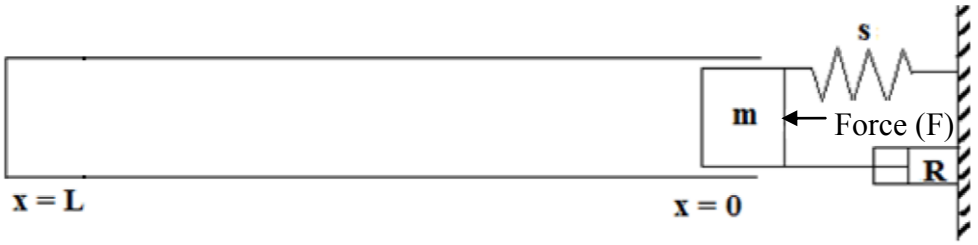

Figure 5-9: Schematic representation of a driver-duct system

Input mechanical impedance of the duct (Z_{m0})

$$Z_{m0} = S\rho c \frac{\alpha L - jCos\,kL\,Sin kL}{Sin^2 kL + (\alpha L)^2 Cos^2 kL},$$

Input mechanical impedance of the driver (Z_{md})

$$Z_{md} = 2\xi\omega m + \left(\omega m - \frac{S\rho cs}{\omega}\right) j,$$

where

S is the cross-sectional area of the testing duct (m^2)

ρ is the density of air (kg/m^3)

c is the sound velocity in air (m/s)

k is the wave number, $k=\omega/c$

L is the length of the testing duct (m)

α is the absorption coefficient in the air, $\alpha = \frac{2.78x10^{-5}\sqrt{f}}{a}$

a is the radius of the testing duct (m)

s is the spring constant (Take s = 324)

The input mechanical impedance Z_m of the system is the series combination of Z_{m0} and Z_{md} and can be written as: $Z_m = Z_{m0} + Z_{md}$. Therefore,

$$Z_m = \frac{S\rho c\alpha L}{Sin^2 kL + (\alpha L)^2 Cos^2 kL} + 2\xi m\omega + \left(\omega m - \frac{S\rho cs}{\omega} - \frac{S\rho c\, CoskL\, SinkL}{Sin^2 kL + (\alpha L)^2 Cos^2 kL}\right) j \tag{5-1}$$

The pressure amplitude *P (L)* at the rigid end is,

$$P(L) = \rho c \frac{F}{Z_m} \frac{1}{\sqrt{Sin^2 kL + (\alpha L)^2 Cos^2 kL}} \tag{5-2}$$

Assume that the driven duct has a rigid termination at x = L, the frequencies of mechanical resonance can be found by putting the imaginary part of Equation (5-1) to be zero, and we have:

$$\omega m - \frac{s}{\omega} - \frac{S\rho c\, CoskL\, SinkL}{Sin^2 kL + (\alpha L)^2 Cos^2 kL} = 0$$

$$\omega m - \frac{s}{\omega} = \frac{S\rho c\, CoskL\, SinkL}{Sin^2 kL + (\alpha L)^2 Cos^2 kL} \tag{5-3}$$

Plotting both sides of Equation (5-3) against frequency on the same set of axes, the intersection points are the resonances of the duct system. As is shown in Figure 5-10, the resonances are approximately at 41Hz, 87Hz, 137Hz and 191Hz.

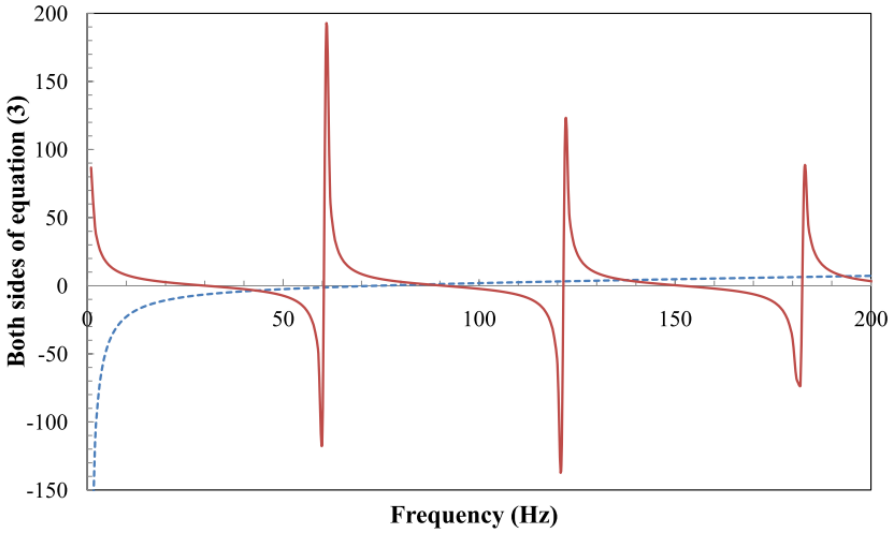

Figure 5-10: Graphical solution of Equation (5-3) for the resonances of the driver-duct system rigidly terminated at x=L; - - -, reactance of the mechanical impedance of the driver; ——, reactance of the mechanical impedance of the duct.

It can be seen from Figure 5-11 that the theoretical and experimental sound pressure levels at the rigid end of the testing duct are nearly identical. Reasonable agreement between measurements and theoretical prediction is achieved. The result has confirmed the validity of the theory for calculating the sound pressure level at the rigid end of a duct.

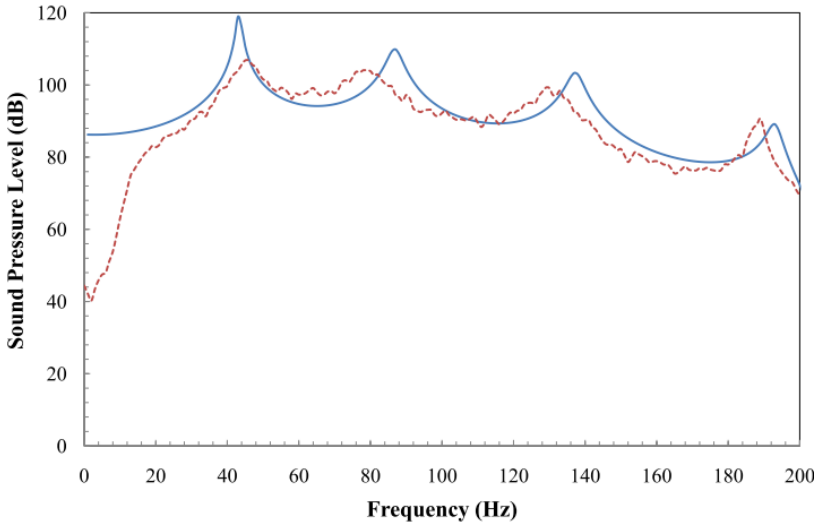

Figure 5-11: Comparison of the theoretical and experimental sound pressure level at the rigid end of the testing duct; ——, theory; – – –, experiment.

5.4 Sound pressure level measurements inside a duct system ended with a cloth membrane backed with an air cavity

5.4.1 Experimental measurements inside a duct system

The experimental configuration is the same as that in Figure 5-1 but with the cloth membrane (See Figure 4-1) at the end backed with an air cavity instead of a rigid end. The side views of different duct end conditions are shown in Figure 5-12 and the mounting condition of the cloth membrane at the end of the duct system is shown in Figure 5-13. According to Figure 5-14, the overall sound pressure level measured at the end of the duct (M2) using a cloth membrane end with a 0.7m air cavity backed has a relatively lower value than that with a rigid end. The resonant

peak is different for different end conditions. The duct with a rigid end has a resonance at about 110Hz. For the duct with the cloth membrane end with a 0.7m air cavity backed, it has resonance at 90Hz where the measured M2 value is about 20dB lower than that of the rigid end condition.

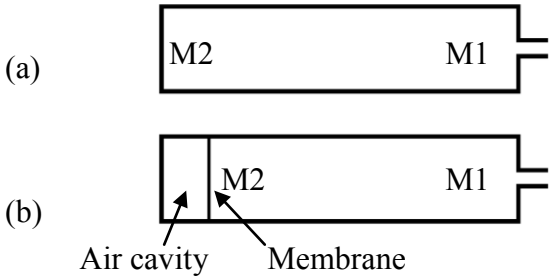

Figure 5-12: Side view of the duct system with different end conditions; (a) rigid end; (b) cloth membrane end backed with an air cavity

(a)

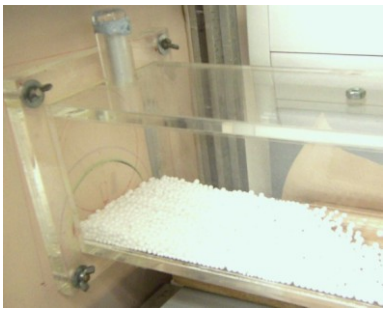

(b)

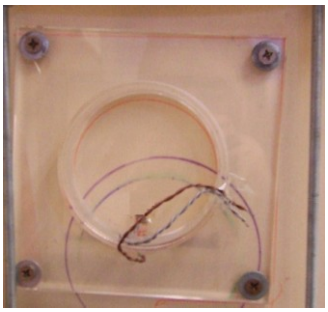

Figure 5-13: (a) Duct system ended with a cloth membrane; (b) the back of the cloth membrane which is connected to the impedance tube

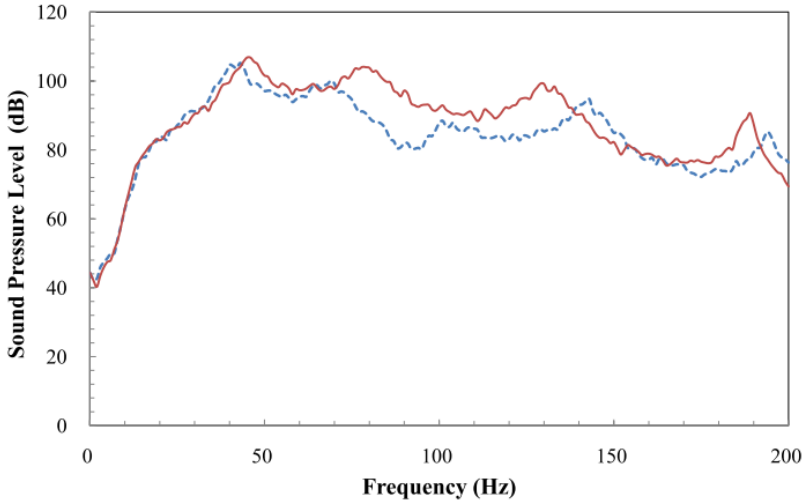

Figure 5-14: Sound pressure level measurements at M2 with different end conditions;——, rigid end;– – –,cloth membrane end backed with an air cavity.

The resonances for the duct with different end conditions can be observed clearly from Figure 5-15. Figure 5-15 reveals that the duct with the cloth membrane end backed with a 0.7m air cavity achieves comparatively greater sound reduction bandwidth (M2-M1) than that with a rigid end. The most significant sound reduction appears in the frequency range from 70 to 140Hz with about 5dB higher than that of the duct with a rigid end. The measured sound pressure level at M1 and M2 for the testing duct with membrane end backed with a 0.7m air cavity is shown in Figure 5-16. The sound pressure level measured at M2 is about 10dB less than that at M1 from 70Hz to 170Hz. For the testing duct with a rigid end, the bandwidth is smaller

and the measured values (M1 and M2) are closer to each others as compared to that with membrane end backed with a 0.7m air cavity (Figure 5-17).

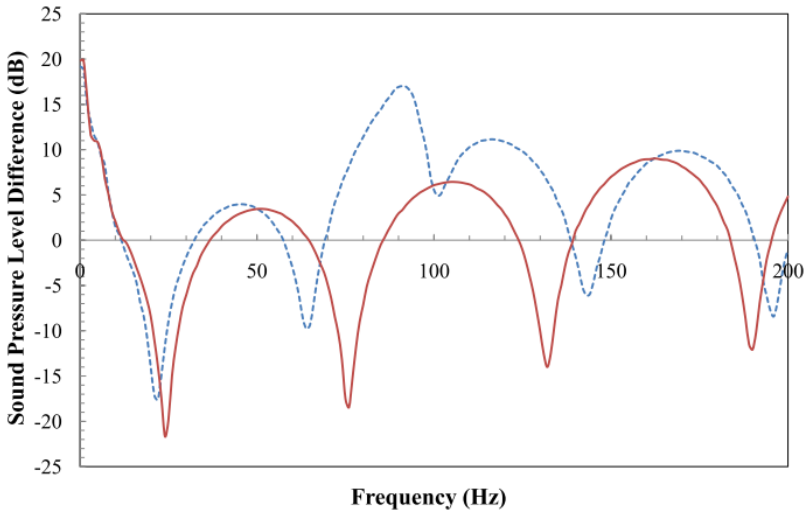

Figure 5-15: Sound pressure level difference (M1-M2) with different end conditions; ——, rigid end; - - -,cloth membrane end backed with an air cavity.

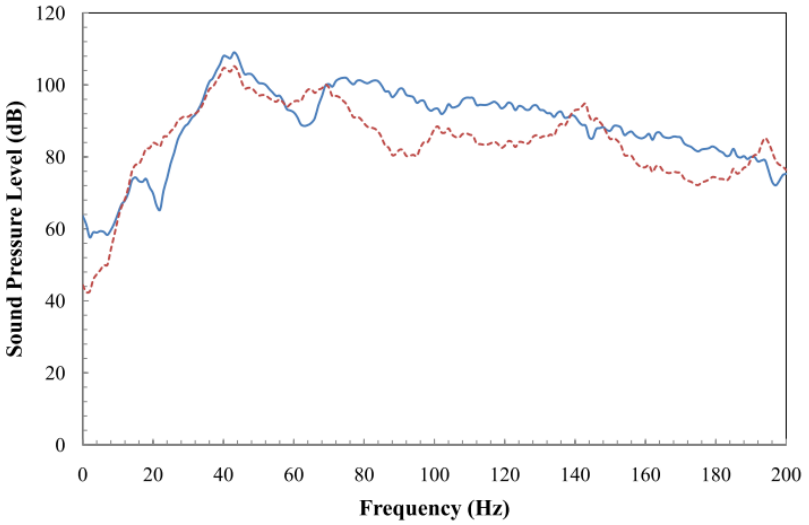

Figure 5-16: Sound pressure level measurements of the duct system with the cloth membrane end backed with a 0.7m air cavity; ——, M1; - - - ,M2.

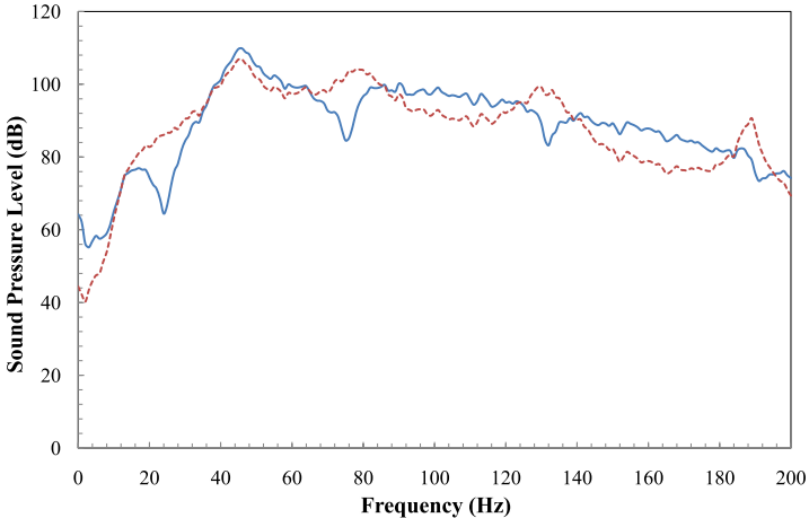

Figure 5-17: Sound pressure level measurements for the duct system with a rigid end; ——, M1; – – –,M2.

Figure 5-18 indicates that the sound pressure level measured at the duct end (M2) will be lower when the cloth membrane is cavity backed. When the air cavity increases, the resonance shifts towards the lower frequencies. It can be seen that when the air cavity is 0.7m, the resonance is around 80–100Hz, while that for 0.5m and 0.2m air cavity are 120-140Hz and 180-195Hz respectively.

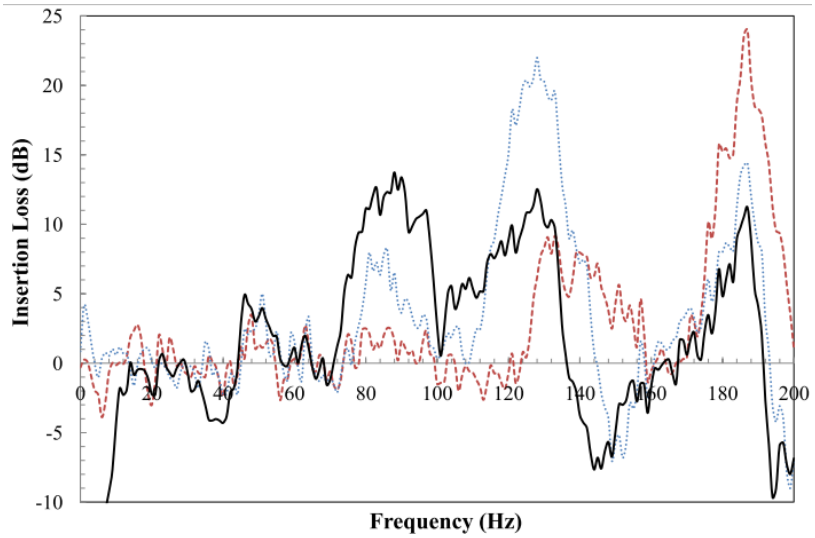

Figure 5-18: Comparison of the insertion loss (M2) of the duct system with the cloth membrane end using different air cavities by the difference of the M2 value from that with no air cavity backed behind; ——, 0.7m air cavity; ·····, 0.5m air cavity; – – –, 0.2m air cavity.

5.4.2 Calculation of the sound pressure level inside the duct system with membrane end backed with an air cavity

Figure 5-19 below demonstrates the driver-duct system with loudspeaker as the driver which is similar to that in section 5.3.2 - Figure 5-9. The rigid end is changed to a membrane end backed with an air cavity in this system.

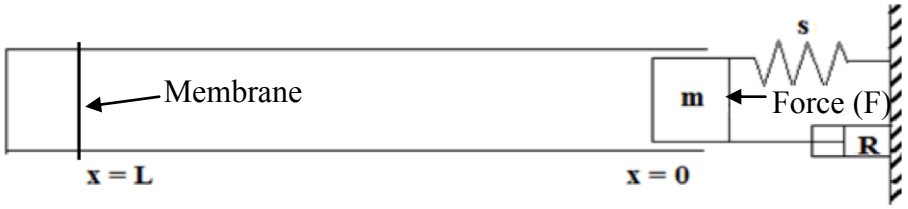

Figure 5-19: Schematic representation of a driver-duct system with a membrane end backed by an air cavity

The normal specific acoustic impedance of the membrane normalized by ρc (Z_M) can be calculated by Equation (3-1) and the normal specific acoustic impedance of the air behind the membrane, again normalized by ρc (Z_D) can be calculated by Equation (3-3). For the overall normal specific acoustic impedance of the membrane backed with an air cavity (Z), Equation (3-4) should be used.

Input mechanical impedance of the duct (Z_{s0})

$$Z_{s0} = S\rho c \frac{Z Cos kL + j Sin kL}{j Z Sin kL + Cos kL} \tag{5-4}$$

Input mechanical impedance of the driver (Z_{md})

$$Z_{md} = 2\xi\omega m + \left(\omega m - \frac{S\rho cs}{\omega}\right) j\,, \tag{5-5}$$

where

S is the cross-sectional area of the testing duct (m^2)

ρ is the density of air (kg/m^3)

c is the sound velocity in air (m/s)

L is the length of the testing duct (m)

The input mechanical impedance Z_m of the system is the series combination of Z_{s0} and Z_{md} where $Z_m = Z_{s0} + Z_{md}$. Therefore, we have

$$Z_m = 2\xi m\omega + Z_{s0} + \left(\omega m - \frac{S\rho cs}{\omega}\right) j \tag{5-6}$$

The pressure amplitude *P(L)* at the membrane end backed with an air cavity is,

$$P(L) = \rho c \frac{F}{|Z_m| \left| j\,SinkL + \frac{CoskL}{Z} \right|} \tag{5-7}$$

To prove the accuracy of the above equation for pressure amplitude calculation, the equation is first applied to the case with a rigid end by putting the overall normal specific acoustic impedance of the membrane backed with an air cavity to be infinitely large, i.e. Z = ∞ at X = L. The comparison of the theoretical and experimental sound pressure level at the rigid end is shown is Figure 5-20. The two curves are very similar with the theoretical peak values are slightly lower than that of the experiment. The overall theoretical result is satisfactory.

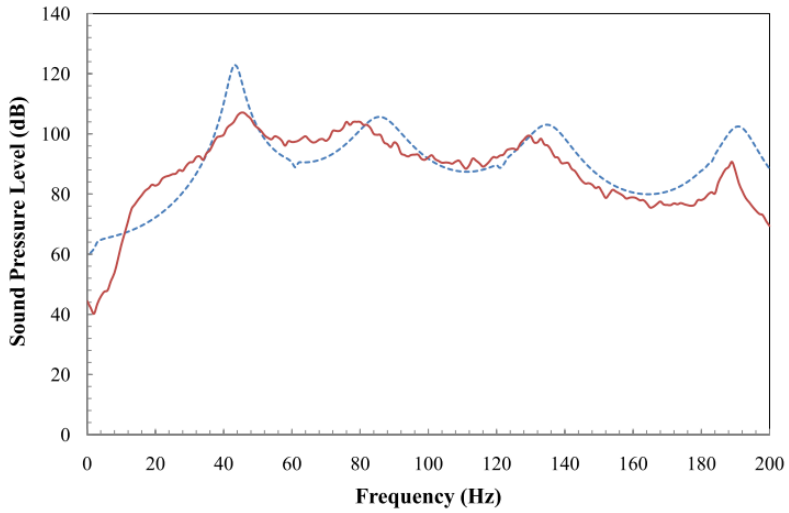

Figure 5-20: Comparison of the theoretical and experimental sound pressure level at the rigid end; – – –, theory; ——,experiment.

The theoretical pressure amplitude *P(L)* at the membrane end backed with an air cavity is calculated. Unfortunately, the above formulations for membrane absorbers are not totally accurate. The curves for experimental and theoretical results shown in Figure 5-21 have similar shapes. Both reach peaks at 35Hz, 65Hz, 105Hz, 150Hz and 195Hz and fell to their lowest points at 80Hz and 170Hz. However, the crest and trough values are slightly different from each other. The membrane system is not as simple as the perforated absorber to model. The mass of the membrane is being treated as a single lump mass, and therefore, the membrane should move as one like a piston. Problems can occur if the membrane is small, because the whole mass may not be able to vibrate freely because it must be secured at the edges. In this case, the actual vibrating mass may be less than expected, and additional losses at the fixings may occur. One solution is to attach the edges of the membrane using resilient foam so that the whole membrane can vibrate including the edges. If such a fixing is used, it is important that the cavity remains air tight.

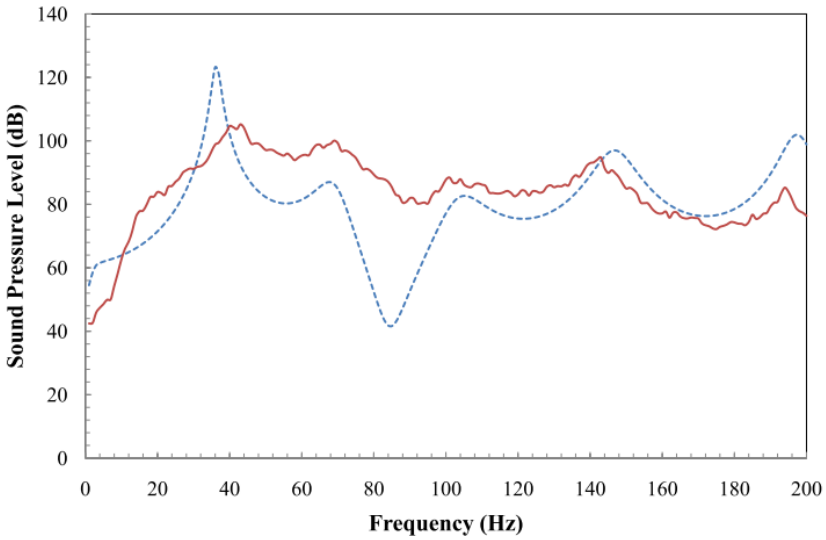

Figure 5-21: Comparison of the theoretical and experimental sound pressure level at the membrane end with a 0.7m air cavity backed ; - - - - , theory; ——,experiment.

An attempt was made to predict the sound absorption performance of the duct ended with a membrane by the finite element analysis (Appendix III). Due to the uncertainties of the boundary conditions of the air-block duct, the results were not satisfactory.

5.5 Sound pressure level measurements inside a duct system ended with two layers backed with an air cavity

5.5.1 Experimental measurements inside an duct system ended with the 13mm thick perforated sheet backed with an air cavity

The configuration of experiment is the same as in Figure 5-1 with the 13mm thick perforated sheet (See Figure 4-8) backed with an air cavity instead of the rigid end. The side view of the duct system can be seen in Figure 5-22. Figure 5-23 shows that for the cases having different air cavities behind the thick perforated sheet (*D*), all have the first resonance at nearly 45Hz. The system with a 0.8m air cavity obtains the greatest bandwidth noise reduction with the frequency range of 40–70Hz. For other cases such as 0.4m and 0.2m air cavity, the bandwidths are about 40–52Hz and 48–55Hz respectively. It can be seen from Figure 5-24, Figure 5-25 and 5-26 that the measured sound pressure level at M2 is relatively smaller than that at M1 at the whole frequency of interest (0–200Hz) for the testing duct with perforated sheet having a 0.8m air cavity as compared to that having 0.4m and 0.2m air cavity.

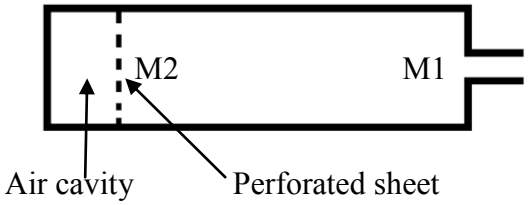

Figure 5-22: Side view of the duct system ended with the thick perforated sheet backed with an air cavity

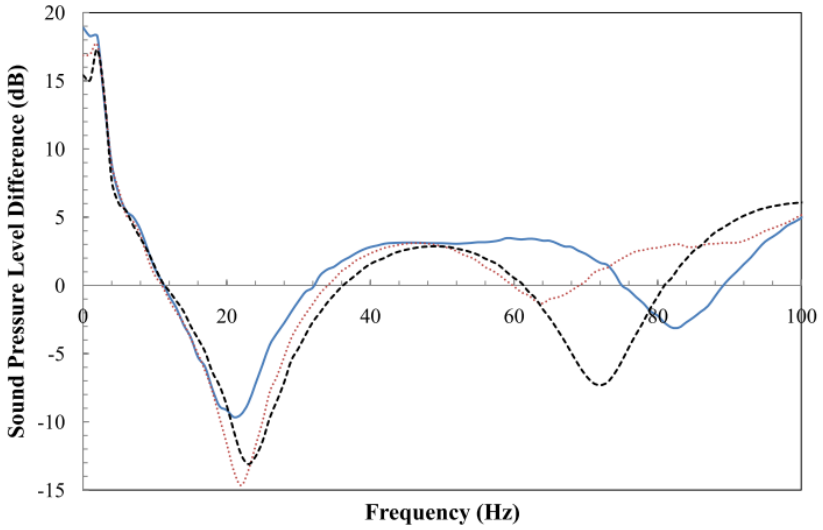

Figure 5-23: Sound pressure level difference (M1-M2) of the duct system ended with the thick perforated sheet backed by different air cavities (*D*); ——, D=0.8m; ·····, D=0.4m; – – –, D=0.2m.

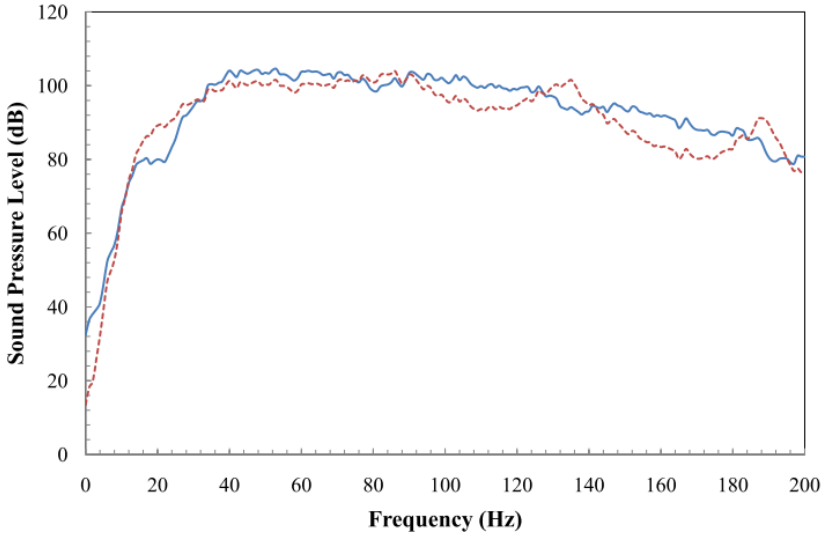

Figure 5-24: Sound pressure level measurements for the duct system ended with the thick perforated sheet backed by a 0.8m air cavity (D=0.8m); ——— ,M1;·····, M2.

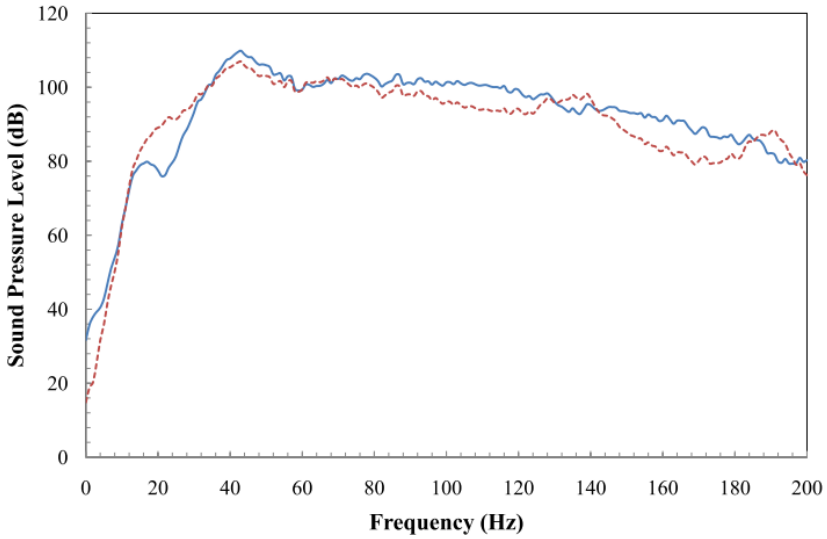

Figure 5-25: Sound pressure level measurements for the duct system ended with the thick perforated sheet backed by a 0.4m air cavity (D=0.4m);——— ,M1;····· , M2.

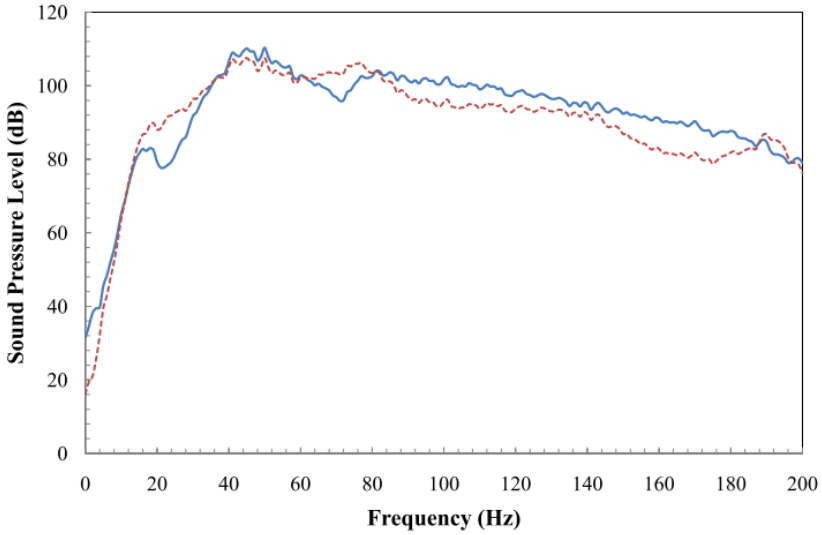

Figure 5-26: Sound pressure level measurements for the duct system ended with the thick perforated sheet backed by a 0.2m air cavity (D=02m); ——,M1;·····, M2.

5.5.2 Experimental measurements inside a duct system with two layers backed with an air cavity (Double layer system)

Sound pressure level difference (M1-M2) of the testing duct with one layer of cloth membrane and one layer of thick perforated sheet at the end was also investigated (same configuration as in Figure 5-1). The side view of the duct system can be seen in Figure 5-27. The cloth membrane was placed in front of the thick perforated sheet. There is an air cavity between the cloth membrane and the thick perforated sheet (D_1) and also behind the thick perforated sheet (D_2) separately. Figure 5-28 shows that a greater bandwidth noise reduction can be achieved when

using a wider air cavity backed behind the thick perforated sheet, keeping the air cavity between the cloth membrane and the thick perforated sheet constant. The first resonance for the case with D_2=0.8m is about 32–74Hz and that for D_2=0.4m and D_2=0.2m are 35–62Hz and 37–60Hz respectively. Figure 5-29, Figure 5-30 and 5-31 show that with greater air cavity behind the thick perforated sheet (D_2) can have lower measured M2 values especially at lower frequency range of 40–70Hz.

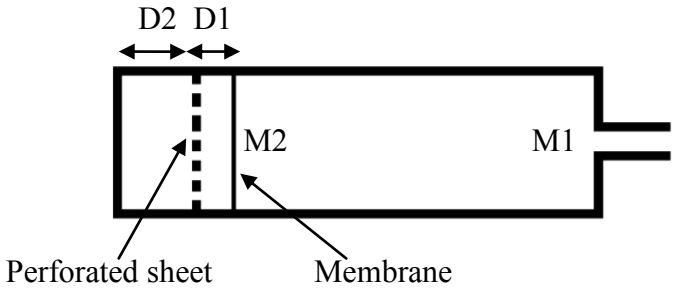

Figure 5-27: Side view of the duct system with the cloth membrane and the thick perforated sheet backed with an air cavity (Double layer system)

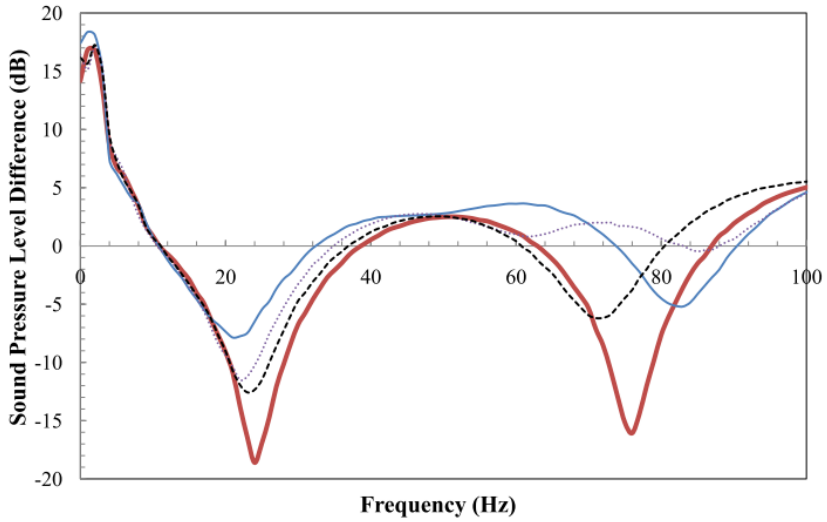

Figure 5-28: Sound pressure level difference (M1-M2) of the double layer system (D_1=0.04m); ——, D_2=0.8m; ····· , D_2=0.4m; – – – , D_2=0.2m; ——, rigid end.

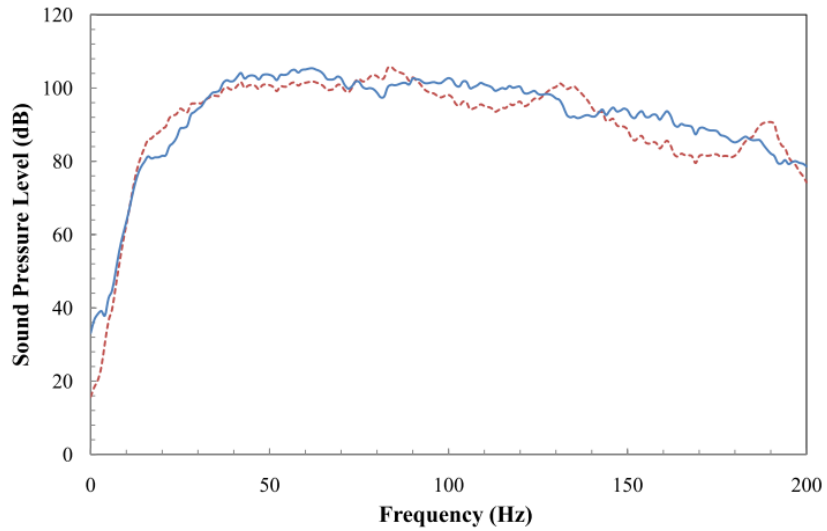

Figure 5-29: Sound pressure level measurements of the double layer system (D_1=0.04m, D_2=0.8m); ——,M1; ····· , M2.

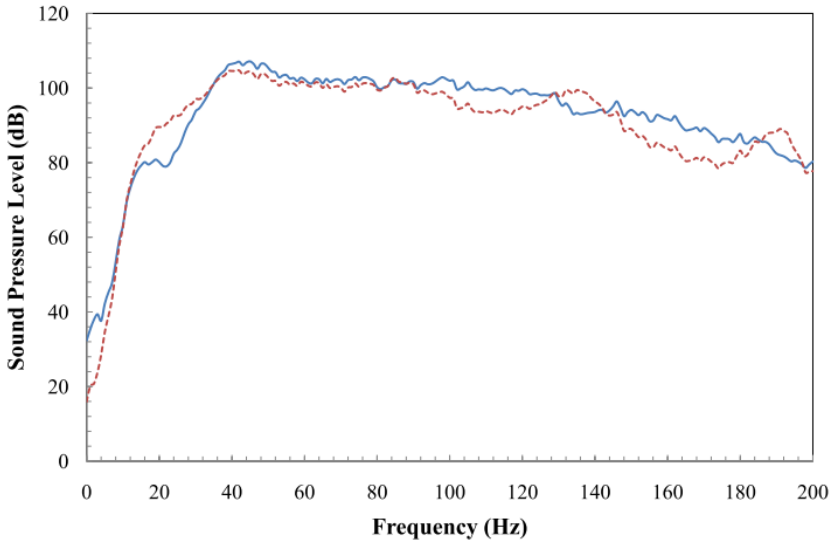

Figure 5-30: Sound pressure level measurements of the double layer system (D_1=0.04m, D_2=0.4m); ——,M1; ·····, M2.

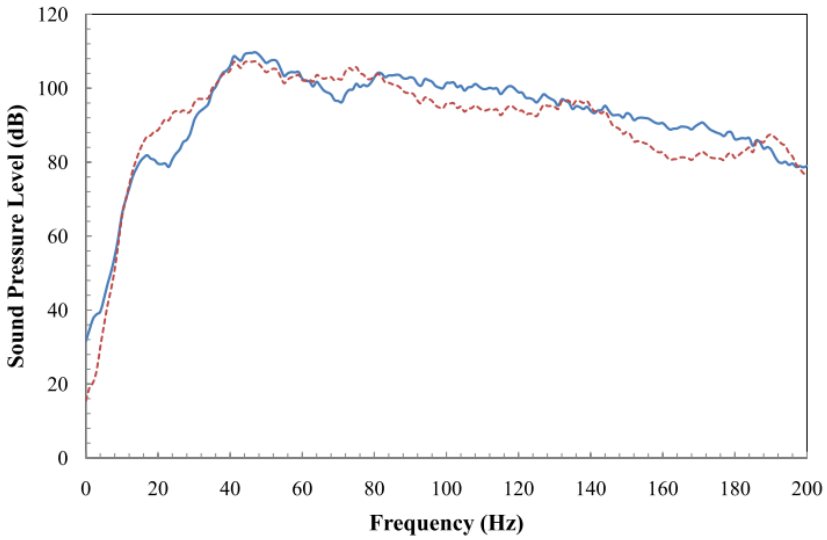

Figure 5-31: Sound pressure level measurements of the double layer system (D_1=0.04m, D_2=0.2m); ——,M1; ·····, M2.

It can be seen from Figure 5-32 that with a fixed cloth membrane to perforated sheet distance (D_1=0.04m), using a greater air cavity backed behind the thick

perforated sheet obtains a greater insertion loss and a broader low frequency bandwidth. For the first resonance in the case of D_2=0.8m, there is more than 5dB insertion loss in the frequency range from 38 to 52Hz, while having insertion loss of above 3dB from 37–60Hz. The sound reduction performance of D_2=0.4m is not as well as the case of D_2=0.8m, it can achieve a 3dB insertion loss in the first resonance in the frequency range from 42 to 60Hz, but it can just have the insertion loss value greater than 5dB at a much narrower bandwidth of about 42–44Hz.

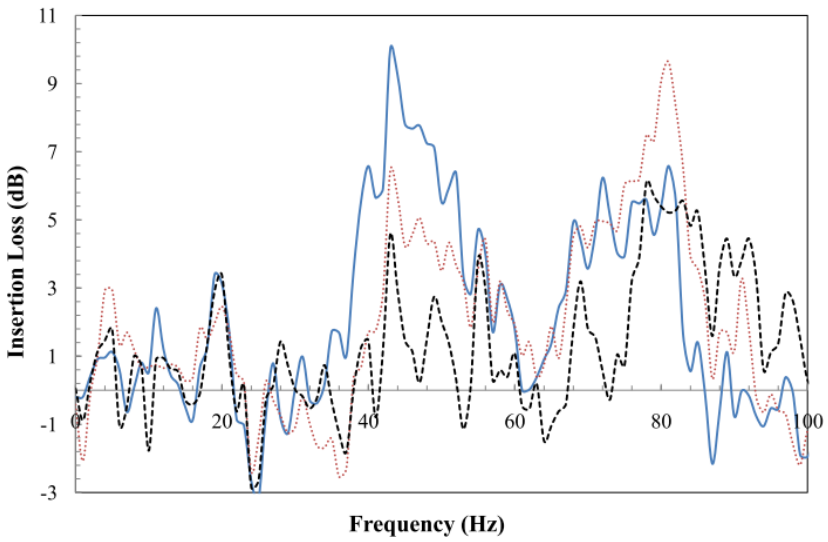

Figure 5-32: The insertion loss of the double layer system (D_1=0.04m); ——— , D_2=0.8m; ····· , D_2=0.4m;– – – , D_2=0.2m.

5.6 Discussion

The testing duct system suggested in this Chapter can be applied to real scale rooms as shown in Figure 5-33. It is shown in Figure 5-33(a) that the room is stimulated by putting n testing ducts together. If each combined-duct has a volume of Vm^3, the volume of the real scale room will be (nV) m^3. Since there will be difficulty in installing multiple small tubes behind the wall, a room of same volume with one big tube instead (Figure 5-33(b)) can also achieve the same performance. If the diameter of each small tube is D m, then the diameter of the big tube should be (nD) m with the same tube length as the small tubes.

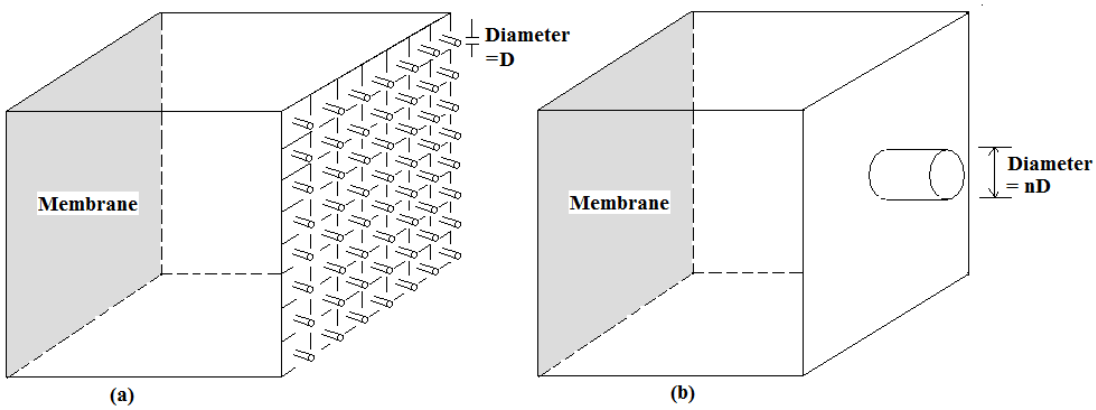

Figure 5-33: (a) Small room consists of n testing duct. (b) Small room with one big duct.

5.7 Summary

There is always limited space in small rooms within which to make acoustic improvements. Porous surface absorption is ineffective at these modal frequencies, because the particle velocity near walls and in corners is essentially zero for these long wavelengths, and also the porous surface would have to be made so deep that significant space within the room would be lost to acoustic treatment. This problem can be solved using a resonant absorber, such as a membrane design combined with Helmholtz resonance at the wall.

To achieve the best sound reduciton in a real scale room, the strategy is to find a membrane having resonant frequency same as the tube Helmholtz resonant frequency. The cloth membrane tested in this chapter has resonant frequency of 60Hz where that for the tube is 43Hz. Better choice of the membrane material or the tube parameters are required.

CHAPTER 6

INFRASOUND INDUCED BY AIRFLOW THROUGH SMALL OPENINGS IN LARGE VENTILATION DUCTS

6.1 Introduction

Internal pressure fluctuations that are induced in rooms through a dominant opening may result from the direct effect of wind turbulence, and/or from Helmholtz resonance. If the Helmholtz resonance frequency of the room lies somewhere in the energy containing region of the freestream turbulence spectrum, and if the damping in the internal pressure system is not high, resonance excitation may take place. Under such circumstances, a significant amplification of internal pressure fluctuations around the Helmholtz resonant frequency can be expected. This tends to produce a higher peak value of internal pressure than the corresponding peak value of external pressure.

The previous chapter reported the control of noise from small ventilation openings. This chapter presents the effect of ventilation openings on rooms with airflow on the infrasound generated in large ventilation spaces. The ventilation space can be a chimney or double skin façade (See Figure 1-1). Infrasound is sound at frequencies less than 20 Hz, which is not audible to the human ear but may annoy

and cause discomfort to exposed persons. As its long waves are able to pass through walls and travel long distances, it may cause annoyance in some neighbourhoods. Infrasound may, therefore, render an environment unacceptable for workers and the residents.

6.2 Literature Review

Infrasound may be rated as harmless at low intensity levels below 120dB; however, at high intensity over 120 dB, it will cause discomfort, mainly nausea due to periodic movement of the stomach and other organs of the body. There is increasing information regarding the adverse effects on the human body caused by exposure to high sound pressure levels of infrasound. The symptoms are summarized as follows: unusual tiredness, concentration difficulties and a feeling of pressure on the head and over the eardrums (Waye et al., 2002); resonant vibrations in some parts of the human body, speech interference and temporary loss of hearing acuity (Adam, 2006); irritation, sleep disturbances and negative social behaviour. The negative influences of infrasound on human health have yet to be fully investigated, but the discomfort caused by infrasound is generally sufficient to call for its reduction to an acceptable level.

The theory of Helmholtz resonance under oblique wind flow was investigated (Sharma and Richards, 2003). Their study showed that Helmholtz resonance under oblique wind flow produces an extremely strong response in internal pressure fluctuations, compared with that obtained under normal onset flow. They verified that "eddy dynamics over the opening" rather than "freestream turbulence" is responsible for the intense excitation at oblique flow angles, which implies that even if the Helmholtz resonant frequency were to be in the tail of the freestream turbulence spectrum, severe excitation would still be possible. However, no study reports on the measurements of infrasound due to air flow.

6.3 Experiments investigating the Helmholtz effect of a top opening in a testing duct

An experiment (Figure 6-1) was carried out to demonstrate the theory for both standing wave and Helmholtz resonance in a real scale size testing duct. The square cross section testing duct was made of concrete. It was 4.4m long with an inner size of 38 x 38cm^2. The duct was used to simulate the effect of a large ventilation space connected to a room through a small opening. Both ends of the duct were rigid and a loudspeaker was installed inside one end of the duct. There was an opening with a

diameter of 105mm on top of the duct that was connected to the room. Two microphones were used for measurements and the positions are shown in Figure 6-1 and Figure 6-2.

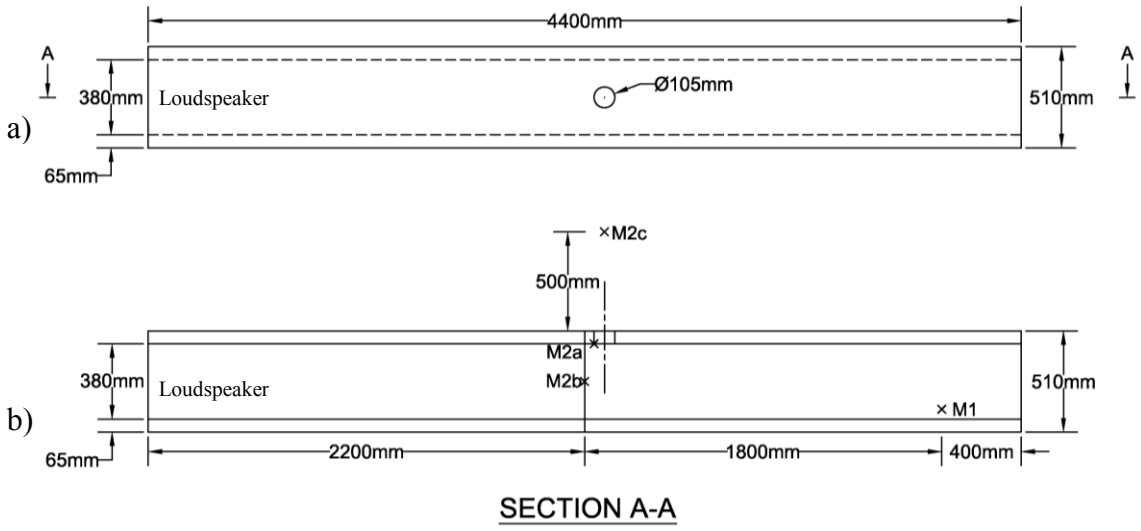

Figure 6-1: Configuration of the concrete duct system (a) Top view (b) Section A-A.

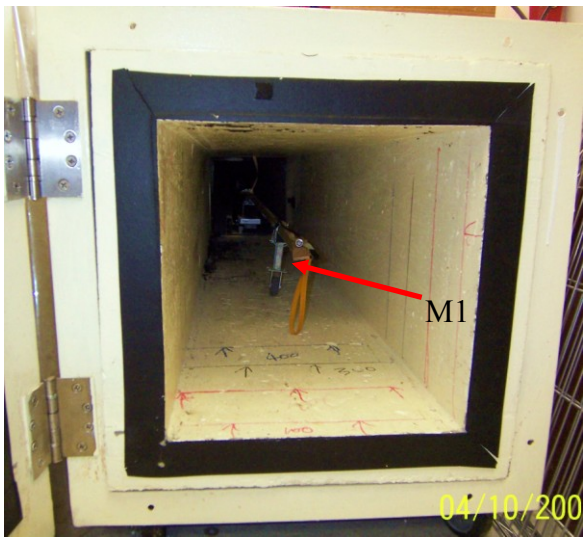

Figure 6-2: Inner view of the concrete duct

The concrete duct was 4.4m long. Using the theory to calculate the resonant frequency of the standing wave $v = f\lambda$, the first resonant frequency was *f1* = 39Hz. Therefore, *f2* = 78Hz and *f3* = 117Hz and so on (See Chapter 5, Figure 5-3). Therefore, there were low sound pressure level measurements at *f1* and *f3* but high sound pressure level measurements at *f2* and *f4* at the mid-length section of the duct. At the two ends of the duct, there were high sound pressure level measurements at all resonant frequencies. The Helmholtz resonance of the opening at the top was calculated by $fr = \frac{c}{2\pi}\sqrt{\frac{S}{VL}}$, the theoretical Helmholtz resonance was 25Hz.

According to Sharma and Richards [1], when there is an air flow through small openings, the natural frequency of the internal pressure system f_{HH} referred to as the Helmholtz frequency is given by $f_{HH} = \frac{1}{2\pi}\sqrt{\frac{0.6S}{VL_e}}$, where L_e ($L_e = L + 0.8\times$diameter of opening) is the effective length of the air slug at the opening. Therefore, if there is air flow through the top opening, f_{HH} = 13Hz.

As shown in Figure 6-3, for a duct system without any opening, the M1 measurements had peak values of about 40Hz, 80Hz, 130Hz and 170Hz, which are standing wave resonances. M2a had peaks only at 80Hz and 170Hz but troughs at

40Hz and 130Hz. These results are in conformity with greater particle vibrations leading to lower sound pressure levels.

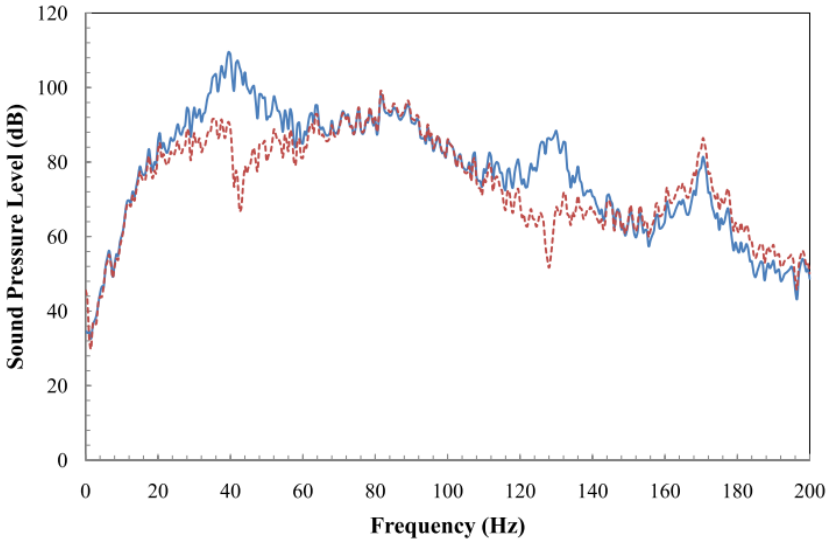

Figure 6-3: Sound pressure level measurements for the duct without an opening; ——, M1; – – –, M2a.

When Figures 6-4 and 6-5 are compared, only the graph in Figure 6-4 has a peak of around 17Hz for both M1 and M2b. Figure 6-4 shows that both the M1 and M2b measurements for the duct with a top opening have the same peak value of about 17Hz. The comparison of the sound pressure level measurements at one position for different duct conditions, that is with and without the top opening, are compared in Figure 6-6 and 6-7. The two curves in Figures 6-6 and 6-7 are nearly the same except for the frequency of 17Hz. There is a peak at 17Hz for the duct with the opening, which further proves that 17Hz is the Helmholtz resonance for the duct

opening. In the experiment the Helmholtz resonance lay between the theoretical Helmholtz resonance without airflow, 25Hz, and with airflow, 13Hz, which shows that the infrasound measured is probably partly due to the air flow through the top opening.

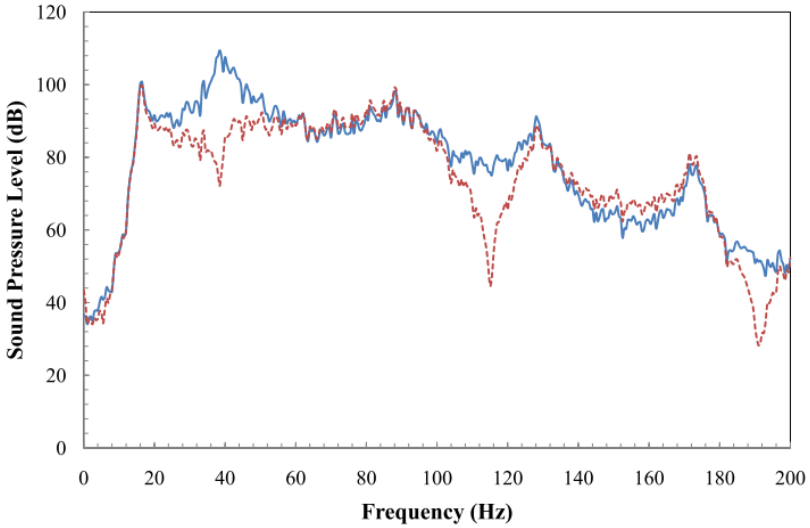

Figure 6-4: Sound pressure level measurements for the duct with the opening; ——, M1; – – –, M2b.

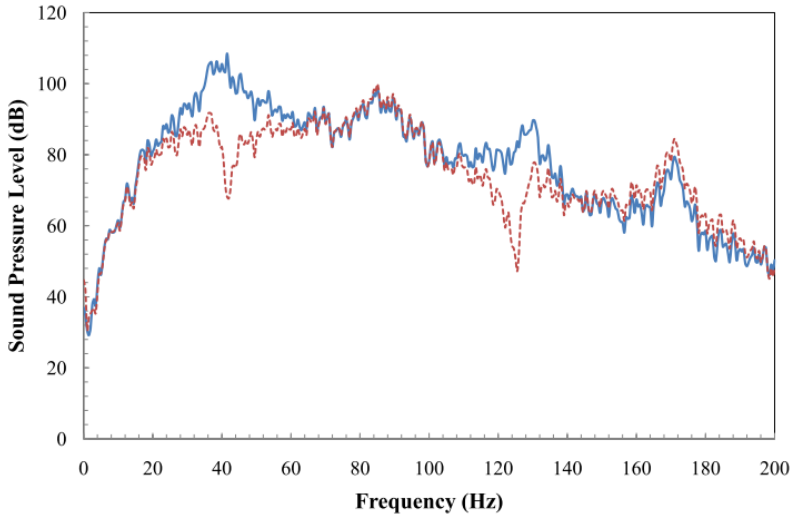

Figure 6-5: Sound pressure level measurements for the duct without openings; ——, M1; – – –, M2b.

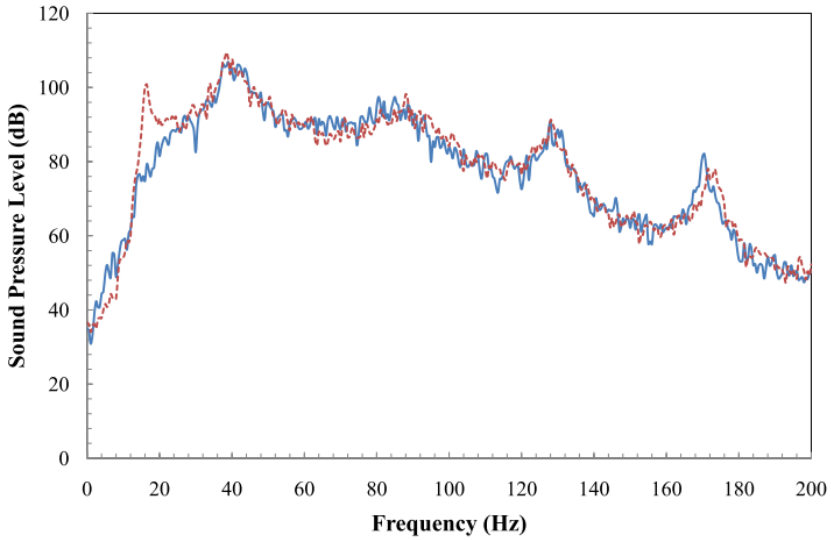

Figure 6-6: Sound pressure level measurements at M1for different duct conditions; ——— , without openings; – – – , with the opening.

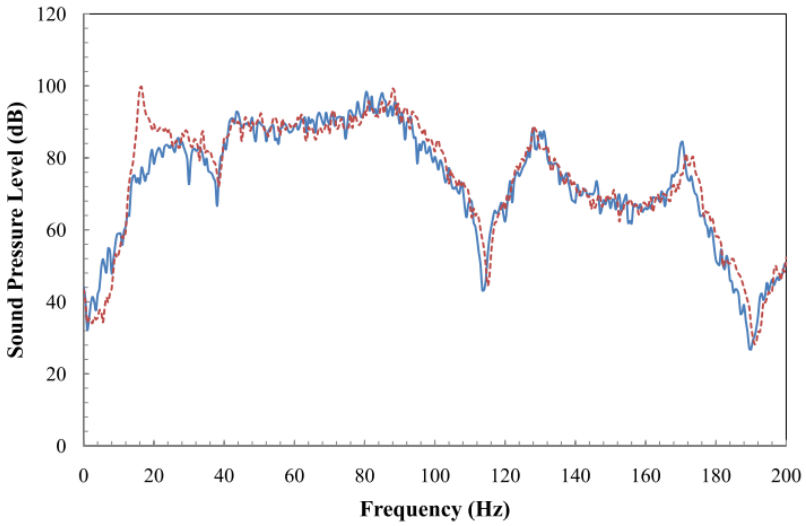

Figure 6-7: Sound pressure level measurements at M2b for different duct conditions; ——— , without openings; – – – , with the opening.

Figure 6-8 shows that even if there is just background noise, such as noise from ventilation ducts or the engines of machines, a sharp low frequency sound at about

17Hz can still be detected at around 75dB inside the concrete duct with the top opening at M2b. The result further proves that the infrasound of 17Hz is due to air flow instead of acoustic excitation. To investigate the adverse effects on humans, the sound pressure level was measured at M2c to demonstrate low frequency sounds detected in rooms with ventilation spaces and the result is shown in Figures 6-9 and 6-10. Figure 6-9 shows that low frequency noise of 80dB at about 17Hz from the loudspeaker was detected. Furthermore, Figure 6-10 shows that there were nearly 87dB for the 1/3 octave band of 16Hz. This is undesirable for humans because sound levels above 80dB at the frequency range below 20Hz cause humans discomfort.

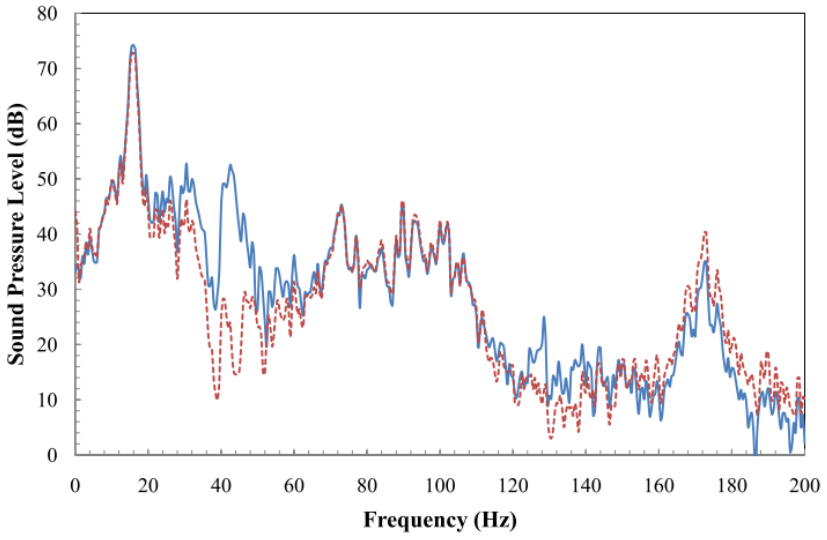

Figure 6-8: Sound pressure level measurements of the background noise for the duct with a top opening; ——, M1; – – –, M2b.

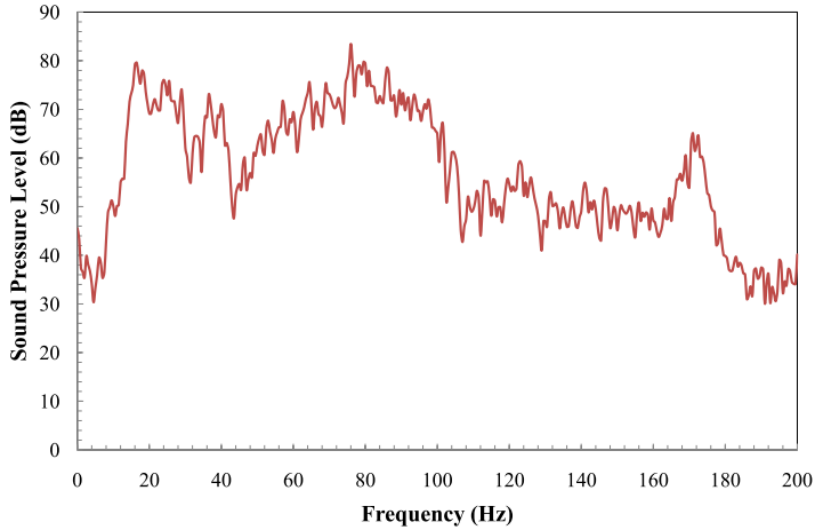

Figure 6-9: Sound pressure level measurements due to the loudspeaker at M2c for the duct with a top opening.

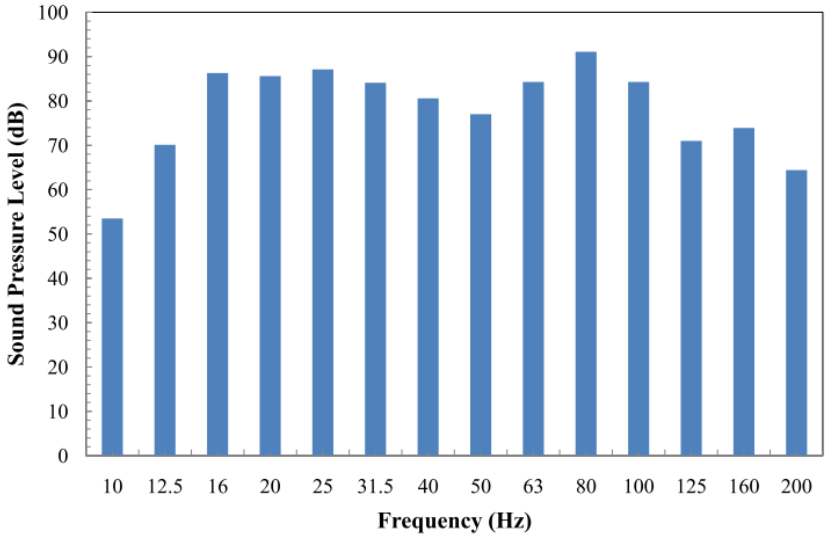

Figure 6-10: Sound pressure level using 1/3 octave measurements due to the loudspeaker at M2c for the duct with a top opening.

6.4 Experiments to investigate the effect of air flow on the Helmholtz effect

The same concrete duct was used with an opening of diameter 105mm on the top of the duct. One end was connected to a small circular tube while the other end was rigid. Two microphones were used to take measurements and the positions are shown in Figure 6-11. The theoretical Helmholtz resonance without air flow ($fr = \frac{c}{2\pi}\sqrt{\frac{S}{VL}}$) of the small circular tube was 21Hz.

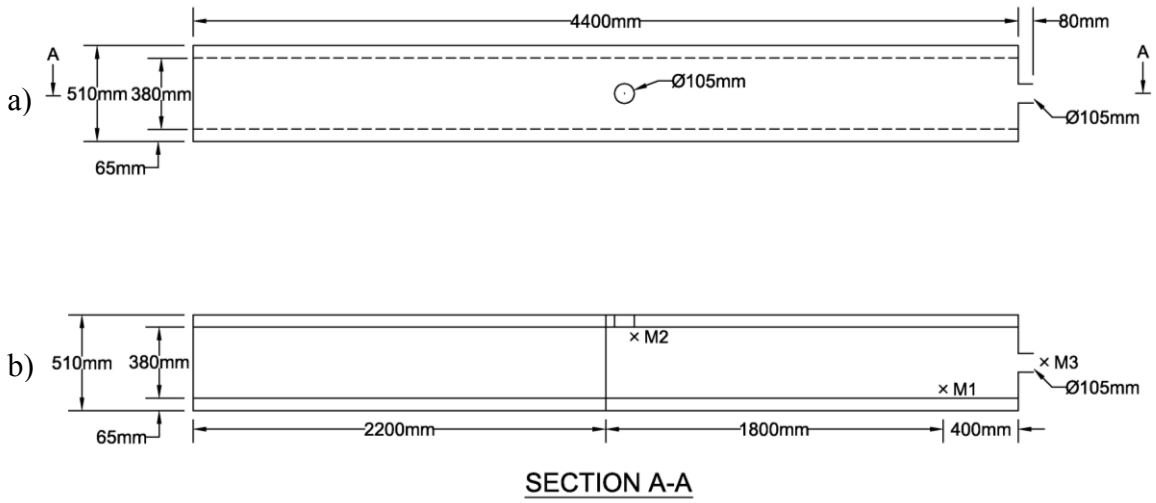

Figure 6-11: Configuration of the concrete duct system. (a) Top view (b) Section A-A.

Figure 6-12 shows that the background sound pressure level measurements outside the duct (M3) was higher than inside the duct (M1) for the whole frequency range, except at frequencies 8Hz, 42Hz and 132Hz. When there was air flow, the

theoretical Helmholtz resonance ($f_{HH} = \frac{1}{2\pi}\sqrt{\frac{0.6S}{VL_e}}$) of the top opening was 13Hz while the theoretical Helmholtz resonance with air flow through the small circular tube was 12Hz. Results show that the high value at M1 was due to the standing wave resonance for frequency 42Hz and 132Hz and was also due to Helmholtz resonance for frequency 8Hz when there was a flow of air passing through the small circular tube or the top opening.

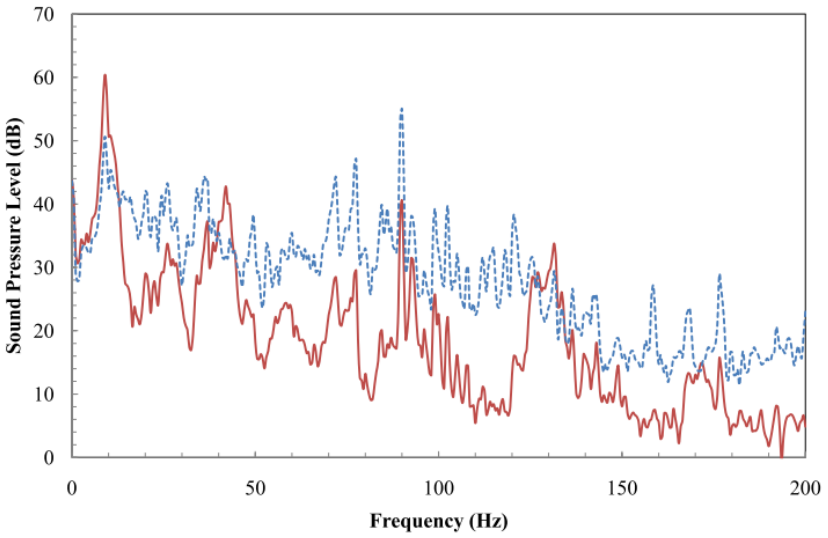

Figure 6-12: Background sound pressure level measurements; ——, M1; – – –, M3.

To strengthen the Helmholtz piston effect, a fan was connected to the small circular tube and was switched on to generate an air flow with a 5.5m/s flow rate (Figures 6-13 and 6-14). Experiments were conducted to measure the noise level of the fan and the results showed that the fan generated about 55dB at 20Hz and about 50dB at 20 – 100Hz. Figures 6-15 and 6-16 show that an air flow will lead to a greater level of sound pressure for the whole frequency range measured in M1 and M2.

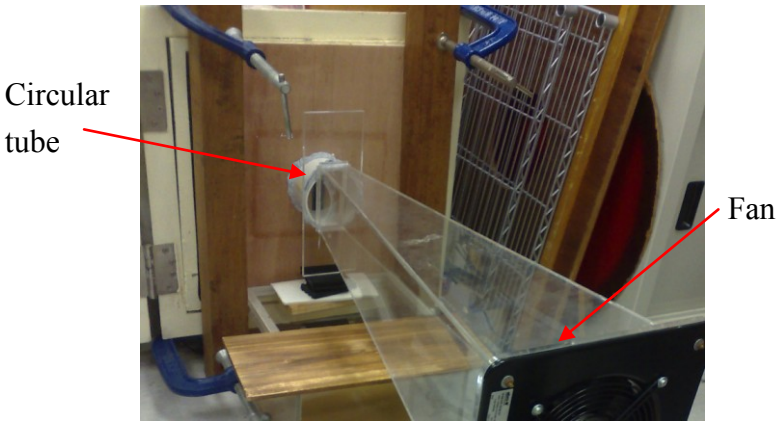

Figure 6-13: A fan connecting to the circular tube

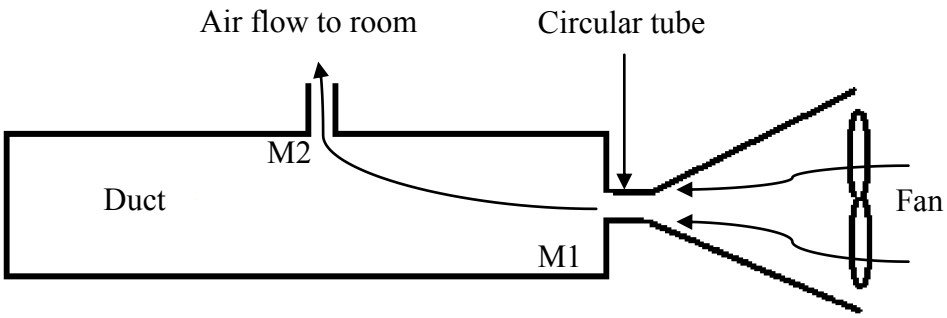

Figure 6-14: A fan is connected to the concrete duct system through a circular tube

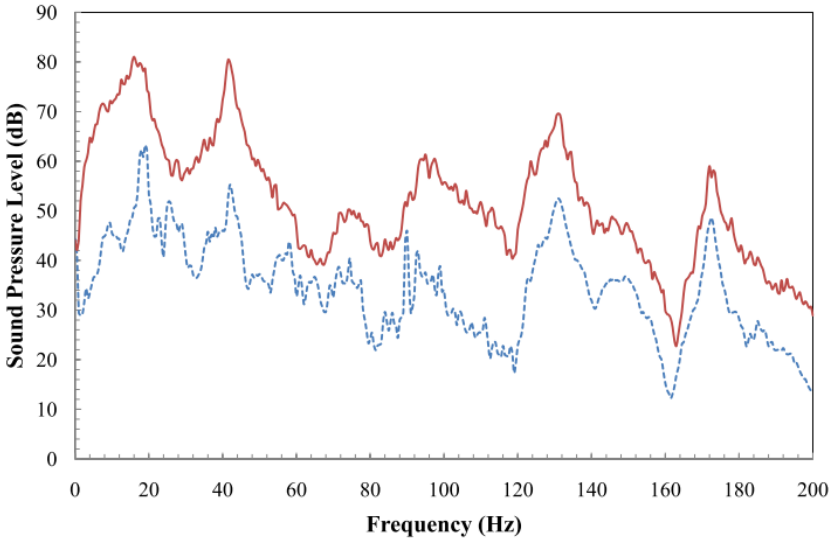

Figure 6-15: Sound pressure level measurements at M1; ——— , fan on; - - - - , fan off.

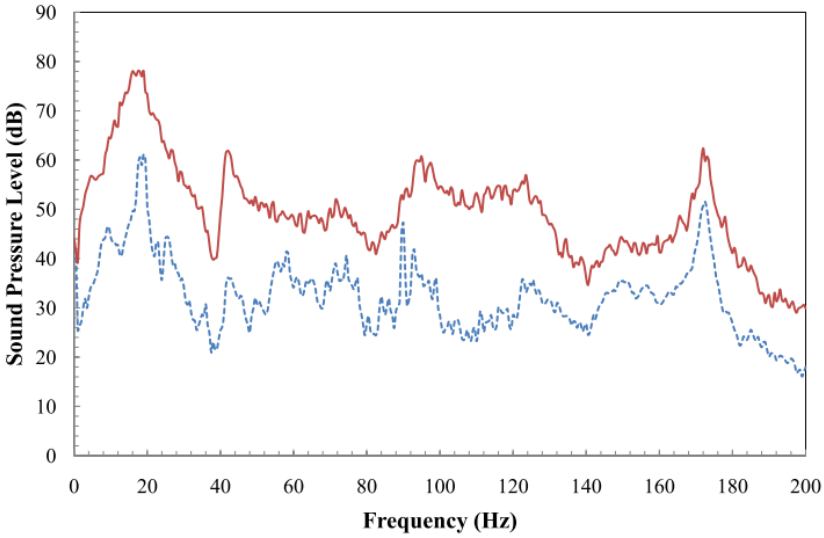

Figure 6-16: Sound pressure level measurements at M2; ——— , fan on; - - - - , fan off.

Figures 6-17 and 6-18 show that there is a shift in the first resonant frequency measured at M1 and M2 when the top opening is closed and the fan is switched on. The first resonant frequency when the top opening is closed is 8Hz and about 16.5Hz when it is open. This shows that the top opening generates a Helmholtz effect by combining with the noise generated by the small circular tube. This changes the first resonant frequency.

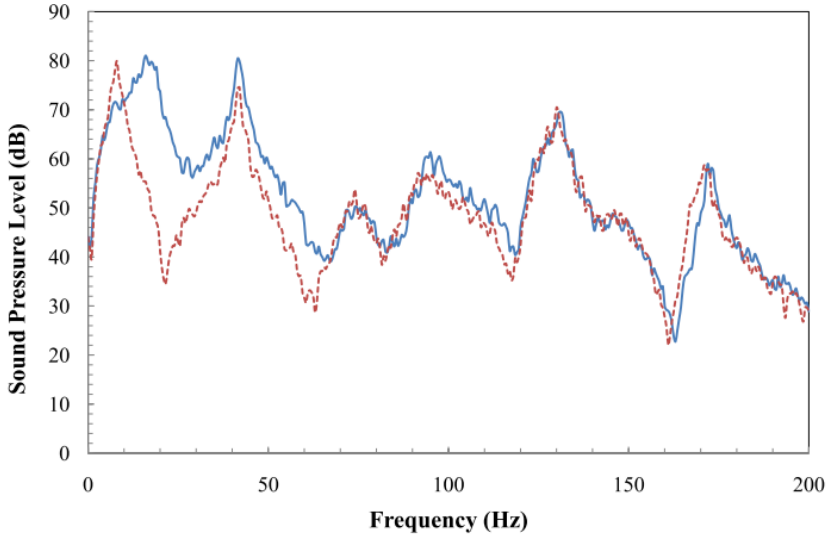

Figure 6-17: Sound pressure level measurements at M1 for different top opening conditions; ——— , open; - - - , closed.

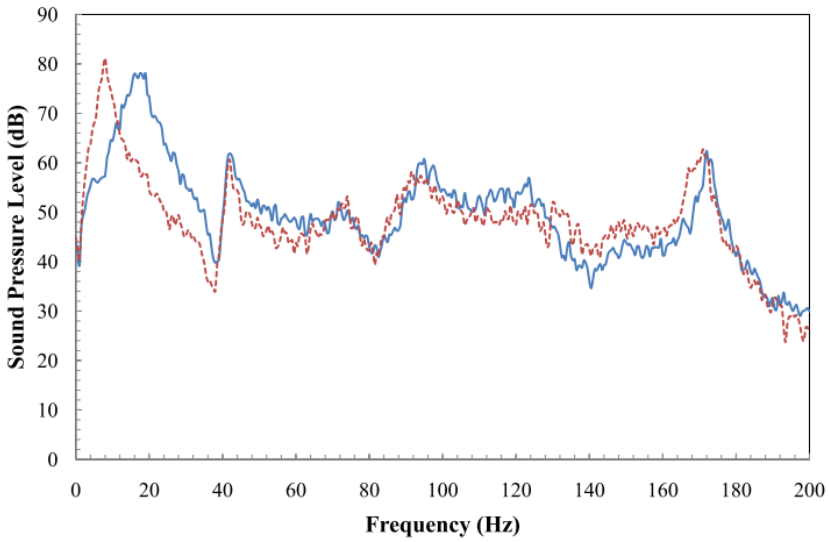

Figure 6-18: Sound pressure level measurements at M2 for different top opening conditions; ——— , open; – – – , closed.

The fan was connected to the concrete duct and switched on. The effect of increasing the size of the top opening on the first resonant frequency is shown in Figures 6-19 and 6-20. Three tubes of different sizes, small (2cm diameter and 6.5cm long), medium (5cm diameter and 26cm long) and large (7.5cm diameter and 26cm long), were connected to the top opening, respectively. The theoretical Helmholtz resonances for the three tubes when there is an air flow passing through them were 3.3Hz and 4.3Hz and 6.2Hz respectively. Results show that increasing the size of the top opening will generate a higher sound pressure level measured at M1 and M2, which shifts the first resonance to the right.

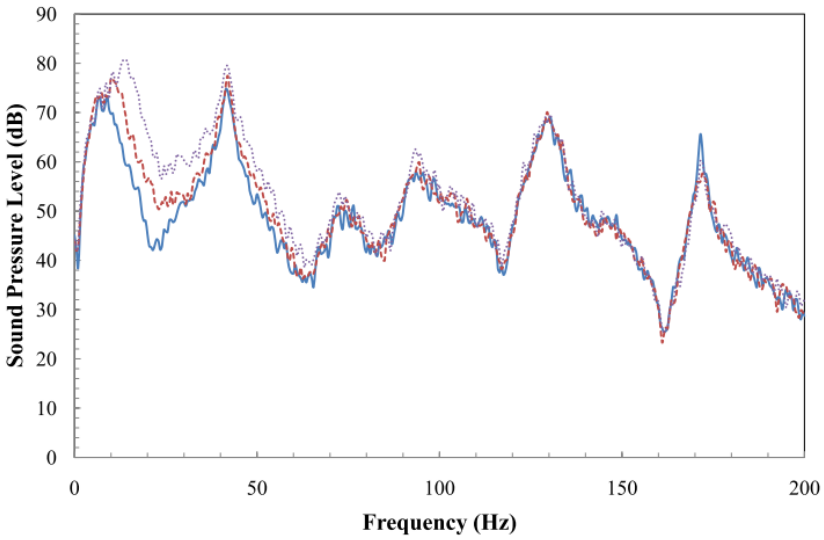

Figure 6-19: Sound pressure level measurements at M1 with different top opening sizes; ——— , small; - - - , medium, ····· , large.

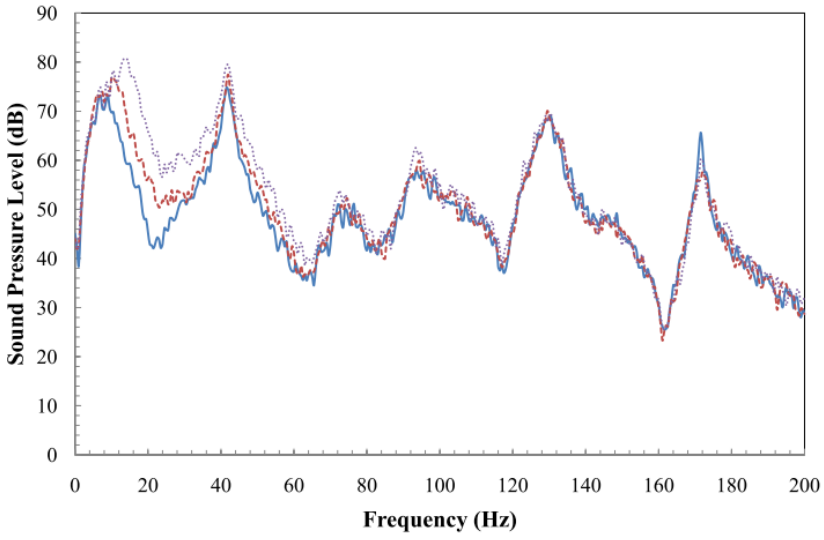

Figure 6-20: Sound pressure level measurements at M2 with different top opening sizes; ——— , small; - - - , medium, ····· , large.

6.5 Experiments to investigate the airflow on the Helmholtz effect in a rectangular duct

The same concrete duct was used with an opening on the top together with a side opening of variable dimensions. The side opening is at one end which is connected to a small rectangular duct and the other end is a rigid. The dimensions of the small rectangular duct are the same as the narrow duct used in Chapter 2 and 3 (See Figure 2-13). The theoretical Helmholtz resonance of the small rectangular duct is 33.6Hz. Two microphones were used for measurements and the positions were shown in Figure 6-21.

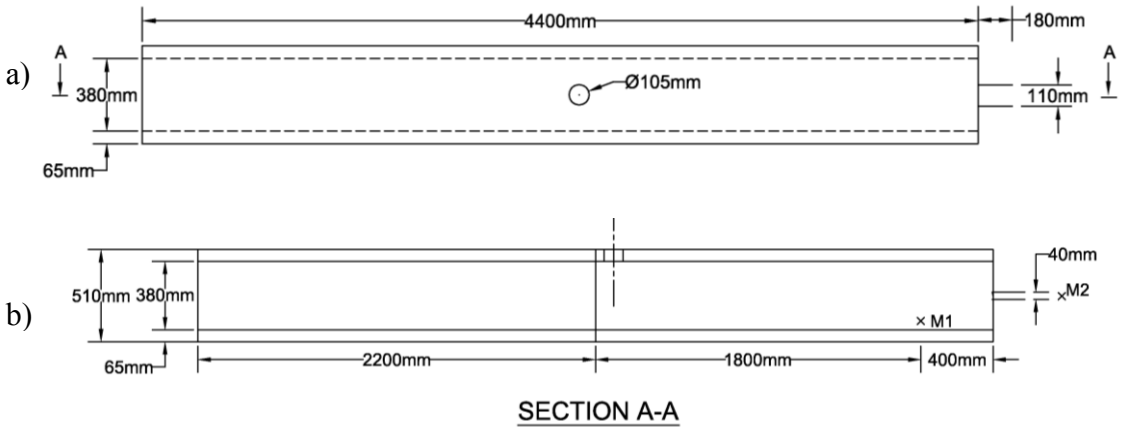

Figure 6-21: Configuration of the duct system (a) Top view (b) Section A-A.

Figure 6-22 shows that there is also a peak at 9Hz about 60dB and 53dB for M1 and M2 measurements respectively even though there is only background noise. This infrasound of 9Hz measured inside the duct (M1) has higher sound pressure level than that outside the duct (M2).

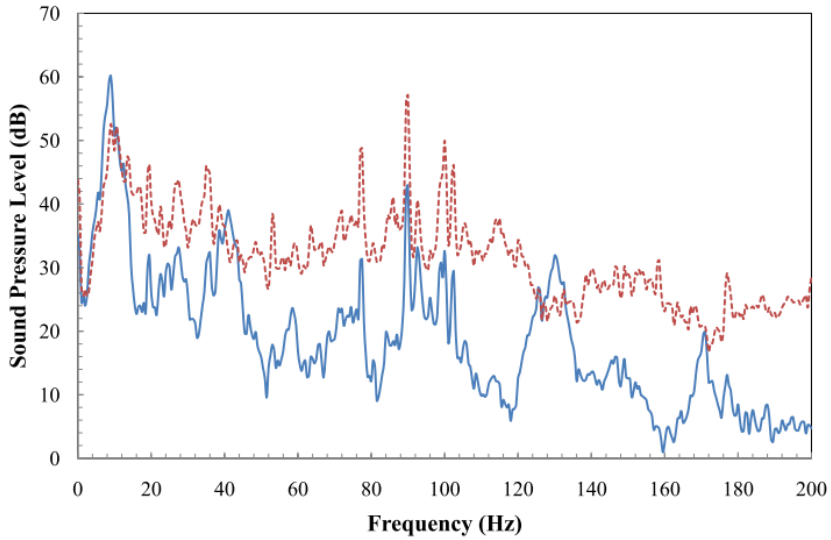

Figure 6-22: Sound pressure level measurements of the background noise; ——, M1; – – –, M2.

Figure 6-23 shows the comparison of the sound pressure level measurements at M2 when there are different activities outside the testing duct. It can be seen that hitting a drum can create a louder sound than other activities at the frequency range from 80Hz to 130Hz and at about 185Hz. Very surprisingly, the sound pressure level is nearly 90dB at 9Hz when slamming a door. Compared to the background noise

measurements in Figure 6-20, nearly 40dB was increased at M2 when a door was slammed at 9Hz. This low frequency is known as infrasound which can cause adverse effect to human when the level is over 80dB.

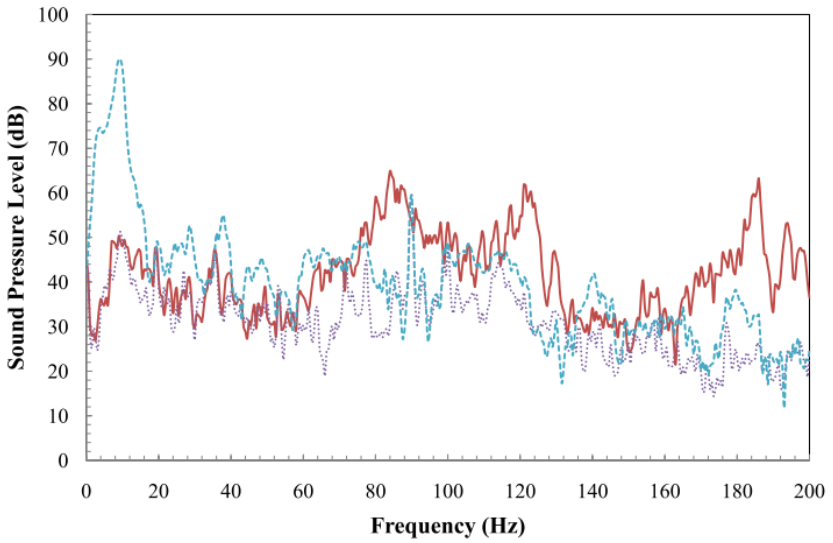

Figure 6-23: Sound pressure level measurements at M2; ——— , drum hitting; ····· , hitting the ground by a falling object; – – – , slamming a door.

Figure 6-24 shows the sound pressure level measured at the moment when the door was closed and slammed. There is a high peak at around 9Hz with nearly 95dB for both M1 and M2 positions. For other frequencies except 9Hz, the measured sound pressure level outside the duct (M2) is about 15dB smaller than that inside the duct (M1). It is also believed that the infrasound is not caused by the vibration of the door but the air flow induced during slamming the door instead. According to the

Helmholtz theory when there is a flow of air through openings, the calculated Helmholtz resonance of the small rectangular duct is 7Hz which further proves that slamming the door induces an air flow and the infrasound is thus generated.

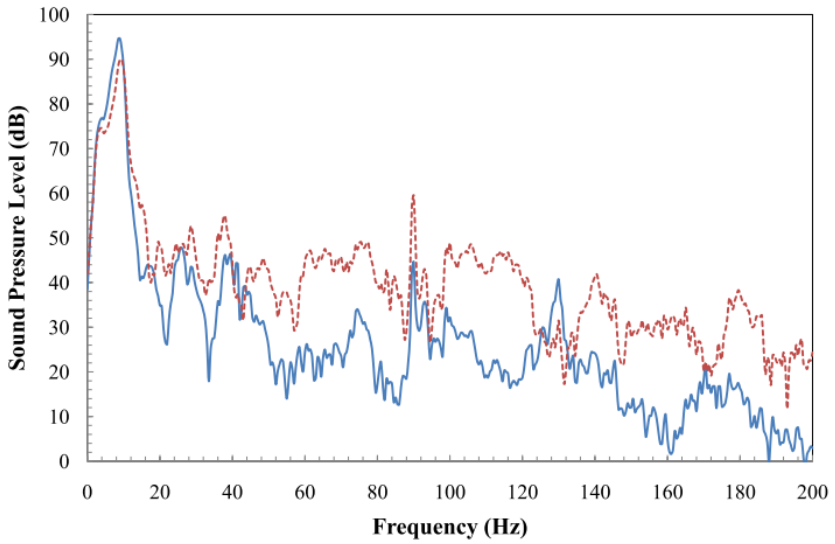

Figure 6-24: Sound pressure level measurements when slamming the door; ——, M1; – – –, M2.

Experiments were done to investigate the effect of the side opening of the concrete duct on sound pressure level measurements. The side opening was open and closed respectively for measurements. Figure 6-25 shows that when there is an opening, several peaks with high sound pressure level are measured. For infrasound measurements, there is a sharp increase from 35dB to about 55dB in the frequency range from 9 to15Hz.

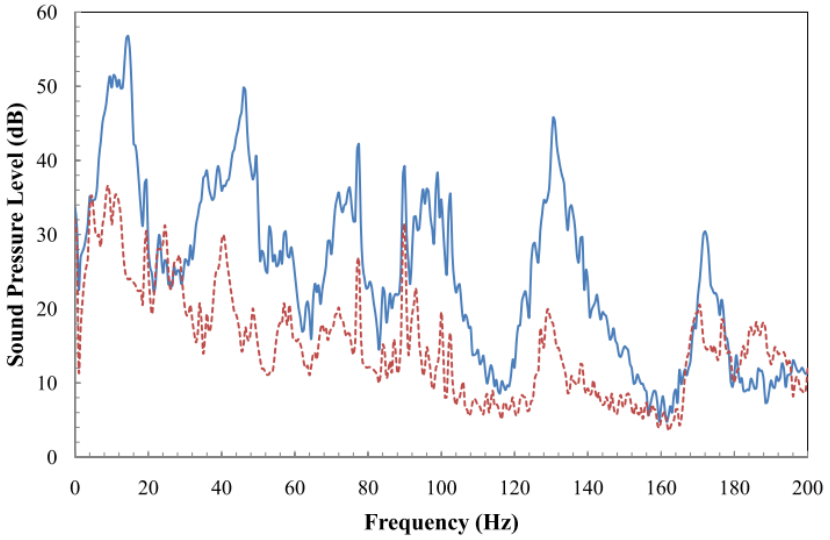

Figure 6-25: Sound pressure level measurements at M1 with different side opening conditions; ——, open; - - -, closed.

Figure 6-26 shows the sound pressure level measurements at M1 with different opening sizes of the small duct. For nearly all frequencies except 9Hz, the smaller the opening size is, the smaller will be the measured sound pressure level at M1. However, for the infrasound of 9Hz, the smaller the opening size is, the higher will be the measured sound pressure level (M1).

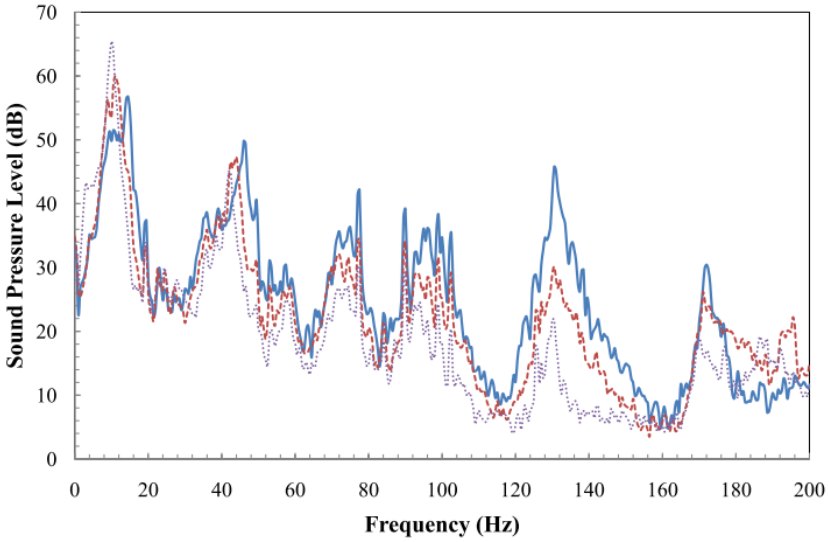

Figure 6-26: Sound pressure level measurements at M1 with different opening sizes; ——— , open; – – –, half open; ·····, 1/4 open.

A fan is connected to the opening of the small duct to increase the piston effect of Helmholtz mechanism inside the small duct (Figure 6-27 and 6-28). The result in Figure 6-29 shows that when wind is generated by turning on the fan, a higher sound pressure level is measured at M1 for the whole frequency range. The average sound pressure level difference measured at M1 for the cases of switching on and off the fan is about 40dB which is quite significant.

a)

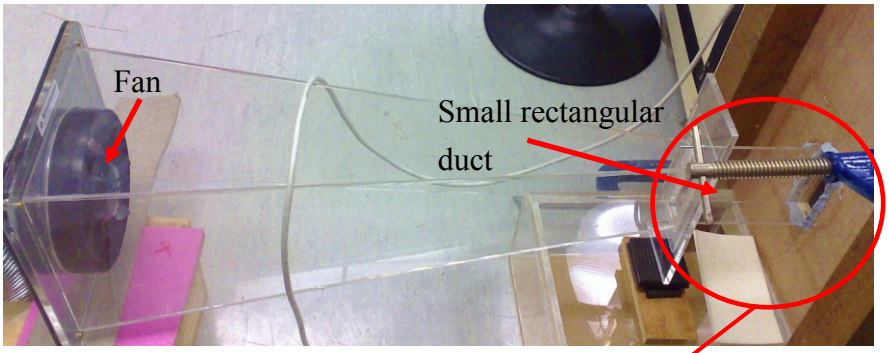

b)

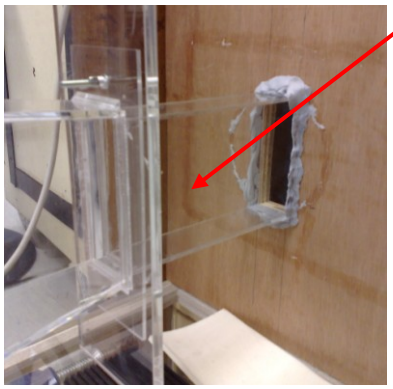

Figure 6-27: (a) A fan connected to the small rectangular duct (b) small rectangular duct

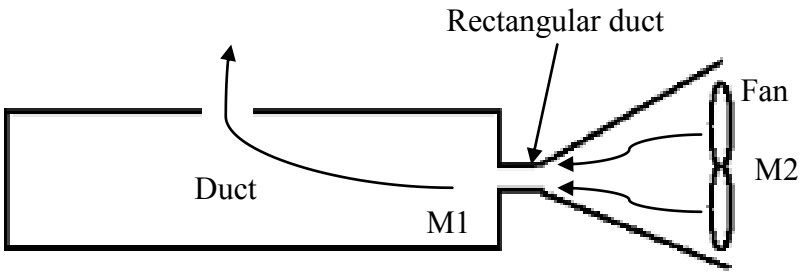

Figure 6-28: A fan connected to the concrete duct

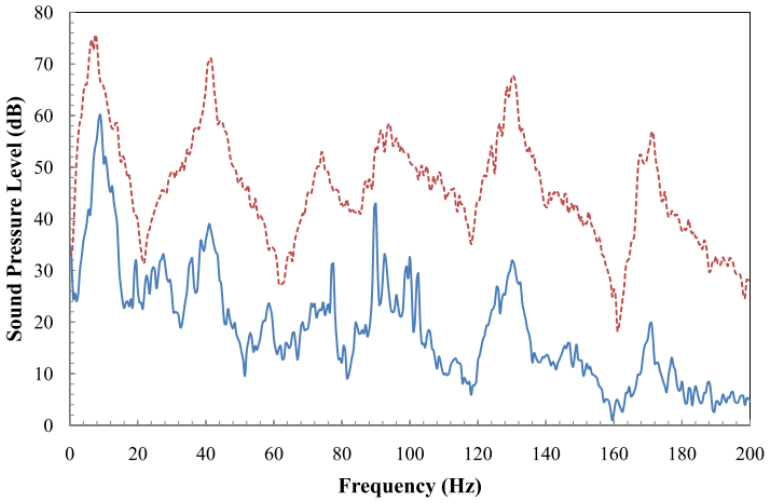

Figure 6-29: Sound pressure level measurements at M1; ——, Fan off; – –, Fan on.

6.6 Summary

An infrasound of 9-11Hz is generated by a flow of air or a door slamming. Most loudspeakers cannot generate sound with frequency lower than 20Hz. Infrasound of over 80dB can cause harm to humans who do not detect it as sound but as a pressure on the body. If there are small ventilation openings in a large ventilation space or room, it is possible for air flow to generate infrasound of significant magnitude which annoys residents. Infrasound cannot be reduced by absorption materials in a small ventilation opening; neither can it be reduced by placing silencers inside the opening or changing the size of the opening. Furthermore, a Helmholtz resonator cannot reduce infrasound due to the large cavity required. Fortunately, as this study has shown, it can be reduced by a membrane absorber.

CHAPTER 7

INTERACTION OF NONLINEAR MEMBRANE VIBRATION WITH ACOUSTIC WAVES

7.1 Introduction

Although the amount of work dedicated to the study of vibrating membranes for sound absorption is not as large as in the case of porous sound-absorbing materials, there have been many attempts to solve for the vibrating response of a homogenous membrane of simply geometry. Dozens of theoretical studies have also been published on membrane vibrations but there is very little experimental work. This chapter presents in detail the experimental work by applying vibrating membrane to achieve sound absorption. It is shown that the behaviour of the absorbing element is mainly determined by the vibrating response at resonances.

When the vibrating membrane follows the linear vibration principle, it can achieve significant sound reduction at particular frequencies. With a greater acoustic pressure acting on the vibrating membrane, both the stiffness of the membrane and the vibrating mode shapes change. This gives rise to non-linear vibration response characteristics. Non linear vibration has adverse effects on noise attenuation. Increasing the tension of the membrane also increase its resonant frequencies.

7.2 Literature Review

There are less than two dozen fundamental experimental membrane vibration studies found in the literature (Jenkins and Korde, 2006). The simplest cases have even not yet been thoroughly investigated. This is partly due to the extreme flexibility and the lightness of membranes. An advanced non-contact measurement methods are thus required. Practical applications of the membrane structures may find value in architectural and civil structures and it can be used to control noise and vibration in buildings.

Currently, wood is more often than not, the preferred surface treatment in general architectural spaces, as well as in critical listening and performance spaces. However, one of the problems is that flat wooden panels may generate problematic reflections compromising speech intelligibility and music quality. To treat offending reflections, upholstered fiberglass or stretch fabric systems are often used.

7.3 Interaction of nonlinear membrane vibration with acoustic waves

Investigations have been made into the feasibility of using the vibrating membrane in a ventilation space to achieve noise reduction (Figure 7-1). A 2.8m long Plexiglas testing duct (the same duct in Chapter 5) with a loudspeaker at one end and

a cloth membrane attached on the other end (Figure 7-2). The cloth membrane used is the same type as that used in Chapter 5. Two microphones were used to find the sound reduction performance of the membrane by dissipating the sound energy into vibration energy. One accelerometer was attached onto the membrane to find its vibration behavior.

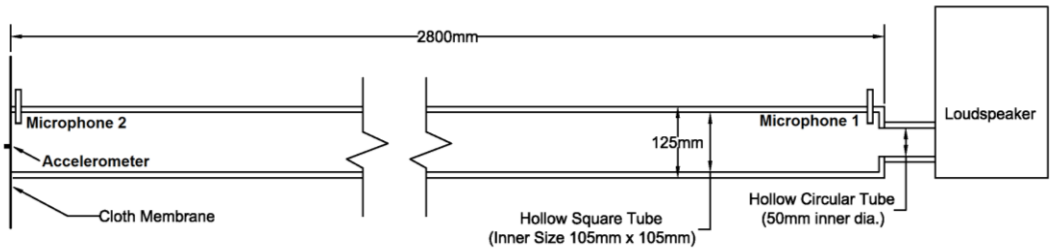

Figure 7-1: Side view of a 2.8m long square testing duct

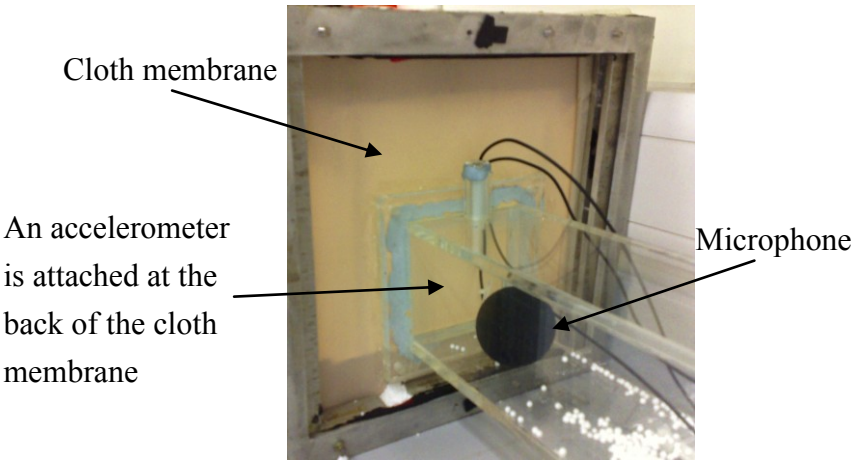

Figure 7-2: Testing duct with a vibrating cloth membrane

Figure 7-3 shows non-linear vibration occurs when there is a sound power input. For the lower sound power inputs such as 0.5mV, 5mV and 50mV, all of them process the same acoustic resonance. When increasing the sound power input to 500mV and 5V, non-linear vibration exists and changes the resonant frequencies. Figure 7-4 also proves that non-linear vibration exists when using a higher sound power input. For the case of 5V, the vibration amplitude is lower at the frequency below 100Hz but higher at the frequency above 100Hz which is totally opposite to that of the lower sound power inputs. It is obvious that the whole vibration pattern for the case of power input of 5V changes due to the non-linear vibration.

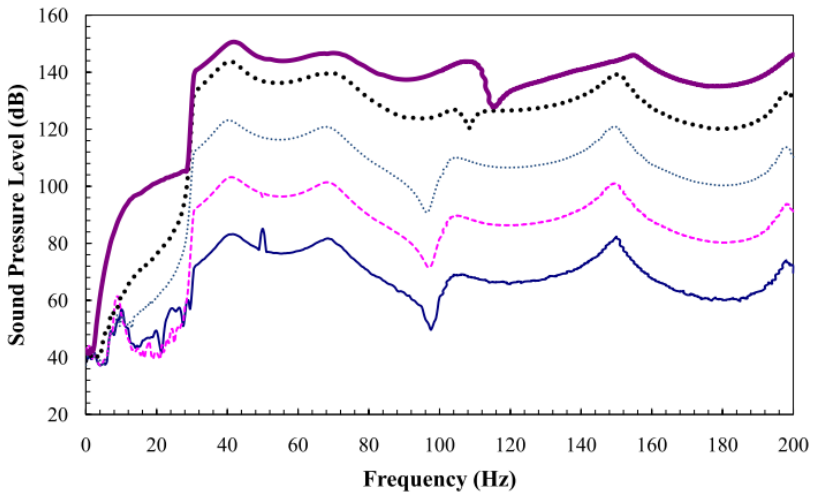

Figure 7-3: Relationships between resonant frequency and sound power input; ——, 0.5mV; – – –, 5mV; ·····,50mV;• • • • •, 500mV; ——, 5V .

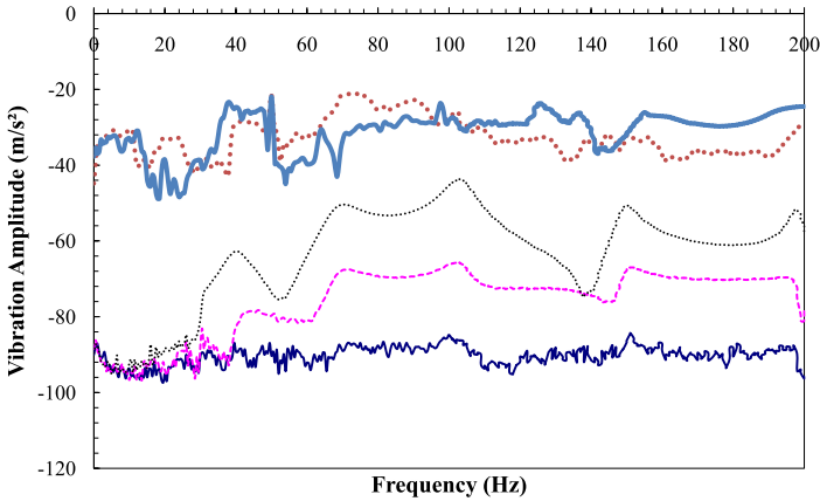

Figure 7-4: Relationships between vibration amplitude and sound power input; ——, 0.5mV; – – –, 5mV; ·····; 50mV; • • • • • 500mV; ▬▬ , 5V .

According to the experimental results as shown in Figure 7-5, for linear vibration, higher vibration amplitude leads to a greater sound reduction. The vibration amplitude is higher at 150Hz than that at 100Hz; however, the sound pressure level is higher at 100Hz than that at 150Hz. Non-linear characteristics can be observed in Figure 7-6. With a higher force, the hardening behavior of membrane becomes more significant. The higher the force acted on the membrane is, the stiffer the membrane will be. It will lead to a reduction in the vibration amplitude and worsens the sound reduction performance by vibration. Thus non-linear vibration which is caused by the high applied force will have adverse effect on sound reduction.

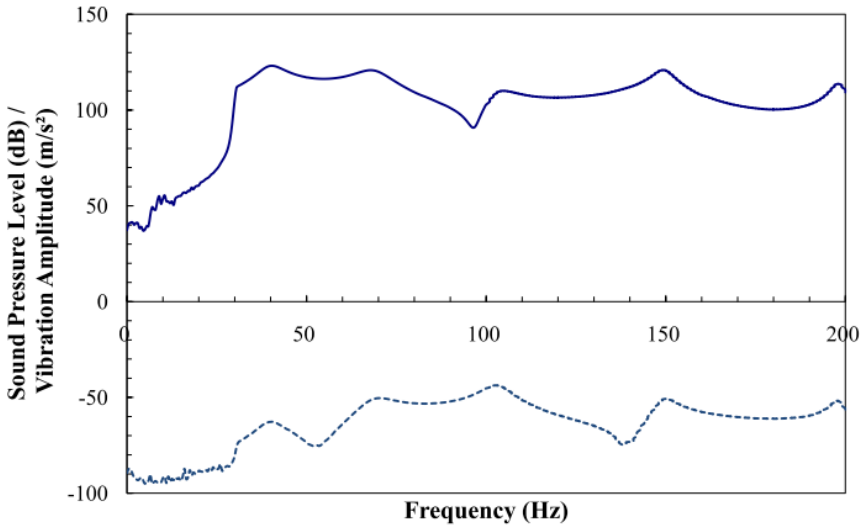

Figure 7-5: Relationships between vibration amplitude and sound pressure level; ——, sound pressure level; - - - , vibration amplitude.

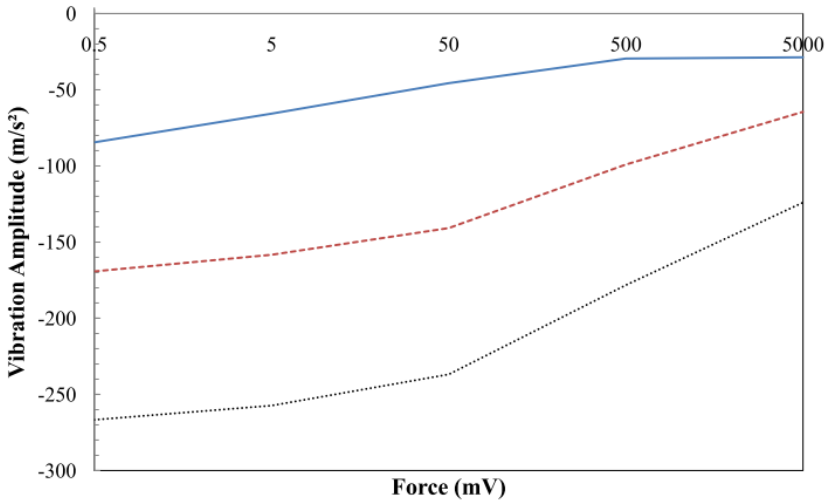

Figure 7-6: Relationships between vibration amplitude and sound power input; - - -, 50Hz; ——, 99Hz; ····· ,200Hz.

Figure 7-7 shows clearly that for the higher sound power inputs at 500mV and 5V, the sound reduction values decrease significantly due to the occurrence of the

non-linear vibration. Thus, non-linear vibration is less effective in sound reduction especially at about 100Hz. Non-linear vibration also leads to a non-pure tone which is proved in Figure 7-8. High sound level can be detected at about 100Hz for all sound power inputs. But for 500mV and 5V where non-linear vibration exists, high sound level is also detected at about 200Hz. The vibrating cloth membrane shows super-harmonic response at 200Hz when non-linear vibration occurs.

The membrane in this study is of small size which requires a high sound power input to excite the membrane for easier observation. If the membrane structure is applied in the real life which must be of a bigger size, a smaller sound power input can already lead to the non-linear effect due to the small thickness of the membrane. One example is that non-linear effect caused by the traffic noise of 100dB.

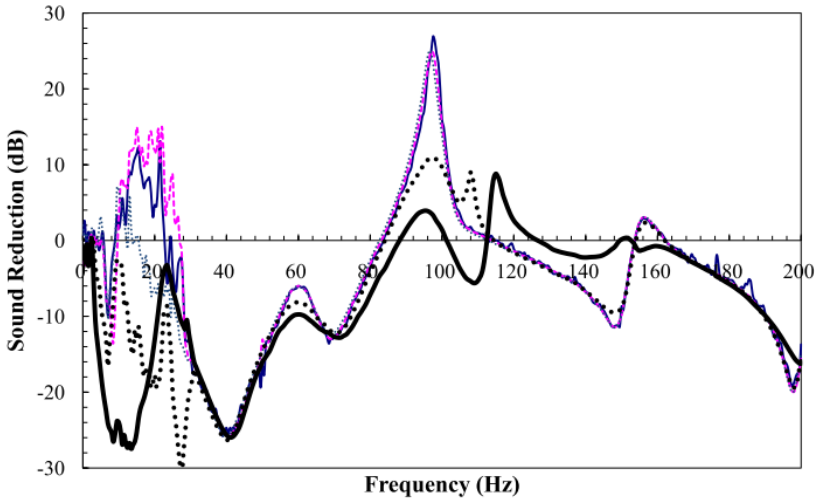

Figure 7-7: Relationships between sound reduction and sound power input; ——, 0.5mV; – – –, 5mV; ·····, 50mV; • • • • •, 500mV; ▬▬, 5V .

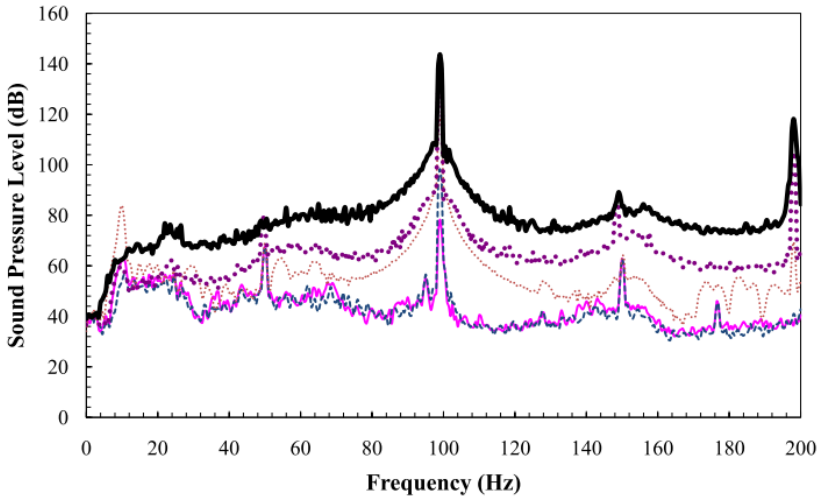

Figure 7-8: Relationships between sound pressure level and sound power input; ——, 0.5mV; – – –, 5mV; ·····,50mV, • • • • •, 500mV; ▬▬, 5V .

7.4 Investigation of the resonant response of the cloth membrane with an increasing one directional tension

7.4.1 Experiment on the resonant response of the cloth membrane by strain gauges

An experiment was conducted to investigate the resonant response of the cloth membrane (Figure 7-9). One microphone was placed at a distance of 350mm from the duct end. Two strain gauges were used to measure the strain and vibration of the cloth membrane due to the sound pressure of the loudspeaker. Strain gauges were used instead of accelerometers to measure the vibration amplitude of the membrane due to its negligible weight.

One was installed on the vibrating cloth membrane at the end of the pipe (Figure 7-10 and 7-11) while the other one was installed on a non-vibrating cloth membrane. The tension on both X and Y directions of the cloth membrane can be adjusted. The Y-direction tension was increased gradually while keeping the X-direction tension to be constant during measurements. Increasing the tension changes the bending stiffness of the membrane and thus alters the resonant frequency.

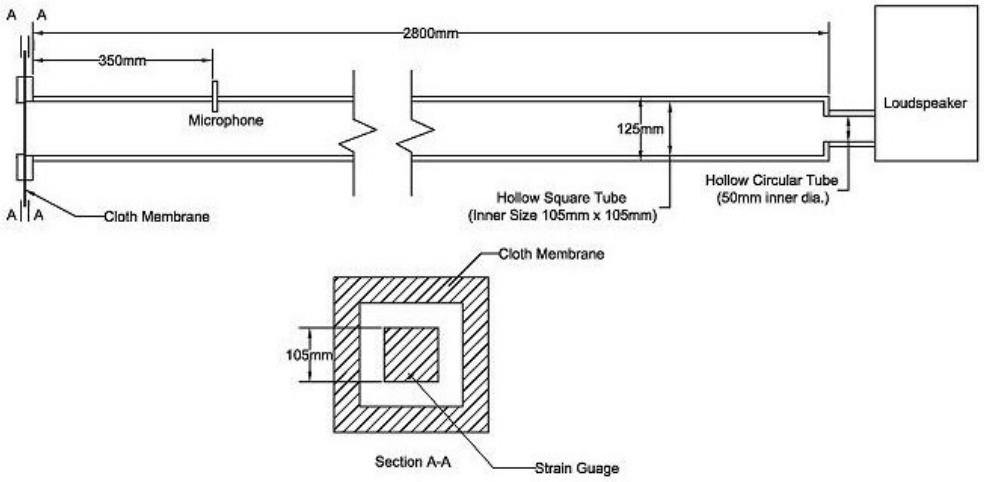

Figure 7-9: Configuration of the testing duct ended with the cloth membrane.

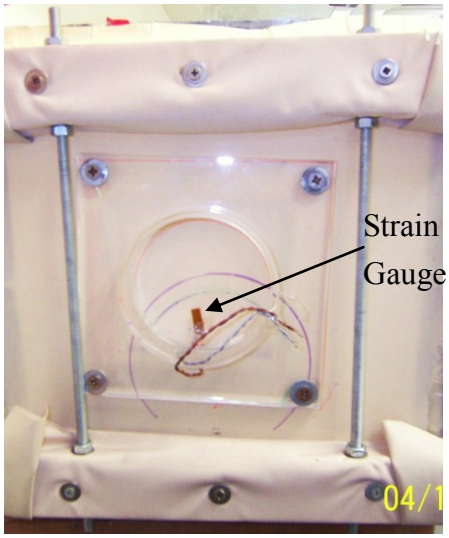

Figure 7-10: A strain gauge fixed on the back of the cloth membrane

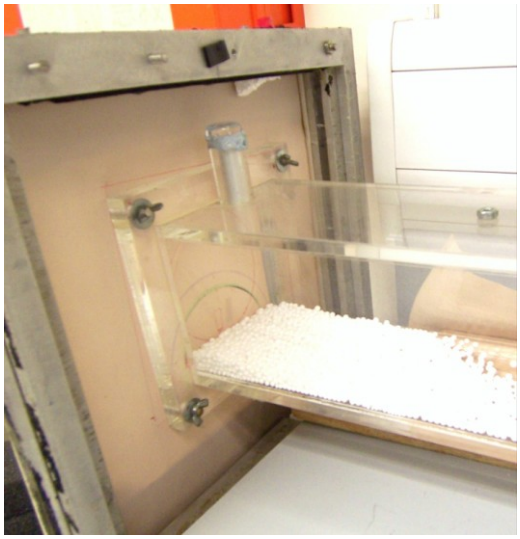

Figure 7-11: The end of the testing duct connecting to the cloth membrane

Figure 7-12 shows that the tension of the cloth membrane has a significant effect on the sound reduction properties. For the Y-direction tension free membrane,

a desirable sound reduction can be achieved in lower frequencies of about 45–85Hz. therefore, the membrane absorber can be used to reduce infra-sound reported in Chapter 6. When increasing the Y-direction tension of membrane, higher sound reduction is achieved at higher frequencies of about 85-105Hz. The results obtained suggest that the membrane having only 1 directional tension is able to achieve low frequency sound absorption than that of having both directions without tension.

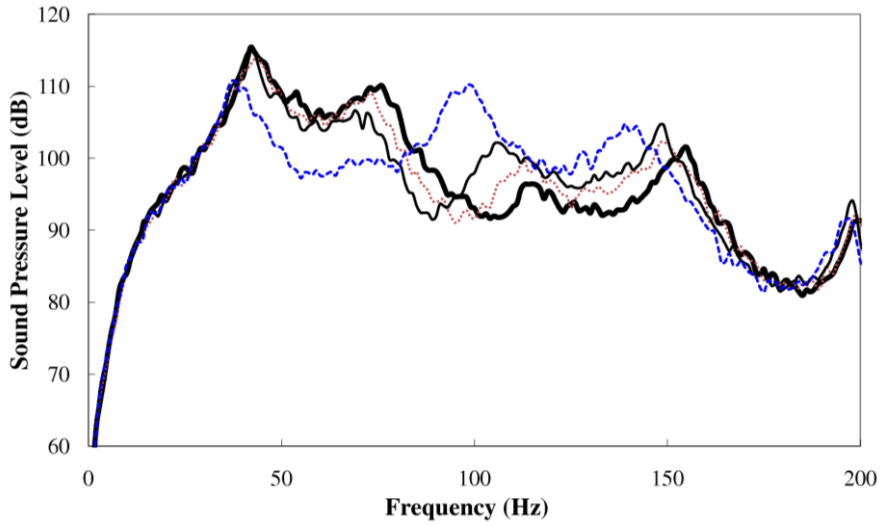

Figure 7-12: Comparison of the sound pressure level at a distance of 350mm from the duct end with the cloth membrane (constant X-direction tension); ▬▬ ,1 unit Y-direction tension; ····· , 1/2 unit Y-direction tension; ——— ,1/3 unit Y-direction tension; – – –, Y-direction tension free.

Figure 7-13 shows that the magnitude of the frequency response changes with the magnitude of the membrane tension. When applying the Y-direction tension free

membrane at the testing duct end, the resonant peak is at around 65Hz. The resonances shifted to the higher frequencies when applying higher Y-direction tension. The duct system has resonant peaks at 80Hz, 100Hz and 110Hz for membrane with 1/3 unit, 1/2 unit and 1 unit Y-direction tension respectively.

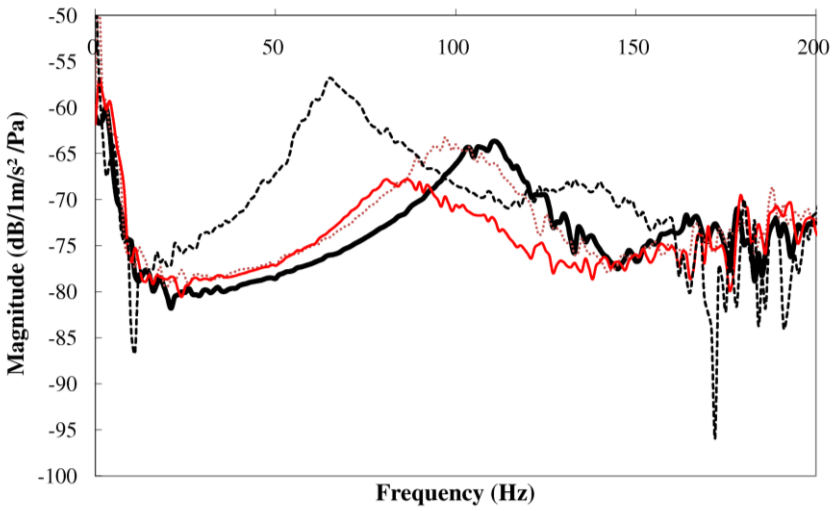

Figure 7-13: Comparison of the frequency response (magnitude) of the duct ended with the cloth membrane (constant X-direction tension); ▬▬ , 1 unit Y-direction tension; ····· , 1/2 unit Y-direction tension; ——— ,1/3 unit Y-direction tension; – – – , Y-direction tension free.

7.4.2 The calculation of the resonant frequency for a free-vibrating rectangular membrane with fixed rims

An elastic two-dimensional solid medium which has the shape of planar domain

in the rest state and whose potential energy in the process of oscillation is proportional to the increment of its area is called a membrane. To obtain the simplest equation of motion, assumptions about the physical properties of the membrane will be required. The membrane is assumed to be thin and uniform with negligible stiffness, to be perfectly elastic with no damping, and to vibrate with small displacement amplitudes. Boundary conditions must include not only the type of support and also the shape of perimeter of the membrane.

Let ρ_s be the surface density of the membrane (mass per unit area) expressed in kg/m² and τ be the membrane tension per unit length in N/m so that the material on opposite sides of a line segment of length dl will tend to be pulled apart with a force τdl. The tension is assumed to be distributed uniformly throughout the membrane.

The equation of motion will be developed in Cartesian coordinates with the transverse displacement of a point expressed as $y = y(x, y, t)$. The force acting on a displaced rectangular surface element of area $dS = dxdz$ is then the sum of the net transverse forces acting on the edges parallel to the X and Z axes.

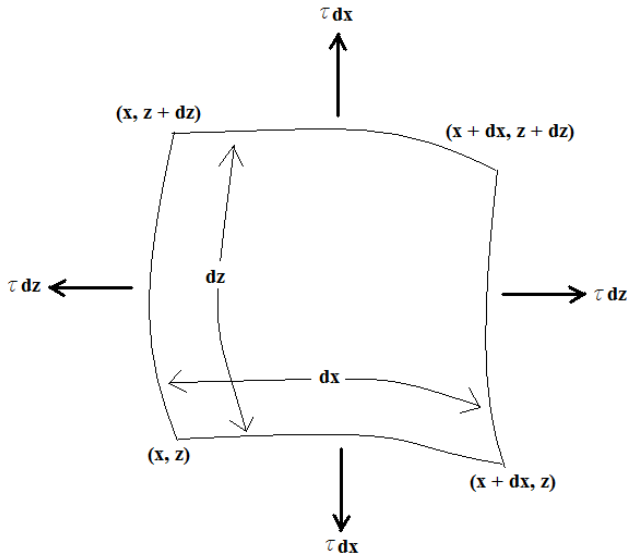

Figure 7-14: Element of a vibrating membrane.

From the incremental area of the membrane shown in Figure 7-14, the net force on the element *dxdz* due to the pair of tension *τdz* is

$$\tau\, dz\left[\left(\frac{\partial y}{\partial x}\right)_{x+dx} - \left(\frac{\partial y}{\partial x}\right)_{x}\right] = \tau \frac{\partial^2 y}{\partial\, x^2} dxdz$$

The net force due to the pair of tensions *τdx* is $\tau(\partial^2 y / \partial\, z^2)dxdz$.

Equating the sum of these two terms to the product of the element's mass $\rho_s\, dxdz$ by its acceleration $\partial^2 y / \partial t^2$ gives

$$\tau\left(\frac{\partial^2 y}{\partial\, x^2} + \frac{\partial^2 y}{\partial\, z^2}\right)dxdz = \rho_s dxdz \frac{\partial^2 y}{\partial\, t^2}\text{, or} \tag{7-1}$$

$$\frac{\partial^2 y}{\partial\, x^2} + \frac{\partial^2 y}{\partial\, z^2} = \frac{1}{c^2}\frac{\partial^2 y}{\partial\, t^2} \tag{7-2}$$

$$\text{where} \quad c = \sqrt{\frac{\tau}{\rho_s}} \tag{7-3}$$

Equation (7-2) can be expressed in a general form, appropriate to any coordinate system, as

$$\nabla^2 y = \frac{1}{c^2}\frac{\partial^2 y}{\partial t^2} \tag{7-4}$$

where ∇^2 is the Laplacian operator, two-dimensional in this case.

In the Cartesian coordinates used above, the Laplacian is expressed as $\nabla^2 = \frac{\partial^2}{\partial x^2} + \frac{\partial^2}{\partial z^2}$ where this form is appropriate for rectangular membranes.

For calculating normal modes it is conventional to recast Equation (7-4) by assuming the solution:

$$y = \Psi e^{jwt} \tag{7-5}$$

where Ψ is a function only of position.

Substitution into Equation (7-4) and the definition of $k = \omega / c$ yields

$$\nabla^2 \Psi + k^2 \Psi = 0 \tag{7-6}$$

which is the Helmholtz equation. The solutions of Equation (7-5) and Equation (7-6) for a membrane of specified shape and boundary conditions are the normal modes of vibration of that membrane.

Assume a stretched membrane fixed at its edges at x = 0, x = L_x, z = 0, and z = L_z.

The appropriate boundary conditions are

$y(0, z, t) = y(L_x, z, t) = y(x, 0, t) = y(x, L_z, t) = 0$

Let us assume a solution of the form $y(x,z,t) = \Psi(x,z)e^{j\omega t}$, so that Equation (7-2) reduces to the Helmholtz Equation (7-6) in Cartesian coordinates,

$$\frac{\partial^2 \Psi}{\partial x^2} + \frac{\partial^2 \Psi}{\partial z^2} + k^2 \Psi = 0 \tag{7-7}$$

Furthermore, let us assume that Ψ is the product of two functions, each dependent on only one of the dimensions, $\Psi(x,z) = X(x)Z(z)$, then Equation (7-7) becomes

$$\frac{1}{X}\frac{d^2 X}{d x^2} + \frac{1}{Z}\frac{d^2 Z}{d z^2} + k^2 = 0 \tag{7-8}$$

The first term in this expression, being a function of x alone, is independent of z. Therefore, the second term must also be independent of z; otherwise the three terms cannot sum to zero for all z. The first two terms must thus each be constant for all x and z. This results in the pair of equations

$$\frac{d^2 X}{d x^2} + k_x^2 X = 0 \quad and \quad \frac{d^2 Z}{d z^2} + k_z^2 Z = 0 \tag{7-9}$$

where k_x^2 and k_z^2 are the respective constants related by $k_x^2 + k_z^2 = k^2$

Solutions of Equation (7-9) are seen to be sinusoids, so that

$$y(x, z, t) = A\sin(k_x x + \varphi_x)\sin(k_z z + \varphi_z)e^{jwt} \tag{7-10}$$

where φ_x and φ_z must be determined by the boundary conditions and $|A|$ is the maximum amplitude of transverse displacement. For the case in question, the

conditions y(0, z, t) and y(x, 0, t) yield $\varphi_x = \varphi_z = 0$, and the conditions y($L_x$, z, t) and y(x, L_z, t) require sin $k_x L_x = 0$ and sin $k_z L_z = 0$. Thus, the normal modes of vibration are given by

$$y(x, z, t) = A \sin k_x x \sin k_z z \, e^{jwt} \tag{7-11}$$

where

$k_x = n\pi / L_{x,}$ n =1, 2, 3, …

$k_z = n\pi / L_{z,}$ n =1, 2, 3, …

Equations (7-10) and (7-11) are seen to limit each of the constants k_x and k_z to a discrete set of values. These limitations, in turn, restrict the characteristics frequencies for the allowed modes of free vibration to

$$f_{nm} = \frac{\omega_{nm}}{2\pi} = \frac{c}{2}\sqrt{\left(\frac{n}{L_x}\right)^2 + \left(\frac{m}{L_z}\right)^2} \tag{7-12}$$

For the case in our experiment, we have different tension values applied to X and Y directions, by $c = \sqrt{\frac{\tau}{\rho_s}}$ Equation (7-3), we have $c_1 = \sqrt{\frac{\tau_1}{\rho_s}}$ and $c_2 = \sqrt{\frac{\tau_2}{\rho_s}}$ for X and Y directions respectively. Substituting c_1 and c_2 into Equation (7-12), we have the frequencies for the membrane with different tension values applied to X and Y directions which is:

$$f_{nm} = \frac{1}{2}\sqrt{c_1^{\,2}\left(\frac{n}{L_x}\right)^2 + c_2^{\,2}\left(\frac{m}{L_z}\right)^2}$$
$$= \frac{1}{2}\sqrt{\left(\frac{\tau_1}{\rho_s}\right)\left(\frac{n}{L_x}\right)^2 + \left(\frac{\tau_2}{\rho_s}\right)\left(\frac{m}{L_z}\right)^2}$$
$$= \frac{1}{2\sqrt{\rho_s}}\sqrt{\frac{\tau_1 n^2}{L_x^{\,2}} + \frac{\tau_2 m^2}{L_z^{\,2}}}$$

For the test in the duct system, $L_x = L_z = 0.105$m, $\rho_s = 0.399$kg/m² and by substitution of $n = m = 1$, the fundamental frequency is

$$f_{nm} = \frac{\sqrt{\tau_1 + \tau_2}}{2\left(\sqrt{0.399}\right)(0.105)} \tag{7-13}$$

Knowing the resonant frequencies which are 65Hz, 80Hz, 100Hz and 110Hz from Figure 7-13, by Equation (7-13), the tension values in both X and Y directions can be calculated and the results are shown in Table 7-1 and Figure 7-15. It can be seen from Table 7-1 that the higher the resonances, the higher will be the Y-Direction tension calculated while keeping the same X-direction tension. Figure 7-15 shows us that the Y-Direction tension is directly proportional to the resonant frequency. The comparison of the relative experimental and calculated Y-direction tension values for different resonant frequencies is shown in Table 7-2. The relative experimental and calculated Y-Direction tension values (in Units) are very similar for each resonance which further proves the validity of the Equation (7-13) in calculating the resonant

frequency of membrane with different X and Y direction tensions applied to it.

Resonant Frequency (Hz)	Tension (N) X-direction	Tension (N) Y-direction
65	74	0
80	74	38
100	74	91
110	74	142

Table 7-1: Tension in X-direction and Y-direction for different resonant frequencies

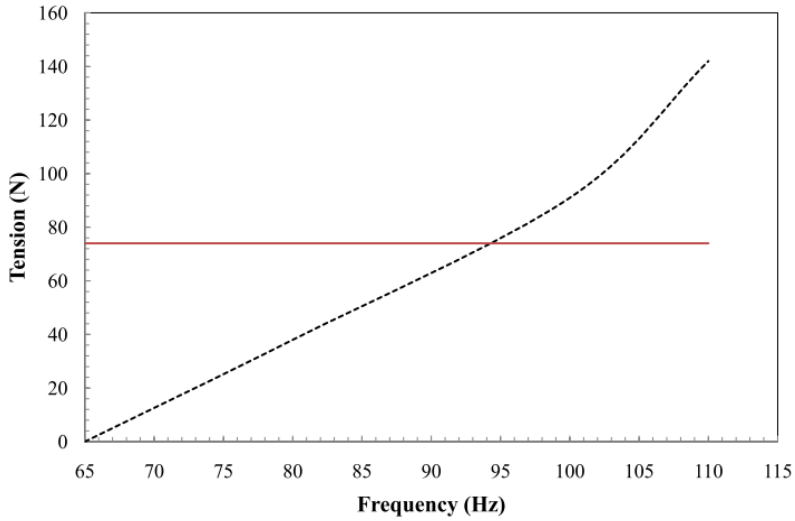

Figure 7-15: Tension against resonant frequencies;
———, X-direction; – – –, Y-direction.

Resonant Frequency (Hz)	Experimental Tension Values (Unit)	Calculated Tension Values (N)	Dividing the Calculated Tension Values by 142 (N)
65	0	0	0
80	0.333	38	0.28
100	0.5	91	0.64
110	1	142	1

Table 7-2: Comparison of the relative experimental and calculated Y-direction tension values for different resonant frequencies.

7.5 Summary

Experiments proved that using large intensities will change the impedance due to the non-linear effects. Non-linear vibration of membrane has adverse effects on noise reduction. To further improve the accuracy of the experimental results, strain gauges and a force transducer are used instead of accelerometers to measure the vibration amplitude of the membrane due to its negligible weight. Increasing the tensile strain of the membrane will increase the resonant frequencies. Membrane absorber can be used to reduce infra-sound reported in Chapter 6 by adjusting the tension of the membrane. There is not necessary to have an enclosed cavity behind membrane. An appropriate tensioned membrane can have some degree of stiffness which is beneficial to the building structure.

CHAPTER 8

DISCUSSION

8.1 Introduction

Cooling strategies have been used for centuries in warm climates; however, research concerning passive cooling strategies is relatively new (Hyde, 2008). It was only at the beginning of the 1980s that interest in cooling increased, by which time the use of air-conditioning systems had already become standard in most warm countries. There are a number of possible reasons for this more recent interest in natural cooling systems; certainly, the increase in energy prices as well as the environmental damage done to ecological cycles has played a significant role in refocusing attention in this area. Bioclimatic strategies can be used to lower the inner temperature of buildings to temperatures near annual average outer temperatures.

The need for daylight and noise abatement can have a significant bearing on the use of passive cooling systems. For example, the use of highly effective shading can reduce daylight, while the extensive use of roof lights can admit unwanted heat through flues. Furthermore, the external acoustic environment may require ventilation if there are high levels of unwanted intrusive noise. This explains the need to investigate strategies for noise abatement. There are strategies to mitigate external

noise including using longer separation distances, avoiding zones of directional sound and screening. It has been established, as a general rule, that a given barrier will be most effective when it is as near to the source of noise as possible. The second best position is near the building that is to be protected, while the least effective position is halfway between the source and the building. Screening or barriers in the path of sound can create an 'acoustic shadow' if the sound is of a high frequency. At low frequencies, diffraction will occur at the edge of the barrier; thus the 'shadow' effect will be blurred. If the dimensions of the barrier are less than the wavelength of sound, the shadow effect disappears. Since at 30Hz the wavelength is over 10m, any barrier less than 10m will be ineffective for such low frequency sounds. For rooms with absorbent surfaces, from the viewpoint of inside noise, the situation may be somewhat better since sound will not be reflected from bounding surfaces and there will be no build-up of reverberated sound. Absorption is not very effective at reducing noise penetration as absorptive fibrous materials are mostly vulnerable and, when exposed to changing climatic conditions, may deteriorate.

When it comes to the issue of room lighting, window size should also be considered. The size of a window also strongly affects the first impression of a space. Increasing the window area by up to 50 per cent increases the light level, while also

reducing the luminance contrast and improving visual comfort. Both the increased absolute amount of light and reduced luminance contrast gives a better first impression upon entering such a space. Light levels are markedly higher in a space with light-coloured surfaces as they maximize the impact of daylight.

It is, therefore, important to take into consideration satisfactory amounts of both daylight and noise reduction when considering natural cooling systems for buildings.

8.2 Summary of major findings

Sound can enter buildings through ventilation ducts. Silencers were applied in ventilation ducts to achieve sound reduction and were designed as different types of vibrating panel absorbers: long panels and divided panels. There was a shift in the resonant frequency when using divided panels instead of long panels. The divided panels obtained best sound reduction in the frequency range from 330Hz to 420 Hz with higher peak values. Unfortunately, the panel absorber system with the transparent plastic sheet was ineffective at reducing sound below 250Hz and above 600Hz. However, broadband noise reduction was achieved in a test using the duct combing effect of a muffler and panel absorbers of various sizes.

The broadband sound reduction performance of the panel absorber system using divided panels with two layers, a transparent plastic membrane and a micro-perforated Plexiglas sheet, was also explored. The new optimized structure extends the absorption to lower frequencies as well as maintaining good mid-frequency absorption, and hence becomes a considerably better broadband absorber. Similarly, the new structure cannot work effectively below 200Hz and above 1500Hz. A muffler can be used to help eliminate high frequency sound because of the large ratio of inlet/outlet cross-sectional area to the pathway cross-sectional area between the panel absorbers of the silencer.

Another major finding relates to low frequency sound generated by cavity/ Helmholtz resonance in rooms connected to ventilation openings. If ventilation openings exist in a room, it is possible for air flow to generate an infrasound of a significant magnitude in the openings to irritate the people inside. Helmholtz resonance can be controlled using a membrane structure that is either cavity backed or not. There were significant improvements in low frequency sound reduction when the Helmholtz resonance of the ventilation openings matched with the membrane vibrating resonance. Non-linear vibration of the membrane will have an adverse effect on sound reduction and an appropriately tensioned membrane can have some

degree of stiffness, which is beneficial to the building structure. It is important to choose a membrane with the appropriate tension and at the same time avoid non-linear vibration.

8.3 Significance and applications

While there is a definite trend towards natural ventilation, it is important to ensure suitable ventilation without allowing unbearable noise to enter. The panel absorber systems described in Chapter 2 and Chapter 3 can be used as silencers in common ventilation ducts. They can also be installed in the inlets and outlets of solar chimneys (See Appendix I) or in the ventilation ducts of double skin façade (DSF) buildings (See Appendix II). Compared to the conventional silencer, the silencer with vibrating panel absorbers can absorb medium to high frequencies while also being able to absorb low frequencies. The sound reduction bandwidth was extended from about 100Hz to 1600Hz using the new two-layered panel absorber system, which uses a plastic membrane and a micro-perforated Plexiglas sheet. Frequencies for which panel absorbers cannot achieve sound reduction, such as the frequency range above 1600Hz, can be eliminated by the muffler effect of the testing duct containing

panel absorbers. The Plexiglas sheet and the plastic membrane are fibre free and offer clean and smooth surfaces. Fibre-free sound absorbers ensure a better indoor environment, especially for children and people with respiratory disorders. In addition, the panel absorber system does not absorb moisture, which eliminates fungi and rot. These benefits reduce costs related to sick leave, loss of productivity and maintenance of facilities. Dust from porous materials can be inflammable and create life-threatening hazards because of limited visibility and breathing difficulties in a fire emergency. Furthermore, the use of fibrous materials within the silencers can result in a poor durability of acoustic performance due to weathering and deterioration in the quality of the fibre quality. The panel absorber system that is made of Plexiglas and plastic, therefore, can be maintained easily and have a longer product lifetime compared to conventional fibrous absorbers.

Membrane type absorbers can be applied to rooms to control Helmholtz resonance, which is generated in ventilation openings in rooms, so as to achieve sound reduction in limited spaces. The construction of DSF buildings is one the latest examples of green buildings with ventilation openings in rooms. In these buildings, ventilation openings or ducts connect each floor (Loncour et al., 2004). Noise from

outside, for example traffic noise, can enter rooms; indeed even human conversation from rooms nearby can be transmitted through openings to other rooms and both can affect the working environment. The concrete duct in Chapter 6 can simulate the effect of Helmholtz resonance due to a small opening inside the DSF cavity (Figure 8-1). Infrasound may be generated due to air flow in the openings. Membrane structures can be placed on an end wall or a side wall or on a walkway to reduce the infrasound inside the cavity (Figure 8-1).

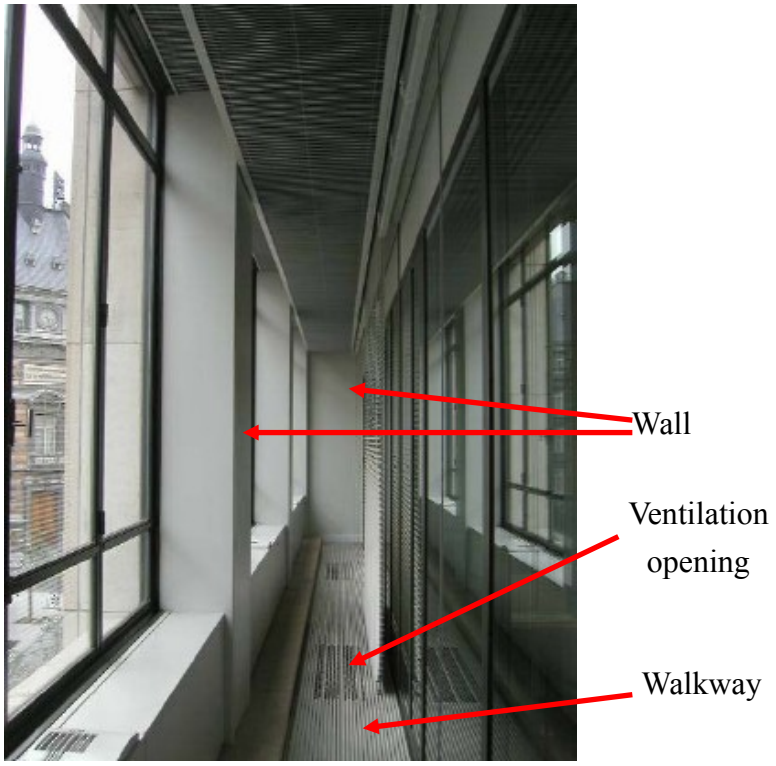

Figure 8-1: Cavity with permanent ventilation openings – membrane can be applied on walls or walkways

Both the silencer and membrane structure are designed to reduce noise inside green buildings with solar stack ventilation effect or double skin façades which promote natural cooling.

Some green groups have pointed out that indoor air pollution is very poor in Hong Kong. Most indoor public places in Hong Kong are air-conditioned with sealed designs where the windows cannot be opened. As a result, poor ventilation occurs in office buildings, shopping centres and on public transport. Occupants inside buildings with poor indoor air quality display symptoms such as headaches, eye or nose irritation, dizziness, difficulty in concentrating and sensitivity to odours. More seriously, there is an increase in the incidence of asthma attacks and personality changes such as depression. As a result of these impacts of poor air quality, natural cooling systems should be widely adopted in buildings in Hong Kong.

Recently, an increasing number of cases of the human swine influenza (H1N1) virus infection have come to light in many countries around the world, with a number of suspected cases of swine flu having been reported in Asia. With such poor ventilation inside buildings, there will be a high risk for serious human-to-human transmission of swine flu to occur once H1N1 reaches Hong Kong. The use of natural ventilation to induce the circulation of fresh air can help prevent the spread of

viruses. Fans can also be used to help generate higher airflow rates across rooms. Air-conditioners should be avoided in cool seasons so as to save energy and prevent the accumulation of harmful gases inside rooms.

8.4 Limitations

There are several limitations to this study that restrict the generalization of its results. The most apparent limitation of the study lies in the lack of a real scale room for testing the performance of vibrating panel absorbers and membrane structures. Real scale rooms should be used to improve the accuracy of the data collected.

Strain gauges were used to investigate the strain behaviour of the vibration membrane (Chapter 7); however the use of lasers to measure the vibration of the membrane would improve the accuracy of the results, but the technology is expensive. There are also many precautions that need to be taken when using lasers. It is accepted that even low-powered lasers with only a few milli-watts of output power can be hazardous to the human eye if the beam from such a laser hits the eye directly or after reflection from a shiny surface. At wavelengths at which the cornea and the lens focus well, the coherence and low divergence of laser light means that it can be focused by the eye onto an extremely small spot on the retina, resulting in

localized burning and permanent damage in seconds or even less.

8.5 Conclusions

Building designs nowadays consider not only noise reduction and aesthetic performance, but also sustainability. Buildings with the double skin façade or using the solar stack ventilation design to achieve natural cooling are the latest examples of sustainable buildings for energy saving. Few researchers combined natural cooling, noise reduction and aesthetic performance together in building designs. The gap can be narrowed using the results in this study.

In this research, noise reduction structures in buildings with chimney or double skin façade are investigated. They are: (1) silencer with combined cavity and membrane absorbers in parallel to control noise in a ventilation duct; (2) membrane absorber to control Helmholtz resonance in a ventilation space or room. One major finding is the broadband sound reduction ability of the silencer using panel absorber system with both transparent plastic sheet and micro-perforated Plexiglas sheet. A formula with a satisfactory accuracy is derived for the two-layered panel absorber system. By adjusting the sizes of the panel absorber, the silencer effect can be obtained for wider frequency range. Another major finding relates to the generation

of infrasound (below 20Hz) by airflow in small ventilation openings connected to rooms. Infrasound cannot be reduced by absorption materials in a small ventilation opening; neither can it be reduced by placing silencers inside the opening or changing the size of the opening. Helmholtz resonator also cannot reduce that infrasound either due to the large cavity required. Fortunately, as this study has shown, it can be reduced by a membrane absorber. There were significant improvements in low frequency sound reduction when the Helmholtz resonant frequency of the ventilation opening matches with the membrane vibrating resonant frequency.

Therefore, the new silencer design and membrane absorber have been proved to achieve desirable broadband noise reduction, offer excellent aesthetical properties and at the same time provide a healthier indoor environment in sustainable buildings.

APPENDIX I

INTRODUCTION OF SOLAR CHIMNEY AND ITS APPLICATIONS

A. The working principle of solar chimneys

A solar chimney is a channel that is glazed on the sunny side and is blacked with a collector wall. It is situated at the top of the room, which should be ventilated. The added height and temperature difference combine to significantly increase airflow, if designed correctly. If there is an opening high in the building and another low in the building, a natural flow will be induced; this is called the stack effect. The sun-warmed air in the duct increases the natural stack effect; therefore, the solar collector is useful in extracting warm room air, which ideally is replaced by cooler air from the shady side of the room.

B. Advantages of using solar chimneys

Solar energy is free. It needs no fuel and moving parts, the whole solar chimney systems are clean and silent. In some sunny countries, solar power can be used where there is no easy way to get electricity to a remote place. Electricity consumption can thus be saved. Most importantly, there is a growing awareness in many parts of the world that some alternative energy sources could have an important role to play in

the production of electricity. However, only the solar energy represents totally nonpolluting inexhaustible energy resource that can be utilized economically to supply man's energy needs for all time. Airflow rates of 0.25m per second and 0.4m per second can be achieved. Night ventilation is also possible

C. Drawbacks of using solar chimneys

During a sunny day, a solar chimney is efficient; in overcast weather, it is less effective but still helps to discharge room air due to the height difference and stack effect. It should be noted that during the design of these elements, a common concern is that the chimney exhaust is too close to the roof, causing problems with the system's effectiveness.

D. Limitations

Occupants must tolerate higher indoor temperatures and more variable ventilation rates than with an electric fan system. During winter conditions, building heat losses may be substantial. Insulated dampers are expensive and are difficult to make airtight.

E. Overseas applications of solar chimneys

E1. Mildura, Australia – Power Plant

The solar chimney in Mildura, Australia (Figure 1) which is one kilometer high is set to be the tallest human made structure in the world. It is set to be the first large-scale attempt to convert solar energy into non polluting electricity.

Solar chimney power stations are particularly suitable for generating electricity in deserts and sun-rich wasteland. No fuel and no cooling water are needed. It provides electricity 24 hours a day from solar energy alone. The material concrete, glass and steel necessary for the building of solar chimney power stations are everywhere in sufficient quantities. Most importantly, it causes no ecological harm.

Details of the solar chimney are as follows:

Type: Solar tower power plant with steel reinforced concrete tower and steel/glass solar air collector.

Features: The base of the tower is 200m. The chimney is a very simple tube with wall thickness of 25cm, diameter of 150m and a height of 1000m.

Power: Up to 500 Giga watt hours per year

The solar chimney system consists of three parts: the collector, chimney and turbines. The collector is the part which is used to produce hot air by green- house effect. The larger the area, the more energy generated from the chimney. The chimney acts as a thermal engine. Turbines are used to convert air current to the mechanical energy.

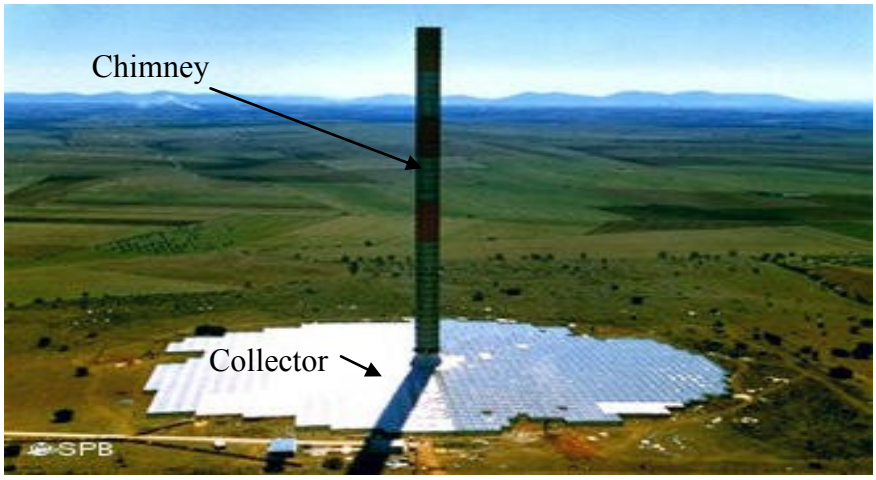

Figure A-1: The Prototype Manzanares Solar Chimney in Australia

E2. Reichstag, Berlin, Germany

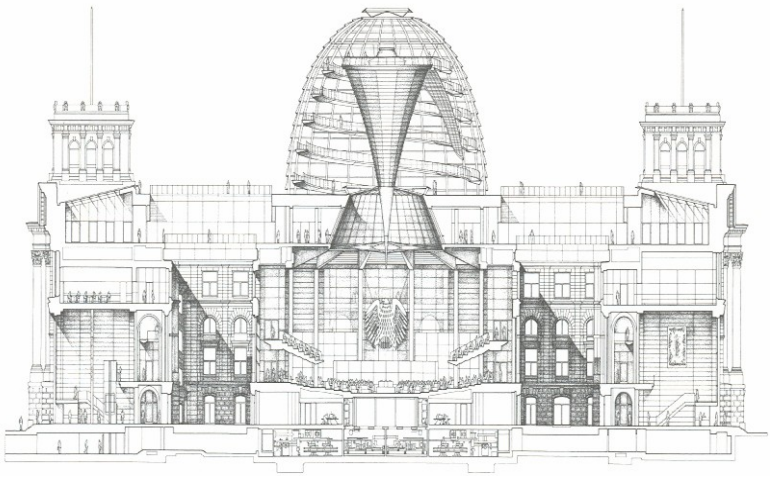

The system is based on the traditional solar chimney and the natural rising of the heated air, encouraged by the “flue” effect of the cone and cupola, is sufficient to maintain the whole process of air circulation. Prevailing winds in Berlin are from west and bring in cool, fresh air. The fresh air intake is conducted via large ducts into a plenum beneath the debating chamber. The air is warmed by various heat sources like lighting and the people in the chamber, air rises to the ceiling and further drawn into funnel-shaped cone. Waste air is emitted at the top of the cone and escapes through the eight-meter-diameter opening in the cupola (Figure 2). The lantern opening is fitted with a wind spoiler to encourage air flow across the top of the cupola (Figure 3) and facilitate the extraction process.

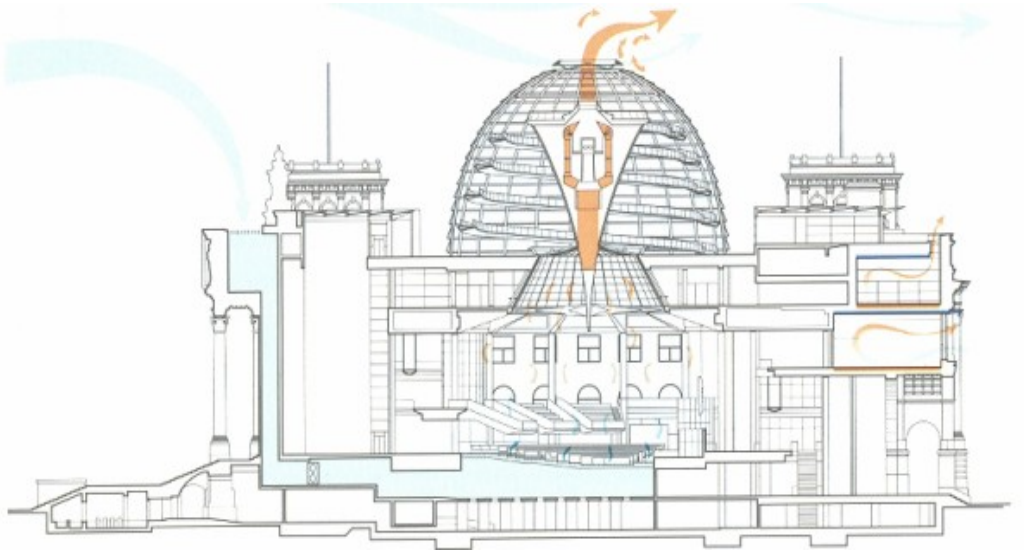

Figure A-2: The natural ventilation of the chamber based on the solar chimney, enhanced by the flue shape of the cone.

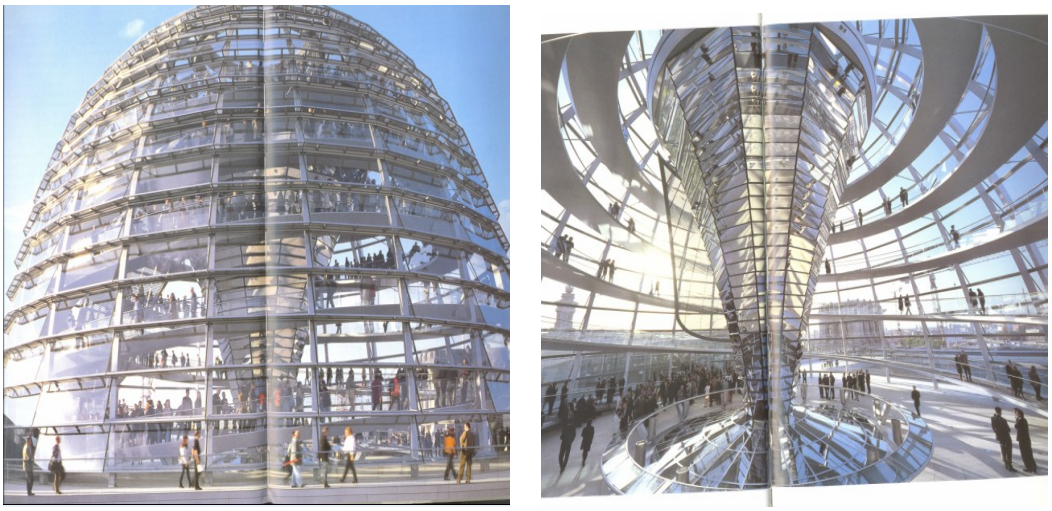

Figure A-3: (a) The cupola with 40m diameter at its base; (b) the glazing allows visitors on the 230m long spiraling ramps an unimpeded view over Berlin

Advantages of solar chimney in Reichstag:

The original design of a huge canopy over the building was justified by the advantages it would bring in terms of day lighting and ventilation. The Reichstag's advance energy-saving system relies on natural light, solar energy, natural ventilation and renewable bio-fuel. Natural warm and cold-water aquifers store surplus energy 300 and 60 meters below ground. The exploitation of natural light is reflected in the energy balanced by a clearly reduced consumption of electricity which would otherwise be necessary for artificial lighting. But the cupola also serves to ventilate the debating chamber via a ventilation system.

Drawbacks of solar chimney in Reichstag:

There is internal noise reflection and the noise due to Helmholtz resonance, sound absorbing material around the lower level of the debating chamber wall is therefore added to reduce the noise reflection due to glass.

The outside hot sunlight heats up the debating chamber .The original openings fitted with a system of intelligent window with two layers of glass are then used to balance out extreme fluctuations of temperature. The inner window can be opened from the inside either manually or automatically. The outer layer is laminated with a protective coating and has ventilation joints which admit air from the outside. The void between houses acts as a solar shading device.

E3. Combining with the mechanism of double skin façade

Solar chimney is considered above the double skin space to strengthen the stack effect (Figure 4 and 5). Increasing the height of the solar chimney makes more ventilation rate and also is profitable to obtain favouable pressure difference distribution.

Double skin façade consists of three parts: an external façade, an immediate space and an inner façade. The external façade can protect against the weather and

improve acoustic insulation against external noise. Air in the immediate space is warmed up due to solar radiation. Flow of air through the immediate space is activated by the stack effect.

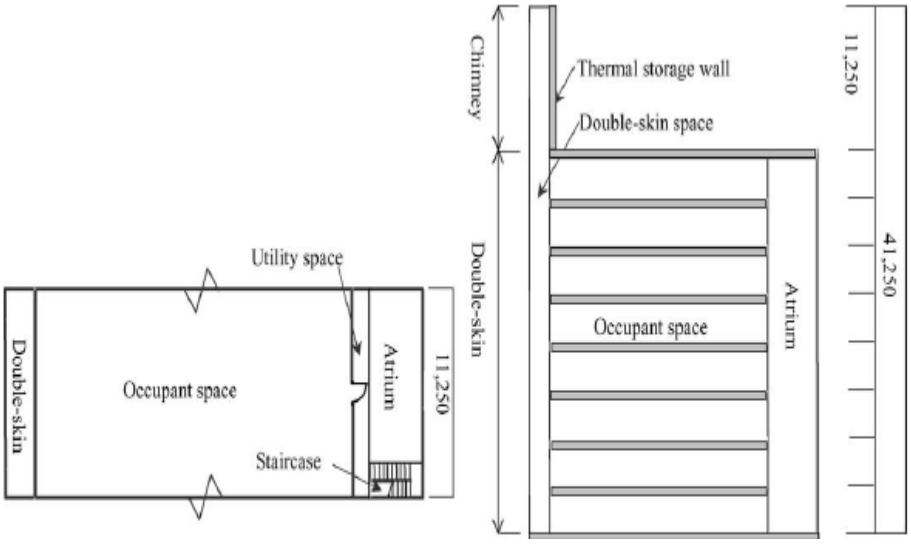

Figure A-4: Outline of the prototype building (units: mm)

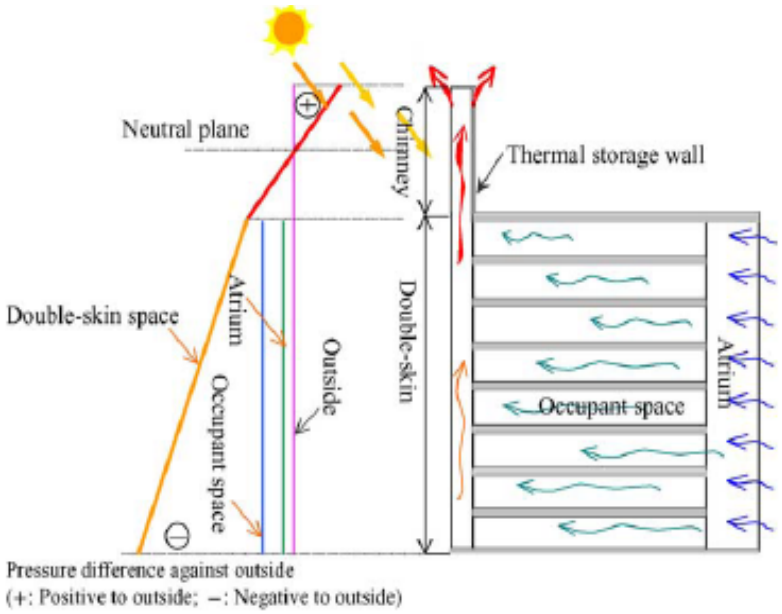

Figure A-5: Concept of natural ventilation in the prototype building

Figure A-6: Picture of the experimental model

E4. Floating solar chimney

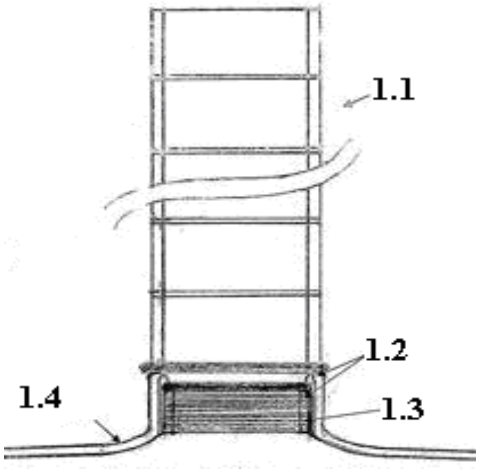

The floating solar chimney is composed by three parts: the main chimney (1.1), the heavy base (1.2) and the folding lower part (1.3). The main chimney is composed by cylindrical balloon rings full of non flammable light gas. This cylindrical balloon rings are tied up between them with the help of supporting rings so that they form a

compact thermo insulated cylindrical chimney.

The solar chimney in this conventional system is manufactured by reinforced concrete. This has the following consequences: High manufacturing cost and limited height of the solar chimneys due to technological restrictions from the construction materials and from exterior limitations such as earthquakes. It is known that the output of such a power station is approximately proportional to the product of the height of solar chimney to the area of the collaborating solar collector. Thus for a given power output from such a solar power station the height of the solar chimney determines the area of its collaborating solar collector. The floating solar chimney is invented to eliminate all pre-mentioned disadvantages by increasing, for a given power output, the height of the solar chimney and decreasing their construction cost and the area of the solar collectors and therefore the total cost of the respective power plant of electricity.

F. Summary

As using solar energy have many advantages as mentioned above, it is becoming more and more popular to use solar energy in order to achieve a non polluted environment. The design of solar chimneys should ensure that the extract stack is as

high as possible above the roof. The exterior of the chimney should be dark to increase the air temperature within. Side openings in the chimney should be avoided in order to prevent potential backward flow. Solar access can be provided, and in such cases the interior surface of a transparent chimney facing the sun acts as an absorber and should be painted black. Inlet openings should be placed to let cold air inside the house, and should be located on a room's windward side to obtain more ventilation pressure due to the prevailing wind. Solar chimneys are useful in low-rise buildings in climates with a high average solar radiation. The channel should be as high as possible and the collector area should be large in order to maximize airflow.

The benefit of using solar chimney to have satisfactory ventilation has already been proved. Other than solar chimney, rooms with high ceilings can also help natural ventilation. These rooms can benefit from airflow derived through stack effects. Good effects can be achieved if the rooms are at least two storeys high. Alternatively, the rooms can be coupled with an open stairwell or tall atria.

APPENDIX II

INTRODUCTION OF DOUBLE SKIN FAÇADE AND ITS APPLICATIONS

A. Introduction

There is a need for a sustainable development in Hong Kong's built environment (Hui, 2000). 53% of energy consumed in Hong Kong accounts for buildings (EMSD, 2005b). One of the most significant technologies for energy savings in a building is the double skin façade (DSF). A ventilated double skin facade can be defined as a traditional single facade doubled inside or outside by a second, essentially glazed facade. A ventilated cavity - having a width which can range from several centimetres at the narrowest to several metres for the widest accessible cavities - is located between these two façades. The ventilation of the cavity can be natural, fan supported or mechanical. There exist façade concepts where the ventilation of the cavity is controllable, by fans and/or openings, and other façade concepts where this ventilation is not controllable. The indoor and outdoor skins are not necessarily airtight. Automated equipment, such as shading devices, motorized openings or fans, are most often integrated into the façade. Apart from the type of the ventilation inside the cavity, the origin and destination of the air can differ depending mostly on climatic conditions, the use, the location, the occupational hours of the building and

the HVAC strategy.

B. Classification of the ventilated Double Façade

The classification worked out here takes into account the modes of working of the façade and introduces two criteria which are independent of one another:

B1. The type of ventilation;

B2. The partitioning of the façade;

B1. First classificatory criterion: The type of ventilation

- Natural ventilation: The two driving forces of natural ventilation are the differences in pressure created by the stack effect and by the effect of the wind.
- Mechanical ventilation: It is defined as being the ventilation with the aid of powered air movement components.
- Hybrid ventilation: It lies in a controlled compromise between natural ventilation and mechanical ventilation. The mechanical ventilation is only triggered when the driving forces of natural ventilation become inadequate and no longer make it possible to achieve the desired performances. A control system permits the shift from one type of ventilation to the other automatic and

controlled manner on the basis of a control algorithm.

B2. Second classificatory criterion: The partitioning of the cavity

Within the ventilated double facades, numerous possibilities of portioning are imaginable and an additional classification can be created. One observes that the partitioning solutions implemented in practice can be classified as follows:

- Ventilated double window: A façade equipped with a ventilated double window is characterized by a window doubled inside or outside by a single glazing or by a second window. From the partitioning perspective, it is thus a window which functions as a filling element in a wall.
- Ventilated double façade:
  - Partitioned by storey with juxtaposed modules: In this type of façade, the cavity is physically delimited (Horizontally and vertically) by the module of the façade which imposes its dimensions on the cavity.
  - The corridor type partitioned by storey (Figure 7 and 8): Corridor type ventilated double facades partitioned by storey are characterized by a large cavity in which it is generally possible to walk. While the cavity is physically partitioned at the level of each storey, it is not limited vertically,

and generally extends across several offices or even an entire floor.

Figure A-7: View of the large cavity and the louvers in vertical position

Figure A-8: Multi-storey naturally ventilated double façade

C. Benefits of double skin façade

The DSFs are touted as providing 30% reduction in energy consumption, providing for natural ventilation even in skyscrapers, and providing valuable noise reduction. They also provide the means to create a far more visually transparent architecture than that is possible with conventional curtain wall facades while improving occupant comfort. If the DSFs include dynamic sun shades in the cavity, they are usually deployed during the cooling season. Consequently, instead of heating the building interior, the solar radiation heats the air in the cavity, causing the air to buoyantly rise out of the cavity (Lee et al., 2002) (Stribling and Stigge, 2003). Thus, the DSF reduces the heat gain of the building. Because the buoyancy of the heated air increases with cavity height, DSFs are typically used in multistory buildings on one or more sides of the building that receive appreciable sun. In addition, when combined with operable windows that open into the air cavity, a DSF can provide natural ventilation to cool spaces adjacent to the DSF without mechanical cooling when the outdoor air enthalpy is less than the indoor air enthalpy (Kurt et al., 2007).

D. Seasonal change in performance of double skin façade

In addition to this continuous dynamic nature, there is also an unusual seasonal fluctuation in how the façade performs. During the cooling season, air is introduced into the cavity to carry away heat that would otherwise accumulate in the cavity. The temperature of the inner membrane is theoretically thus kept lower than it would otherwise be. This reduces the conduction, convection and radiation from the inner pane to the occupied space within. The result is that less heat transfers from the outside to the inside, and less energy is required to cool the space. Also, the occupant is more likely to be comfortable because the mean radiant temperature of the space is reduced. As the sun warms the air in the cavity, the stack effect is improved, so that relatively cool air is drawn in at the sill at an even faster rate as the temperature increases. Paradoxically, the heat of the sun thus contributes to the cooling of the façade.

E. Examples of double skin façade building in Hong Kong

Many architects and their clients prefer buildings with all-glass facades. There are a number of buildings incorporating DSFs in Hong Kong (Matthias et al., 2007). Examples are Kadoorie Biological Science Building, Building 5 of Hong Kong Science Park and Dragonair Building.

E1. The Kadoorie Biological Sciences Building

The Kadoorie Biological Sciences Building (Figure 9) is the first building in Hong Kong to fully exploit the green possibilities of a second skin: an external glazed screen which is 2.5m away from the external wall (Figure 10). The space between the double skins is not only used to accommodate the building services, but also used as an external buffer zone between the two layers of glazing, which acts as a stack that channels hot air upwards for discharge into the air, thus reducing the building's solar heat gain. An open metal grille installed at each floor allows free air circulation while serving as walkways for maintenance access. Heat gain is further reduced by locating heat emitting equipment in the external services zone outside the building, where they release their heat into the void rather than the interior. The design means that the building's air conditioning system is used only to cool the space and not to overcome solar heat gain, thus dramatically improving the system's energy efficiency.

Figure A-9: The Kadoorie Biological Sciences Building

Figure A-10: Exterior of the double skin façade

E2. Building 5 of Hong Kong Science Park

The double skin façade system on the west elevation of Building 5 of Hong Kong Science Park helps to shield traffic noise from Tolo Highway and reduce solar heat gain, while the double-glazed curtain wall system, sun shading devices and the metal roof also enhance the building's thermal and acoustic performance.

E3. Dragonair Building

The problem of aircraft noise in the Dragonair Building was addressed by the adoption of a double- skin cavity wall system which provides 60dBA of sound attenuation.

The features of these buildings were collated and analysed and the results show that considerable energy consumption savings (up to 9.18%) is possible. Double skin façades (DSFs) offer several advantages (Oesterle et al., 2001). They provide an additional layer that helps to reduce the acoustic impact on a building. Their cavities provide a space for positioning advanced sunshading devices that reduce heat gain but allow in natural daylight (Grabe, 2002). Allowing natural daylight to be filtered into a building for lighting appears to reduce the heat load for artificial lighting on air

conditioning (Bodart and Herde, 2002). Finally, the buoyancy flow in DSF cavities may reduce solar heat gain and also supports HVAC (heating, ventilation and air-conditioning) systems. This can help to minimize the size of such systems, thereby reducing the building's energy consumption (Andersen, 2003).

Perhaps the most common acclamation of the DSF is that they are energy efficient, but there is more to the story. They have also been installed for exterior sound reduction, user adjustability and occupant comfort, pollution avoidance, and nighttime security for operable windows. Occupant productivity is also increased. Other reasons include cost savings of reduced mechanical plant and reduced dependence on artificial lighting. Architectural benefits include transparency, and a "high-tech" image.

F. Precautions in the design of double skin façade

DSFs can reduce the transmission of outdoor noise sources into the building if the cavity entrances and exits are not too large. However, if the DSF provides natural ventilation, the magnitude of the required airflows tends to increase the size of the cavity entrances and exits and windows open into the cavity. As a result, outdoor sounds can more readily enter the cavity and sound transmission between spaces

with windows openings into the cavity increases. Other concerns about DSF performance include fire safety (fires spreading between floors via the cavity) and maintenance (keeping more glazing surfaces clean and dynamic shading operational) (Kurt et al., 2007). The reason for the DSF of not being popular in the world is its high cost. When there is extreme weather like too hot or too cold, natural ventilation is still a difficulty to fulfill.

APPENDIX III

PREDICTION OF THE ABSORPTION PERFORMANCE OF THE MEMBRANE BY COMPUTER ANALYSIS

A. Modeling of the air-block duct by the finite element analysis

Computer analysis was conducted on the vibrating cloth membrane (same cloth membrane as described in Chapter 4) attached at the end of the testing duct for sound absorption properties analysis using the finite element analysis. Air inside the duct was simulated as a long duct which consisted of many block-like elements. There were 100 blocks at the cross-sectional area and 10 blocks along the length. Restraints and springs were added to represent the air moving patterns inside the duct for the cases with the cloth membrane or not (Figure A-1 and A-2).

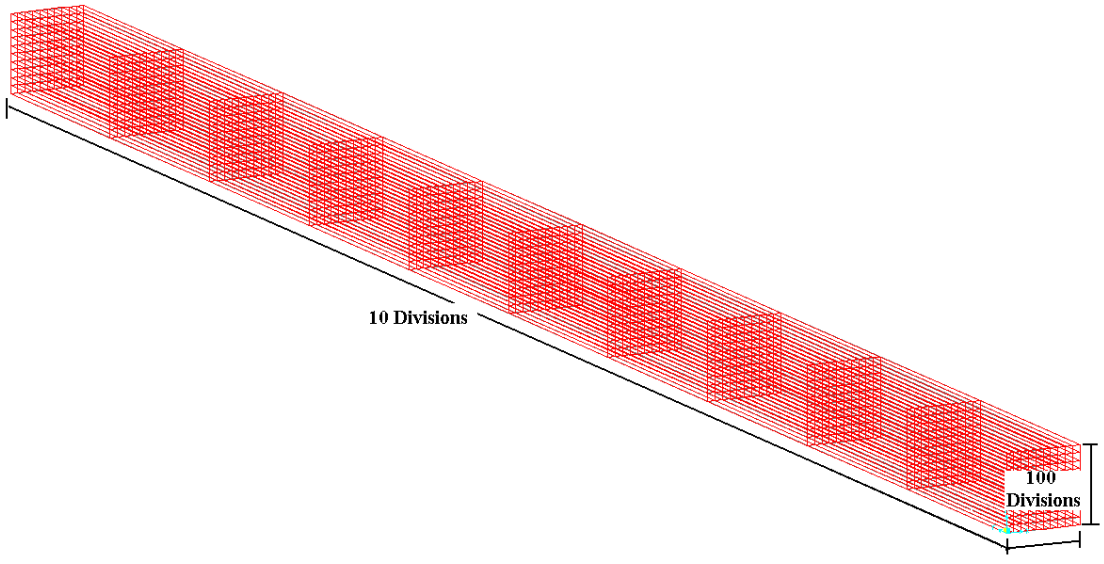

Figure A-1: Model simulating the air inside the duct which is divided into blocks

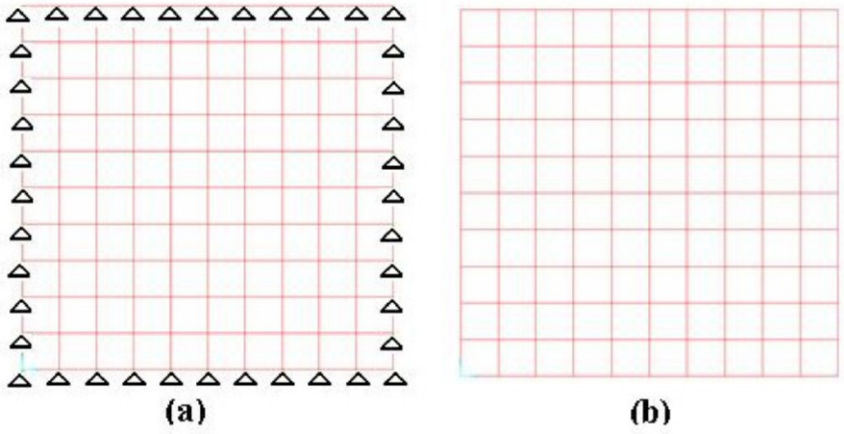

Figure A-2: Cross section at the duct end for the cases: (a) with a membrane (b) without a membrane (free end).

Computer programming was also used to demonstrate the sound pressure level measured at different joint positions along the air-block duct by adding forces at one end of the duct (Figure A-3). Since the velocity is proportional to the sound pressure level, thus velocity response measurement can be used to predict the sound pressure level at different positions. Figure A-4 and A-5 shows that the resonances are the same for all positions but the values is much higher at the end of the duct (Joint A) for the duct of both conditions.

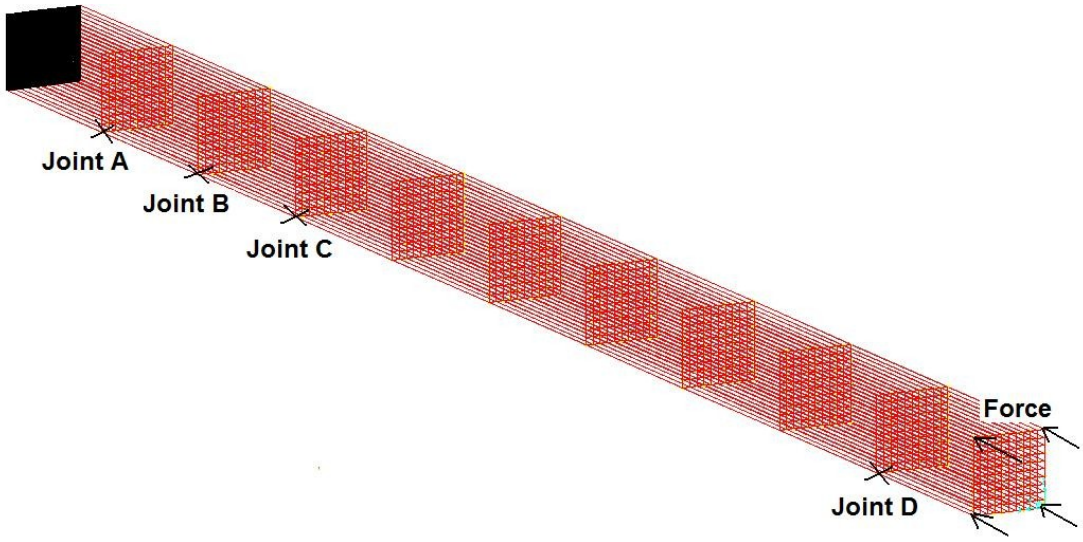

Figure A-3: Different joint positions on the computer model with the applied forces.

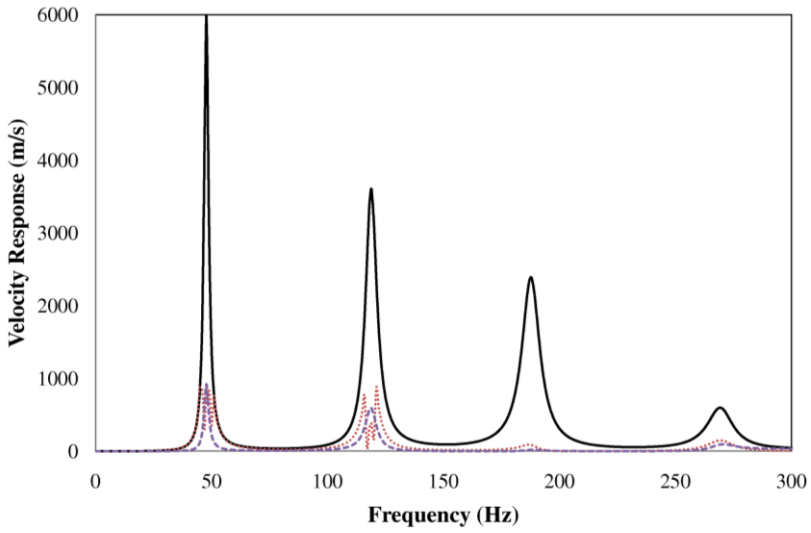

Figure A-4: Velocity response along the direction of the applied forces at different positions for the duct with free end;
——, Joint A, – – –, Joint B; ·····,Joint C.

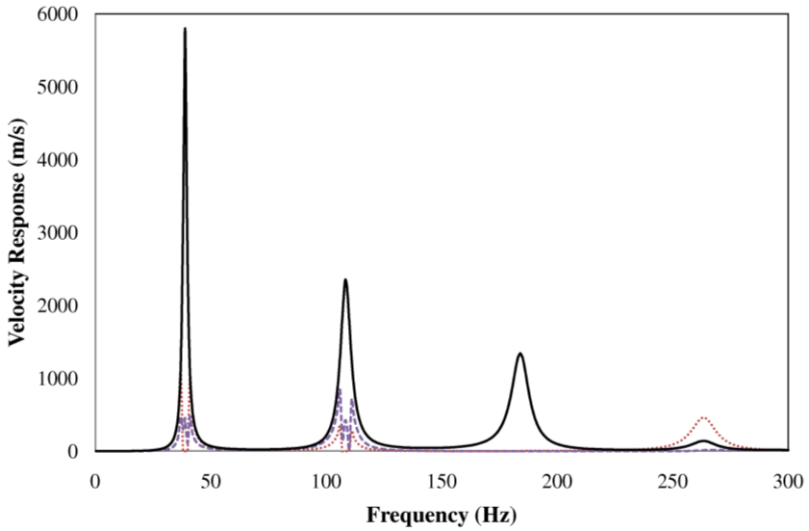

Figure 5: Velocity response along the direction of the applied forces at different positions for the duct with the membrane end; ——— , Joint A, - - - , Joint B; ····· ,Joint C.

By comparing the velocity response results of the air-block duct with and without a membrane, it can be observed that the velocity response peaks shift to the left for the case with a vibrating membrane (Figure A-6, A-7, A-8 and A-9).

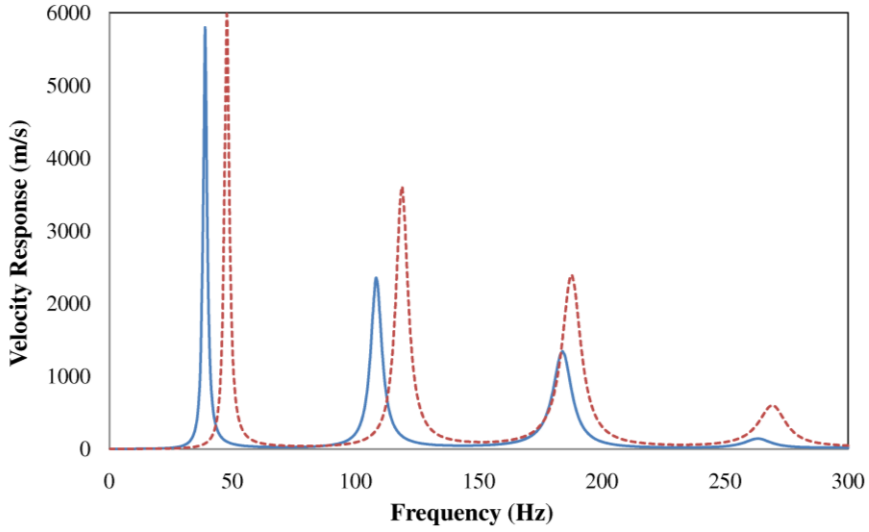

Figure A-6: Velocity response along the direction of the applied forces at Joint A for the duct; ———, membrane end, - - -, free end.

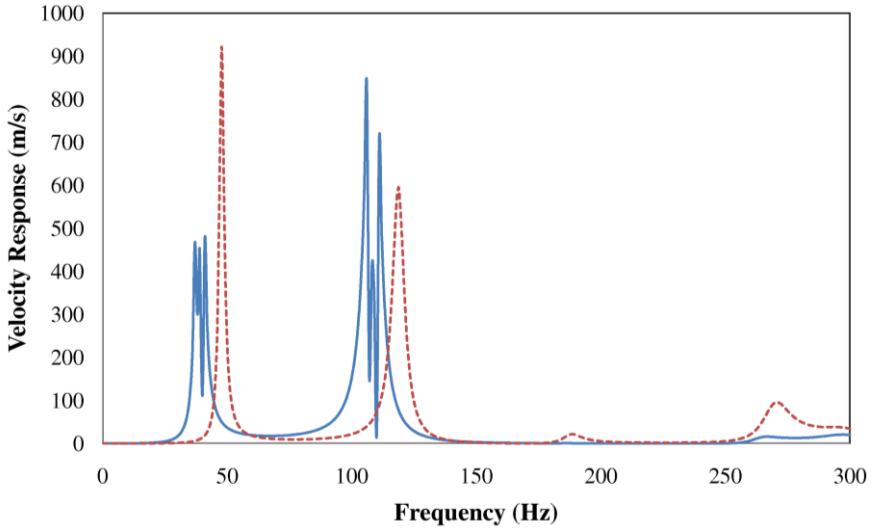

Figure A-7: Velocity response along the direction of the applied force at Joint B for the duct; ——— , membrane end, – – – , free end.

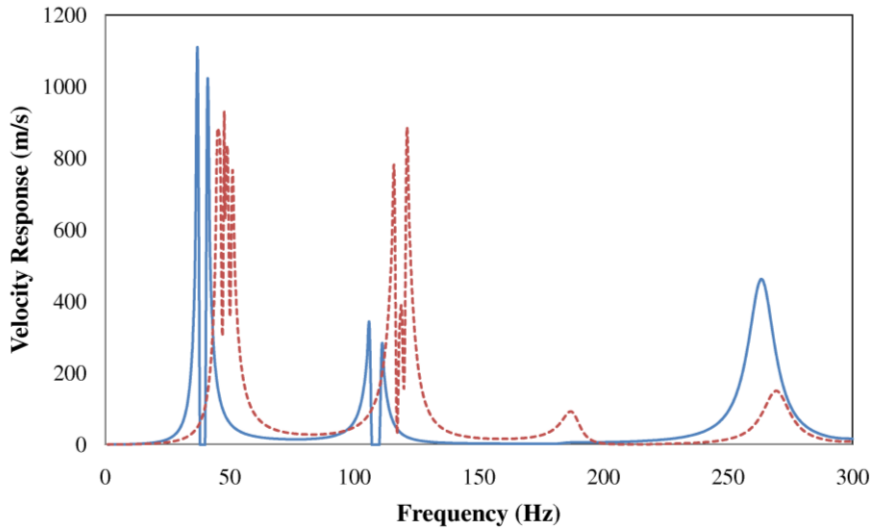

Figure A-8: Velocity response along the direction of the applied force at Joint C for the duct; ——— , membrane end, – – – , free end.

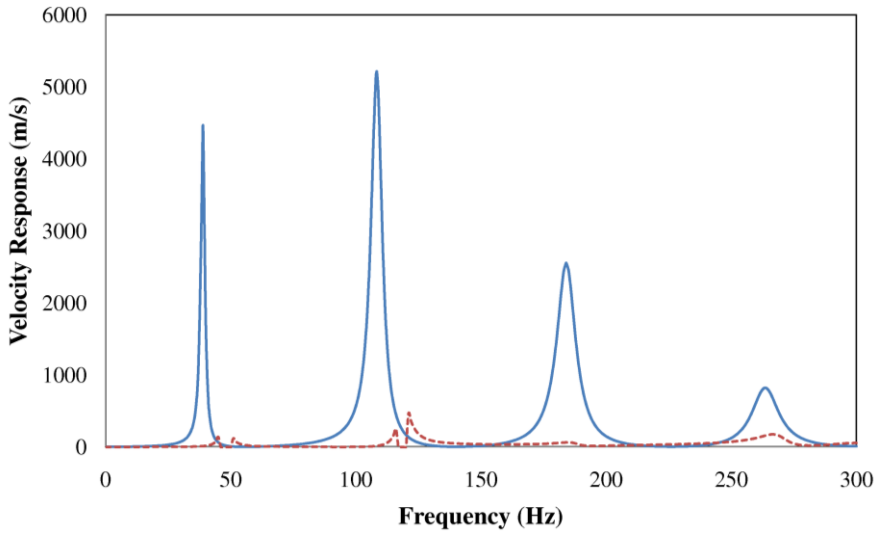

Figure A-9: Velocity response along the direction of the applied forces at Joint D for the duct; ——— , membrane end, – – – , free end.

B. Summary:

From the finite element analysis, a shift of resonant frequencies can be observed when using different end conditions: membrane end and free end. However, the sound absorption performance of the duct ended with a membrane cannot be determined. Further improvement on the boundary conditions is required to pursue a more accurate prediction on the air-block duct using the finite element analysis.

LIST OF BIBLIOGRAPHY

Adam, D. Proposed criteria for assessing low frequency noise annoyance in occupational settings. *International Journal of Occupational Medicine and Environmental Health* 2006, 19(3), 185-197.

Andersen, K.T. Theory for natural ventilation by thermal buoyancy in one zone with uniform temperature. *Building and Environment* 2003, 38(11), 1281-1289.

Asdrubali, F., Buratti, C. Sound intensity investigation of the acoustic performances of high insulation ventilating windows integrated with rolling shutter boxes. *Applied Acoustic* 2005, 66, 1088-1101.

Ballagh, K.O. Investigation into hygienic attenuators. *Applied Acoustics* 1993, 40, 107-122.

Bodart, M., Herde, A.D. Global energy savings in offices by the use of daylight. *Energy and Buildings* 2002, 34(5), 421-429.

Christopher, D.F., Fergus R.F. An attenuator for buildings using natural ventilation. *Noise Control Engineering Journal* 2001, 49(6), 258-264.

Cox, T.J., Antonio, P.D. *Acoustic Absorbers and Diffusers - Theory, Design and Application*, Spon Press, Oxford: UK, 2004.

Electrical and Mechanical Services Department (EMSD). *Hong Kong energy end-use data 2005*, Hong Kong, 2005b.

Frommhold, W., Fuchs, H.V., Sheng, S. Acoustic performance of membrane absorbers. *Journal of Sound and Vibration* 1994, 170, 621-636.

Fuchs, H.V., Zha, X. Acrylic-glass sound absorbers in the plenum of the Deutscher Bundestag. *Applied Acoustics* 1997, 51(20), 211–217.

Fujiwara, K., Miyajima, T. A study of the sound absorption of a quadratic-residue type diffuser. *Acustica* 1995, 81, 370-378.

Grabe, J.V. A prediction tool for the temperature field of double facades. *Energy and Buildings* 2002, 34(9), 891-899.

Huang, L.X. A theoretical study of duct noise control by flexible panels. *The Journal of the Acoustical Society of America*1999, 106(4), 1801-1809.

Hui, S.C.M. Solar Hong Kong – present applications and future prospects. *Renewable Energy World* 2000, 3(1), 76-83.

Hyde, R. *Bioclimatic Housing: Innovative Designs for Warm Climates,* Earthscan Publications Ltd., UK and USA, 2008.

Jenkins, C.H.M., Korde, U.A. Membrane vibration experiments: An historical review and recent results. *Journal of Sound and Vibration* 2006, 295, 602-613.

Kang, J. (2008). Using micro-perforated absorbers for sustainable building envelop development. Proceedings from INTER-NOISE 2008: *The 37th International Congress and Exposition on Noise Control Engineering*. China, Shanghai.

Kang, J., Brocklesby, M.W. Feasibility of applying micro-perforated absorbers in acoustic window systems. *Applied Acoustics* 2005, 66(6), 669–689.

Kang, J., Fuchs, H.V. Predicting the absorption of open weave textiles and micro-perforated membranes backed by an air space. *Journal of Sound and Vibration* 1999, 220(5), 905-920.

Kurt, R., Tyson, L., James, B. Double Skin Facades. *ASHRAE Journal* 2007.

Lee, E., Selkowitz, S., Bazjanac, V., Inkarojrit, V., Kohler, C. *High-performance commercial building facades*. Building Technologies Program, Environmental Energy Technologies Division, Ernest Orlando Lawrence Berkeley National Laboratory, University of California, Berkeley, 2002

Lee, J., Swenson, G.W. Compact sound absorbers for low frequencies. *Noise Control Engineering Journal* 1992, 38(3), 109–117.

Loncour, X., Deneyer, A., Blasco, M., Flamant, G., Wouters, P. *Ventilated double facades classification and illustration of façade concepts.* Belgian Building Research Institute: Department of Building Physics, Indoor Climate & Building Services, 2004.

Matthias, H., Felix, W., Alex, A. Double skin facades for Hong Kong. *Surveying and Built Environment* 2007, 18(2), 17-32.

Oesterle, E. Lieb, R.D., Lutz, G., Heusler, B. *Double-skin facades: integrated planning: building physics, construction, aerophysics, air-conditioning, economic viability*. Prestel, Munich, 2001.

Sakagami, K., Morimoto, M., Yairi, M., Minemura, A. A pilot study on improving the absorptivity of a thick microperforated panel absorber. *Applied Acoustic* 2008, 69, 179-182.

Salikuddin, M., Syed, A.A., Mungur, P. Acoustic characteristics of perforated sheets with throughflow in a high intensity noise environment. *Journal of Sound and Vibration* 1994, 169, 145-177.

Sharma, R.N., Richards, P.J. The influence of helmholtz resonance on internal pressures in a low-rise building. *Journal of Wind Engineering and Industrial Aerodynamics* 2003, 91, 807-828.

Stribling, D. and Stigge, B. *A critical review of the energy savings and cost payback issues of double facades*. CIBSE/ASHRAE Conference: Building Sustainability, Value and Profit, Edinburgh, Scotland, 2003.

Takahashi, D., Sakagami, K., Morimoto, M. Acoustic properties of permeable membranes. *The Journal of the Acoustical Society of America* 1996, 99(5), 3003-3009.

Thomson, W.T. *Theory of Vibration with Applications*. Prentice-Hall, New Jersey, 1981.

Wang, C.Q., Han, J., Huang, L.X. Optimization of a clamped plate silencer. *The Journal of the Acoustical Society of America* 2006, 119, 2628-2368.

Waye, K.P., Bengtsson, J., Rylander, R., Hucklebridge, F., Evans, P., Clow, A. Low frequency noise enhances cortisol among noise sensitive subjects during work performance 2002. *Life Science*, 70(7), 745-758.

Wen, H.L. (2008). Noise reduction window with natural ventilation. Proceedings from INTER-NOISE 2008: *The 37th International Congress and Exposition on Noise Control Engineering*. China, Shanghai.

White, R.G., Walker, J.G. Noise and vibration. *The Journal of the Acoustical Society of America*1983, 74(4), 1312-1313.

Wu, T., Cox, T.J., Lam, Y.W. A profiled structure with improved low frequency absorption. *The Journal of the Acoustical Society of America* 2006, 110, 3064-3070.